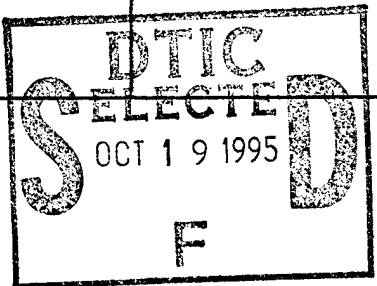


REPORT DOCUMENTATION PAGE			Form Approved OMB No. 0704-0188	
Public reporting burden for this collection of information is estimated to average 1 hour per response, including the time for reviewing instructions, searching existing data sources, gathering and maintaining the data needed, and completing and reviewing the collection of information. Send comments regarding this burden estimate or any other aspect of this collection of information, including suggestions for reducing this burden, to Washington Headquarters Services, Directorate for Information Operations and Reports, 1215 Jefferson Davis Highway, Suite 1204, Arlington, VA 22202-4302, and to the Office of Management and Budget, Paperwork Reduction Project (0704-0188), Washington, DC 20503.				
1. AGENCY USE ONLY (Leave blank)		2. REPORT DATE 10 Sep 95		3. REPORT TYPE AND DATES COVERED
4. TITLE AND SUBTITLE Temporal and spatial Variability of Surface Temperature Over Texas			5. FUNDING NUMBERS	
6. AUTHOR(S) Anthony David Moninski				
7. PERFORMING ORGANIZATION NAME(S) AND ADDRESS(ES) AFIT Students Attending: Texas A&M University			8. PERFORMING ORGANIZATION REPORT NUMBER 95-112	
9. SPONSORING/MONITORING AGENCY NAME(S) AND ADDRESS(ES) DEPARTMENT OF THE AIR FORCE AFIT/CI 2950 P STREET, BLDG 125 WRIGHT-PATTERSON AFB OH 45433-7765			10. SPONSORING/MONITORING AGENCY REPORT NUMBER	
11. SUPPLEMENTARY NOTES				
12a. DISTRIBUTION/AVAILABILITY STATEMENT Approved for Public Release IAW AFR 190-1 Distribution Unlimited BRIAN D. GAUTHIER, MSgt, USAF Chief of Administration			12b. DISTRIBUTION CODE	
13. ABSTRACT (Maximum 200 words)				
<div style="font-size: 2em; font-weight: bold; margin: 20px 0;">19951017 163</div>				
DTIC QUALITY INSPECTED 5				
14. SUBJECT TERMS			15. NUMBER OF PAGES 90	
			16. PRICE CODE	
17. SECURITY CLASSIFICATION OF REPORT	18. SECURITY CLASSIFICATION OF THIS PAGE	19. SECURITY CLASSIFICATION OF ABSTRACT	20. LIMITATION OF ABSTRACT	

**TEMPORAL AND SPATIAL VARIABILITY OF SURFACE
TEMPERATURE OVER TEXAS**

A Thesis

by

ANTHONY DAVID MONINSKI

Submitted to the Office of Graduate Studies of
Texas A&M University
in partial fulfillment of the requirements for the degree of

MASTER OF SCIENCE

Accession For		
NTIS CRA&I		<input checked="checked" type="checkbox"/>
DTIC TAB		<input type="checkbox"/>
Unannounced		<input type="checkbox"/>
Justification		
By		
Distribution/		
Availability Codes		
Dist	Avail. and/or Special	
A-1		

August 1995

Major Subject: Meteorology

TEMPORAL AND SPATIAL VARIABILITY OF SURFACE
TEMPERATURE OVER TEXAS

A Thesis

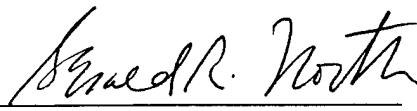
by

ANTHONY DAVID MONINSKI

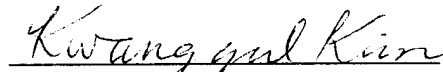
Submitted to Texas A&M University
in partial fulfillment of the requirements
for the degree of

MASTER OF SCIENCE

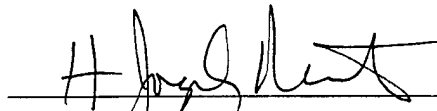
Approved as to style and content by:



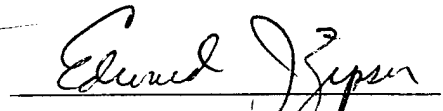
Gerald R. North
(Chair of Committee)



Kwang-Y. Kim
(Member)



H. Joseph Newton
(Member)



Edward J. Zipser
(Head of Department)

August 1995

Major Subject: Meteorology

ABSTRACT

Temporal and Spatial Variability of Surface Temperature
over Texas. (August 1995)

Anthony David Moninski, B.S., Pennsylvania State University

Chair of Advisory Committee: Dr. Gerald R. North

Surface temperature is one of the most fundamental aspects of the climate system, and its study has been the focus of extensive research in the field of climatology for years. Examination of its temporal and spatial fluctuations can provide scientists with information on the behavior of the atmospheric circulation. Many researchers have also been interested in the physical processes and mechanisms at work in producing the observed distribution of the surface temperature field over the globe.

Various analytical methods are used in the study of temperature variability on the Earth. White and Wallace (1978) documented the annual march of surface temperature by mapping amplitudes and phases of the seasonal cycle. The latter were obtained through Fourier analysis of the data. Kim and North (1991, 1992) routinely use second-moment statistics such as variance and spatial correlation to study the fluctuations of temperature in energy balance models as compared with observations. Empirical orthogonal function (EOF) analysis has become a popular and convenient method for representing the variability of climatic parameters since the groundbreaking work of Lorenz (1956). The first several EOFs, or patterns of covariability in a meteorological field, can sometimes be explained in a physical sense based on their shapes.

While most previous efforts have concentrated on the global or hemispheric scale, this research examines the fluctuations of surface temperature on a regional scale, namely the state of Texas. Texas is an ideal location for a study of this

type due to its vast areal extent, diverse topography, and expanse across different climatic regimes. Some of the methods used in the study of temperature variability are applied to the state of Texas.

DEDICATION

This thesis is dedicated to my mother, Alice, for her continued love and encouragement over the years. She always urged me to be diligent and to do the best that I could, regardless of the situation. Instead of pursuing a career for herself, she chose to commit her life to being the best mother any son could have. She sacrificed her time and prayed many prayers so that her children could have a better life than she did. While I may have gained some knowledge about the complex atmosphere over me during my years here, the basics of life taught to me by my mother at a young age are what have carried me this far.

ACKNOWLEDGMENTS

Many individuals were integral parts of this research effort. Above all, I would like to thank Almighty God for His grace and His blessings during my time here at Texas A&M. My relationship with Jesus Christ has grown stronger as a result of this academic experience.

I am deeply indebted to the United States Air Force for providing me this opportunity to further my education at their expense. This service organization has allowed me to complete both undergraduate and graduate work through their financial support.

I thank the chair of my committee, Dr. Gerald R. North, for first suggesting this topic to me and attempting to tailor it to the needs of the Air Force. His comments and recommendations were both insightful and beneficial. He was a source of motivation for me to pursue this work.

I owe a special token of gratitude to Dr. Kwang-Yul Kim of the Climate System Research Program (CSRP), who served as a committee member. He spent countless hours and days teaching me about the concepts studied in this research. He also provided nearly all of the computer codes needed to perform this study. I could not have completed this work in a timely manner without him.

I thank Dr. H. Joseph Newton from the Statistics Department for teaching me about time series analysis in his course. He is an excellent instructor.

In addition, I would like to thank members of the CSRP for their support and assistance in this research: Ms. Yuhong Yi, my office mate, who was continually interrupted by my inquisitiveness; Mr. Mark Stevens, with whom I enjoyed many discussions; and Mr. Neil Smith, the computer genius for the group who often came to my rescue during workstation crises and related dilemmas.

Finally, I would like to extend thanks to Professor John F. Griffiths and Dr.

James P. McGuirk, both of the Meteorology Department, for their fruitful discussions with me about the finer points of EOF analysis. I also thank Iwan Gunawan of the Geography Department for assisting me in the creation of Thiessen polygons for my station data.

TABLE OF CONTENTS

	Page
ABSTRACT	iii
DEDICATION	v
ACKNOWLEDGMENTS	vi
TABLE OF CONTENTS	viii
LIST OF TABLES	ix
LIST OF FIGURES	x
1 INTRODUCTION	1
1.1 Present Status of the Problem	1
1.2 Reason for Texas Study	4
1.3 Objectives	6
2 DESCRIPTION OF DATA	9
2.1 Sources and Format of Data	9
2.2 Possible Errors Associated with the Data	12
3 METHODS OF ANALYSIS	14
3.1 Fourier Analysis	14
3.2 Analysis Of Second-Moment Statistics	18
3.3 Empirical Orthogonal Function Analysis	20
4 RESULTS AND DISCUSSION	28
4.1 Fourier Analysis	28
4.2 Second-Moment Statistics	43
4.3 Empirical Orthogonal Function Analysis	67
5 SUMMARY AND CONCLUSIONS	83
REFERENCES	87
VITA	90

LIST OF TABLES

TABLE		Page
1	A listing of the stations used in this study, along with pertinent information.	10
2	Phase and amplitude of the annual cycle with an estimate of the standard error for each quantity.	32
3	Correlation between the first 8 EOFs computed with and without an area weighting for each station.	68
4	Total variance, percent variance, and cumulative percent variance associated with the first 8 EOFs for January, April, July, October and the entire year.	70

LIST OF FIGURES

FIGURE		Page
1	Map showing the layout of orography across the region of interest. ..	5
2	The ten climatic divisions of Texas.	7
3	Procedure for defining Thiessen polygons.	26
4	Plot of the region of study showing each station's location and its area weighting as defined by a Thiessen polygon.	27
5	Plot of amplitude and phase lag of the annual cycle of mean monthly temperature at each station.	30
6	Plot of standard error for amplitude and phase of the annual cycle of mean monthly temperature at each station.	31
7	Same as in FIG. 5, but for mean daily maximum temperature.	34
8	Same as in FIG. 5, but for mean daily minimum temperature.	36
9	Plot of amplitude and phase lag of the semiannual cycle of mean monthly temperature at each station.	39
10	Same as in FIG. 9, but for mean daily maximum temperature.	40
11	Same as in FIG. 9, but for mean daily minimum temperature.	41
12	Distribution of variance of the mean monthly temperature field for the months of January, April, July and October.	44
13	Same as in FIG. 12, but for mean daily maximum temperature. ...	47
14	Same as in FIG. 12, but for mean daily minimum temperature.	48
15	Plot of spatial correlation function for mean monthly temperature for the months of January, April, July and October.	50
16	Same as in FIG. 15, but a station in central Texas is used as the reference point.	51
17	Same as in FIG. 15, but a station in mountainous west Texas is used as the reference point.	52

FIGURE		Page
18	Plot of spatial correlation function for mean daily maximum temperature for the months of January, April, July and October. ..	54
19	Same as in FIG. 18, but a station in central Texas is used as the reference point.	55
20	Same as in FIG. 18, but a station in mountainous west Texas is used as the reference point.	56
21	Plot of spatial correlation function for mean daily minimum temperature for the months of January, April, July and October. ..	57
22	Same as in FIG. 21, but a station in central Texas is used as the reference point.	58
23	Same as in FIG. 21, but a station in mountainous west Texas is used as the reference point.	59
24	Plot of the temporal correlation function for a lag of one month for the mean monthly, mean daily maximum and mean daily minimum temperature field.	62
25	Plot of the temporal correlation function for a lag of one year for the mean monthly temperature field.	64
26	Same as in FIG. 25, but for mean daily maximum temperature. ...	65
27	Same as in FIG. 25, but for mean daily minimum temperature.	66
28	First four spatial EOFs of mean monthly temperature for the year.	71
29	Same as in FIG. 28, but for mean daily maximum temperature. ...	72
30	Same as in FIG. 28, but for mean daily minimum temperature.	73
31	First spatial EOF for mean monthly temperature for the months of January, April, July and October.	75
32	Second spatial EOF for mean monthly temperature for the months of January, April, July and October.	78

FIGURE

Page

33	Third spatial EOF for mean monthly temperature for the months of January, April, July and October.	80
34	Fourth spatial EOF for mean monthly temperature for the months of January, April, July and October.	82

1. INTRODUCTION

1.1. Present Status of the Problem

Surface temperature is one of the most fundamental aspects of climate, and its study has been the focus of extensive research in climatology. It is instructive to study both the spatial and temporal fluctuations of surface temperature, whether forced or natural, for they provide some information on the energy budget of the Earth and some clue as to the behavior of the atmospheric circulation. Records from observation stations worldwide have been analyzed using various methods over the years, and maps of the analysis results have been created for further study. Many researchers have also been interested in the physical processes and mechanisms at work in producing the observed distribution of the surface temperature field and its temporal and spatial fluctuations.

Kendrew (1953) noted that the pattern and variation of the observed surface temperature over the continents are largely due to the geography of the land and sea over the Earth. He found that locations displaced far from any marine influence, as he called it, have larger annual ranges of surface temperature than those on or near bodies of water, especially on the continental littorals. The annual temperature cycle over land not only possesses a greater amplitude, but also occurs earlier in phase than the marine counterpart. The extremely small thermal inertia of land and atmosphere compared with water is considered to be the main factor in producing this contrast, known as the continentality effect.

Prescott and Collins (1951) calculated the lag of surface temperature behind solar radiation on a global basis and for the United States using Fourier analysis. They found phase lags of up to one-and-a-half to two months for locations at or near

The thesis style is that of the *Journal of Climate*.

coastal areas, while inland sites had lags of about one month. They concluded that phase lag could be considered an index of continentality. Griffiths and Driscoll (1982) later summarized the primary factors which shape the annual cycle of temperature as observed at various locations over the globe: latitude, elevation, and continentality.

White and Wallace (1978) documented the annual march of surface temperature over the Earth by mapping the amplitudes and phases of the annual and semiannual cycles in a vectorial format. These were obtained after subjecting the monthly mean temperatures to harmonic analysis. Their results confirmed those of previous investigators while presenting the annual cycle in a compact and objective format suitable for future use in climate studies.

Since the climate can be defined as the long-term average condition of the Earth (Griffiths and Driscoll 1982), the variability of climate variables from their mean values is often studied. The temperature field at the surface exhibits both temporal and spatial variability (Kim and North 1991, 1992). The latter is primarily due to the effects of latitude and continentality (Griffiths and Driscoll 1982). The interannual variability is an important current issue in climatology and is a measure of the year-to-year variation of climatic variables (Shea 1986). There are also significant monthly fluctuations in the variance. The winter months in the Northern Hemisphere experience much greater interannual variability than the summer months due to the higher frequency and strength of transient synoptic systems.

Empirical orthogonal function (EOF) analysis has become a popular and convenient method for representing the variability of climate variables. EOFs have been widely used to study dominant spatial patterns (Kim and North 1993) and the time history of these patterns. They also provide a compact means of representing the main variability in a dataset, allowing us to discard much that is insignificant. Different sources of variability are ultimately separated into modes, and these modes are subsequently arranged in descending order based on the amount of the variance

“explained.” The first several patterns, or EOFs, associated with these modes can sometimes be explained in a physical sense based on their shapes. Other higher modes occur on decreasing space scales and generally represent local variations and noise.

Grimmer (1963) processed 80 years of monthly surface temperature anomalies from 32 stations in northwest Europe using an EOF analysis. His first eight modes contain over 80% of the variance in the data, permitting the original dataset to be reduced by 75%. The dominant patterns he observed occur more or less unchanged throughout the year, signifying that the physical agencies which cause them are prevailing at all seasons. For example, the first EOF indicates the great importance of continentality in the monthly anomaly fields, showing the strong temperature gradient over the European littoral due to the land-sea configuration. Likewise, the second pattern seems to be associated with thermal advection in zonal currents. Nearly all of the important information about the surface temperature field is contained in the first few EOFs.

Kutzbach (1967) studied the two-dimensional fields of three climatic variables, including the monthly surface temperature, at 23 stations in North America during 25 years of Januarys using an EOF analysis. Nearly 88% of the total variance in the temperature field could be explained by the first five EOFs. He was also able to decipher known climatological fields in the patterns.

Kidson (1975) attempted to evaluate the usefulness of EOFs as climatological indices. He analyzed 10 years of monthly surface data, including temperature, for nearly 1900 stations around the world. Over 98% of the variance in the Northern Hemisphere temperature data could be explained by the first 10 modes, with nearly 95% accounted for by the first mode.

Statistical estimates derived from meteorological fields are widely used as aids in verifying the accuracy of model-generated data, especially those produced in con-

junction with climate change research. Preisendorfer and Barnett (1983) used EOFs as a primary tool in testing model output against observational data. Kim et al. (1984) studied the relationship between local and large-scale climate in the state of Oregon through the use of EOFs. Hyde et al. (1989) tested energy balance model runs with the amplitudes and phase lags of the annual and semiannual cycles of the observed surface temperature.

The study I propose to undertake is similar to that of Shea (1986), who provided a complete statistical analysis of 30 years of global atmospheric data by mapping such quantities as mean, interannual variability, EOFs, and amplitude and phase of the annual cycle of temperature. He reasoned that historical datasets were necessary to describe and understand the mean state of the atmosphere and its variability, assess its predictability, and validate climate simulations. The resolution of observed global data fields, however, is not adequate for use in regional climate model simulations, which are becoming more prevalent as researchers seek to gain a better understanding of the regional impacts of global climate change (Giorgi et al. 1993). The use of a denser network of stations, which is roughly equivalent to a scale reduction, would make it possible to resolve smaller scales of variability (Kutzbach 1967).

Therefore, I propose to calculate various statistical quantities for the state of Texas in order to learn more about the temporal and spatial fluctuations of the surface temperature field, and hence the climate, on a regional scale.

1.2. Reason for Texas Study

The state of Texas is the largest in the conterminous United States in terms of total land area, covering over 267,000 square miles. It extends from 25°50' to 36°30'N in latitude and from 93°31' to 106°38'W in longitude. The elevation ranges from sea level at the Gulf of Mexico to over 8,700 feet in the extreme west, where

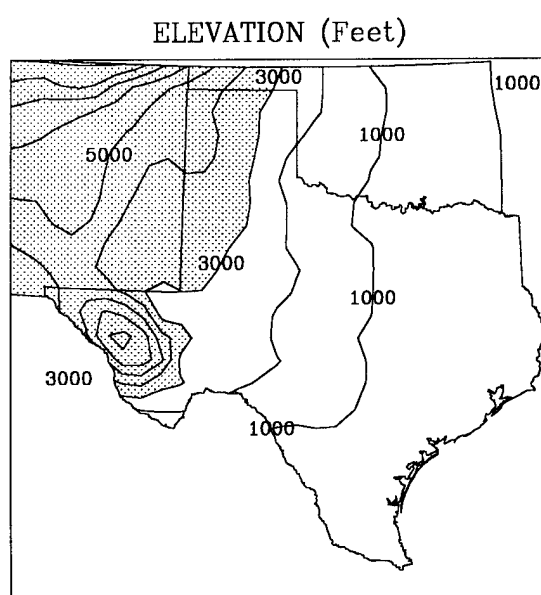


FIG. 1. Map showing the layout of orography across the region of interest. Contours are labelled in units of feet. Elevations of 3,000 feet and greater are shaded.

the Rocky Mountains traverse the state. Figure 1 is a map depicting the general orography across the state of Texas. This vast extent in size and elevation produces many different types of climate around the state, from the cool and dry temperate of the High Plains (north) and Trans-Pecos (west) to the humid subtropical temperate of the East and the Gulf Coast. Extreme southern areas even experience near-tropical weather. As a result of this diversity, the state has been divided into ten climatic regions by the National Weather Service (Griffiths et al. 1987), as indicated in Figure 2.

While similar studies have been conducted on a global scale (Shea 1986), no study has yet focused on the depiction and the variability of the regional temperature field over Texas and the adjacent area. Texas provides an ideal setting for a study in regional climate.

1.3. Objectives

The goal of this research is to provide a comprehensive analysis of the variability of the surface temperature field over the state of Texas. Therefore, I propose the following objectives in order to meet this goal:

- (1) Depict the extent of continentality in the state of Texas through analysis of the surface temperature field. Specifically, I will perform a Fourier analysis to determine amplitude and phase lag of the annual and semiannual cycles of temperature.
- (2) Examine variability of surface temperature in Texas by providing a limited analysis of second-moment statistics such as variance.
- (3) Perform an EOF analysis of the surface temperature field in Texas to show the dominant modes of variability for different frequency bands. I will also determine the percent variance explained by each EOF mode.

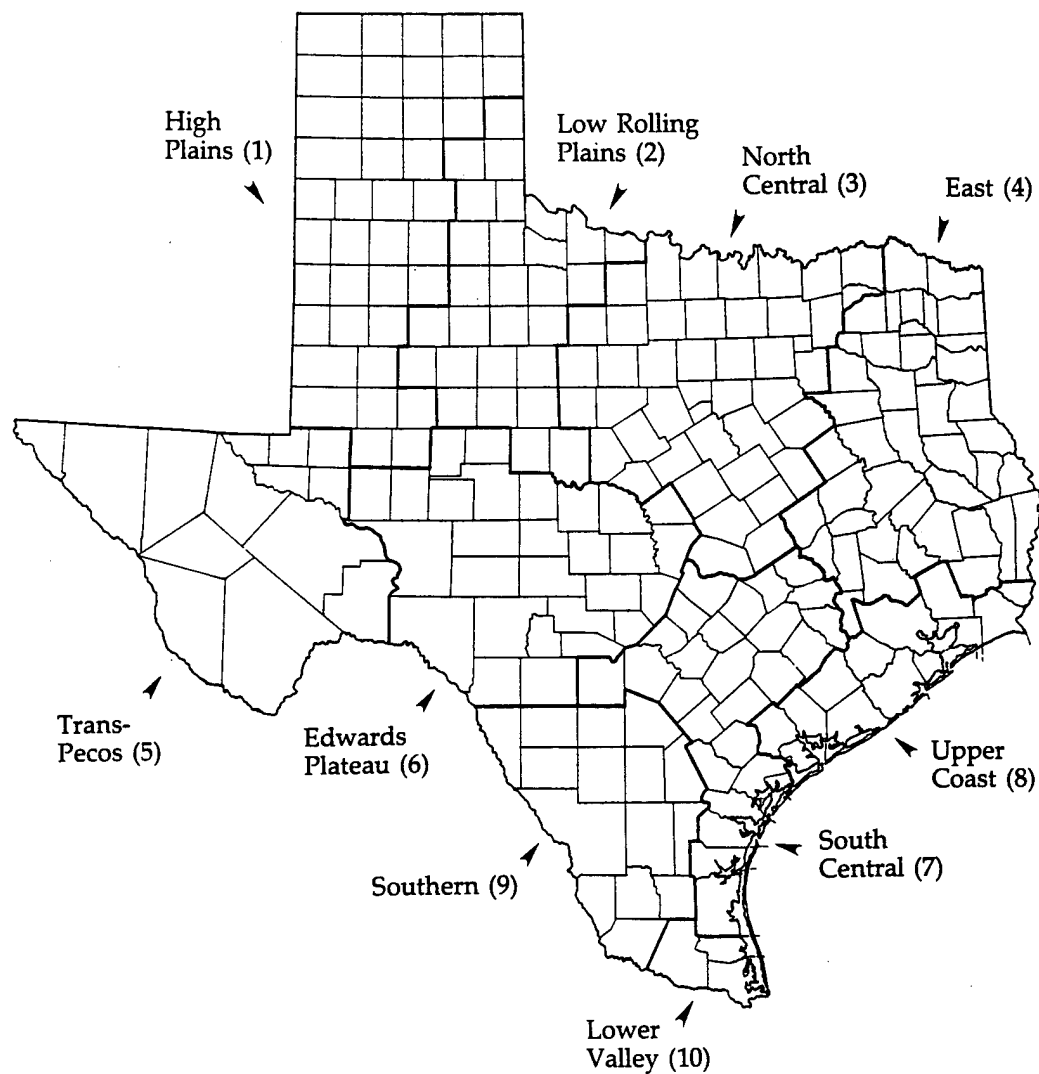


FIG. 2. The ten climatic divisions of Texas (Griffiths et al. 1987).

- (4) Attempt to relate the dominant EOF patterns observed in (3) to known synoptic and climatological features of the atmospheric circulation over Texas.

This thesis will cover the following areas. In section 2, the data used in this study are described, along with possible errors associated with them. Section 3 discusses the different types of analyses performed on the data. Results from the respective analytical methods are presented and discussed in section 4. Finally, section 5 gives a summary of and provides conclusions drawn from this research.

2. DESCRIPTION OF DATA

2.1. Sources and Format of Data

The data used in this study consisted of mean monthly temperatures from a vast spatial network of observing stations in Texas, Oklahoma, and eastern New Mexico. A listing of each station and pertinent information about the station is in Table 1. Each location's data underwent a crude quality control check to ensure accuracy and completeness. The following criteria were adhered to during the selection process:

- (a) Period of record for each station must equal or exceed fifty continuous years ending in December 1992, i.e. minimum 600 consecutive data points per station.

Thus, a minimum record consists of monthly values from January 1943 through December 1992.

- (b) Number of missing monthly values in a station's record must be no greater than 5% of the total.

Utilization of the above criteria allowed for a large number of stations to be included in this study while also serving to reduce some of the sampling error inherent in the statistical analysis.

Temperature data for the states of Texas and Oklahoma were extracted from EarthInfo, Inc.'s National Climatic Data Center (NCDC) Summary of the Day WEST2 1993 CD-ROM. New Mexico data through the year 1987 were obtained from United States Historical Climatology Network Serial Temperature and Precipitation Data (rev. 1990), located on Volume One of the Carbon Dioxide Information Analysis Center's Numeric Data Packages CD-ROM, version 1.02. The remaining years' data for New Mexico, 1988 through 1992, were transcribed from *Climatological Data Annual Summary, New Mexico* for the respective years.

All temperature data in this study are in the form of mean daily maximum and mean daily minimum temperatures. The mean monthly temperatures were gener-

TABLE 1. A listing of the stations used in this study, along with pertinent information. The last two columns will be referred to in section 3.

Station	Lon.	Lat.	Elev. (feet)	Yrs of Data	Thiessen Number	Polygon Area (m ²)
Ada, OK	96 41 W	34 47 N	1020	86	22	6276545055.54
Austin, TX	97 42 W	30 17 N	590	63	70	4388800506.36
Ballinger, TX	100 03 W	31 44 N	1640	91	60	20760357938.46
Beeville, TX	97 42 W	28 27 N	250	91	89	18973190355.87
Bell Ranch, NM	104 06 W	35 32 N	4500	89	12	8410273057.47
Blanco, TX	98 25 W	30 06 N	1370	69	71	3171920656.01
Boerne, TX	98 43 W	29 48 N	1420	89	75	13405642873.78
Brenham, TX	96 24 W	30 10 N	310	91	67	14766511392.55
Bridgeport, TX	97 46 W	33 13 N	750	58	36	7035294707.96
Carrizozo, NM	105 53 W	33 39 N	5440	85	26	35586128500.07
Cimarron, NM	104 57 W	36 28 N	6540	89	3	7223833279.46
Clayton, NM	103 09 W	36 27 N	4670	80	5	20313353317.66
Cleburne, TX	97 24 W	32 20 N	780	80	50	6550534292.21
Clarksville, TX	95 02 W	33 38 N	440	50	23	18360852722.48
Coleman, TX	99 26 W	31 50 N	1730	84	55	8176011081.14
Corsicana, TX	96 28 W	32 05 N	420	91	56	9704337232.94
Crosbyton, TX	101 15 W	33 39 N	3010	93	31	9695852885.02
Danevang, TX	96 14 W	29 03 N	70	96	79	2417251409.85
Denison Dam, TX	96 34 W	33 49 N	610	53	29	9007534558.45
Eagle Pass, TX	100 29 W	28 42 N	810	91	86	20850349613.91
Encinal, TX	99 25 W	28 02 N	590	78	80	24105421398.78
Enid, OK	97 52 W	36 25 N	1250	90	10	9759903710.77
Flatonina, TX	97 07 W	29 40 N	520	85	73	3734930056.47
Fredericksburg, TX	98 52 W	30 16 N	1750	54	69	14307421053.90
Frederick, OK	99 01 W	34 24 N	1300	84	20	12589894026.12
Goliad, TX	97 24 W	28 40 N	140	56	88	7967410486.56
Graham, TX	98 35 W	33 06 N	1050	64	39	7340396422.60
Greenville, TX	96 13 W	33 12 N	610	92	38	6060856361.11
Harlingen, TX	97 40 W	26 12 N	40	74	83	2698400804.32
Haskell, TX	99 44 W	33 10 N	1610	92	42	8621527170.71
Henderson, TX	94 48 W	32 10 N	420	52	51	7665985762.31
Henrietta, TX	98 12 W	33 49 N	900	91	28	9591842230.11
Hico, TX	98 02 W	31 59 N	1020	77	54	8692420503.52
Hillsboro, TX	97 07 W	32 01 N	550	84	57	5654786636.91
Hallettsville, TX	96 57 W	29 28 N	270	96	78	5024465192.81
Holdenville, OK	96 24 W	35 05 N	860	92	14	26040102056.47
Hollis, OK	99 55 W	34 42 N	1630	69	18	9844841321.63
Jacksboro, TX	98 09 W	33 14 N	1100	52	41	3334428390.85
Jefferson, OK	97 48 W	36 43 N	1050	71	8	8728323576.23
Jemez Springs, NM	106 41 W	35 46 N	6260	83	1	44627156723.31
Kaufman, TX	96 16 W	32 33 N	420	93	49	7639717413.40
Kingfisher, OK	97 54 W	35 51 N	1100	96	13	16926119982.76
Lamesa, TX	101 56 W	32 42 N	2970	66	46	22476751191.00
Lampasas, TX	98 11 W	31 03 N	1020	93	64	7435594329.15
La Tuna, TX	106 36 W	31 58 N	3800	50	58	7908326117.66
Liberty, TX	94 48 W	30 03 N	40	88	85	16622857616.76
Livingston, TX	94 56 W	30 44 N	180	56	66	12093865892.22
Llano, TX	98 41 W	30 45 N	1040	84	65	8467601431.73
Lubbock, TX	101 49 W	33 39 N	3250	79	32	8175145069.83
Lufkin, TX	94 45 W	31 14 N	280	68	61	12459075881.86
Luling, TX	97 39 W	29 40 N	400	92	76	4727092569.13
Marshall, TX	94 21 W	32 32 N	350	84	44	6985143427.20
Matagorda, TX	95 58 W	28 42 N	10	66	87	3130448971.46
McAllen, TX	98 13 W	26 12 N	120	52	82	1548015385.31
McCamey, TX	102 12 W	31 08 N	2450	61	84	40910217191.65
McKinney, TX	96 37 W	33 10 N	600	50	43	5085211014.10
Memphis, TX	100 32 W	34 44 N	2090	76	24	11149987203.82
Miami, TX	100 38 W	35 42 N	2760	87	9	21703607704.49

TABLE 1. (Continued)

Station	Lon.	Lat.	Elev. (feet)	Yrs of Data	Thiessen Number	Polygon Area (m ²)
Mission, TX	98 24 W	26 13 N	130	72	81	8007284783.61
Mount Locke, TX	104 00 W	30 40 N	6790	58	62	26810129915.42
Mount Pleasant, TX	95 00 W	33 10 N	420	74	40	9306859342.66
Muleshoe, TX	102 45 W	34 14 N	3760	65	25	19296313068.80
Munday, TX	99 38 W	33 27 N	1460	55	35	4665346813.84
New Braunfels, TX	98 07 W	29 44 N	710	93	74	5590297062.54
Orogrande, NM	106 06 W	32 23 N	4180	53	47	20674960570.25
Palacios, TX	96 15 W	28 43 N	20	50	90	2784658424.36
Pauls Valley, OK	97 17 W	34 44 N	940	84	19	12629093204.69
Pawhuska, OK	96 21 W	36 40 N	840	87	6	24494960414.93
Pecos, TX	103 30 W	31 25 N	2610	58	53	26735032080.23
Pierce, TX	96 11 W	29 14 N	100	85	77	7668819478.86
Plainview, TX	101 42 W	34 11 N	3370	84	21	12056971480.86
Presidio, TX	104 20 W	29 32 N	2560	64	72	14309006353.70
Quanah, TX	99 41 W	34 15 N	1500	84	27	6464368655.97
Raymondville, TX	97 48 W	26 28 N	30	73	91	10198341986.63
Red River, NM	105 24 W	36 42 N	8680	84	2	10941002381.41
Rising Star, TX	98 58 W	32 06 N	1630	50	52	8851732286.83
Roscoe, TX	100 32 W	32 27 N	2380	56	48	9850853554.94
Roswell, NM	104 32 W	33 18 N	3670	89	30	32518564073.85
Rusk, TX	95 09 W	31 48 N	720	51	59	9796908878.06
San Jon, NM	103 20 W	35 07 N	4230	85	16	13918948483.34
Santa Rosa, NM	104 41 W	34 57 N	4620	70	17	22304225273.74
Seymour, TX	99 15 W	33 36 N	1290	67	33	5228690178.81
Sherman, TX	96 37 W	33 38 N	720	82	34	3865169384.84
Snyder, TX	100 55 W	32 43 N	2340	74	45	8724121242.99
Spearman, TX	101 11 W	36 11 N	3090	65	7	25894369028.86
Springer, NM	104 35 W	36 21 N	5880	89	4	9578255975.85
State University, NM	106 45 W	32 17 N	3880	88	37	13184407409.20
Stillwater, OK	97 06 W	36 07 N	900	100	11	9747212913.36
Taylor, TX	97 25 W	30 34 N	560	64	68	5249419471.98
Temple, TX	97 19 W	31 05 N	630	93	63	10182058150.56
Tucumcari, NM	103 41 W	35 12 N	4090	89	15	5813441591.96

ated simply from an algebraic mean of the maximum and minimum temperatures. All missing data were replaced in the record by the appropriate mean value for the particular month.

2.2. Possible Errors Associated with the Data

Data from the Earth Info, Inc. CD-ROM consisted of daily maximum and daily minimum temperatures for each month and year of the period of record at a station. The mean daily maximum and minimum values which I extracted from this CD were computed upon command by the program software. In some cases, these latter values were calculated from monthly records which were incomplete. In accordance with NCDC procedure, mean values are generated for a month as long as fewer than 10 daily maximum or 10 daily minimum temperatures are missing. If this criterion is not satisfied, the mean is reported missing.

The data for eastern New Mexico followed a slightly different criterion. All mean temperatures for the month were reported, but flags indicating the number of missing daily values in computing the mean were used. Since one of the flags was defined as "1-10 daily values missing", it was impossible to use the same cutoff point as in the EarthInfo, Inc. dataset. Therefore, these New Mexico data include some mean values which were calculated when as many as 10 daily measurements were missing. When over 10 such values were missing, I chose to count the monthly mean as a missing value for the sake of consistency with the Texas and Oklahoma datasets.

In addition, some data for eastern New Mexico were identified as suspect or flaky based on the observation time for the station. The flag code indicated that the temperature data should be used with caution. Such data were not used in this study, but rather were reported missing.

Another possible source of error with the EarthInfo, Inc. data is due to rounding off. All mean daily maximum and minimum temperatures were rounded off to the nearest whole number. However, when mean monthly values and missing values were computed, they were carried out to one decimal place. All New Mexico data were reported to one decimal place, as well.

A source of spatial bias in the representation of the data may be from its interpolation onto a regular grid from irregularly-spaced data points. Missing values may also contribute to bias over the domain of interest.

Since this study wasn't directly concerned with climatic change in the Texas region per se, I didn't seek to homogenize any times series or minimize the effects of urbanization. Only original data as reported in climatological records were utilized.

3. METHODS OF ANALYSIS

3.1. Fourier Analysis

Fourier, or harmonic, analysis permits an objective approach to the study of climatological features. It often allows scientists to be able to distinguish regional and local characteristics, or delineate boundaries between different climatic regimes (Kirkyla and Hameed 1989). Fourier analysis is applied to study periodic variations and is also used commonly in research of the seasonal cycles of meteorological variables such as temperature, precipitation, and geopotential heights (White and Wallace 1978; Hsu and Wallace 1976). White and Wallace (1978) produced charts showing the distribution of the amplitude and the phase of various harmonics resulting from the annual variation of temperature over the globe. Such an analysis provided a more objective basis for identifying various climatic regions on the earth. North and his collaborators (North et al. 1983; Hyde et al. 1989; Kim and North 1991) routinely use harmonics in testing the sensitivity of their two-dimensional surface energy balance model. Griffiths and Driscoll (1982) present a concise discussion of this procedure as it applies to studies in climatology.

A discrete Fourier analysis is the decomposition of a time series into the sum of sinusoids of various frequencies and amplitudes. The basic idea of a harmonic analysis is that one can find a unique set of sinusoids (sines and cosines of differing frequency) which, when added together, reconstruct the mathematical object being studied. Namely,

$$T(t_i) = \sum_{n=0}^{N/2} a_n \cos(2\pi t_i/N) + \sum_{n=1}^{N/2} b_n \sin(2\pi t_i/N), \quad i = 1, \dots, N, \quad (1)$$

where a_n and b_n are, respectively, the cosine and sine expansion coefficients of the n th harmonic. Such a uniqueness representation is based on the mathematical principle that the cosine and sine functions form a complete basis set (Weinberger 1965). Thus,

one can study a complicated object by breaking it up into these simple "frequency components" and studying them separately.

Since the annual variation of mean monthly surface temperature at most stations in the northern Hemisphere mid-latitudes is periodic or quasi-sinusoidal in nature, this type of analysis is appropriate in order to isolate the dominant frequency components of the surface temperature fluctuations. The coefficients resulting from a discrete Fourier transformation are used to compute the amplitude and the phase of each cycle (Newton 1988):

$$\text{Amplitude} = \sqrt{a_n^2 + b_n^2}, \quad (2)$$

$$\text{Phase} = \tan^{-1}(b_n/a_n),$$

where n indicates that the amplitude and phase are for the n th harmonic. The frequency of undulation dominating the variation of a certain climatic variable is revealed by a comparison of the size of the amplitudes. In this study, the amplitude is in degrees Fahrenheit and the phase is in days.

The sinusoid having a period of 12 months is a good representation of the annual cycle of temperature in the Northern Hemisphere mid-latitudes. It accounts for a large portion of the variance in the actual data. The sinusoid corresponding to the semiannual cycle also accounts for some of the variance. Therefore, the amplitude and phase for these two cycles will be computed at each station over the period of record.

3.1.1. Phase Lag

Solar radiation incident upon the surface of the Earth is the primary forcing for surface temperature fluctuations. The temperature field varies latitudinally due to the angle of the surface of the Earth relative to the insolation. It also varies seasonally due to the planet's revolution around the sun and diurnally as a result

of the Earth's rotation about its axis. In the Northern Hemisphere, incoming solar radiation reaches a maximum at the summer solstice and a minimum at the winter solstice. The Earth's surface temperature fluctuates in response to this insolation change. Due to the differing heat capacities of air, land, and water, however, the temperature response to the solar forcing exhibits a lag which varies on the surface of the Earth. Prescott and Collins (1951) calculated this phase lag for the globe and the continental United States and found larger lags over bodies of water than over land areas. Phase lags of up to two months were seen for maritime stations, while inland basins experienced lags of about one month. In addition, those locations near or at coastal regions exhibited greater phase lags than those at continental locations. Their study confirmed that the lag of the temperature field behind solar radiation is an index of continentality. Later studies determined that the higher thermal inertia of water was the main reason for the greater lag.

In order to compute the phase lag of the surface temperature with respect to the insolation forcing, a discrete Fourier transformation was conducted on the insolation forcing cycle at each station. The annual variation of this insolation forcing is well represented in terms of three harmonics, the first harmonic being the annual cycle (North et al. 1983). The insolation reception at each station was computed in terms of the Earth's orbital parameters, namely the declination angle, the ellipticity of the Earth's orbit, and the angle of perihelion relative to the winter solstice. The orbital parameters are the Sun's Keplerian elements referred to on an Earth-fixed frame. Currently, the eccentricity is about 0.017, the perihelion is 348° from the winter solstice in the direction of the planet's revolution, and the obliquity, or the tilt of the earth's spin axis with respect to a line perpendicular to the ecliptic plane, is 23.45° (North et al. 1983). A computational algorithm was developed by Kim (1988). Rubincam (1994) also discusses a convenient computational formula for the insolation. The phases of both the annual and the semiannual cycles were then

calculated according to (2), and each was subtracted from its respective counterpart of the surface temperature field to determine the phase lag.

3.1.2. Estimate of the Standard Error

It is interesting to determine the standard errors of the amplitude and phase estimates for the annual cycle. There is an argument that the phase lag is different for the summer and winter temperature extrema with respect to insolation peaks when the raw data is analyzed (Driscoll et al. 1994). Error bounds for the amplitude and phase of the annual cycle will allow us to assess whether the proposed summer-winter phase discrepancy is significant or not.

In order to estimate the standard error of the amplitude and phase of the annual cycle, we consider the regression problem (Newton, personal communication):

$$Y_t = a \cos(2\pi t/12) + b \sin(2\pi t/12) + \epsilon_t, \quad t = 1, \dots, N \quad (3)$$

where ϵ_t represents random noise added to the sinusoid having a period of 12 months.

The ϵ_t 's are assumed to be independent and have an identical normal distribution.

The error variance, σ^2 , can be estimated by s^2 , where

$$s^2 = \frac{1}{(N-2)} \sum_{t=1}^N (Y_t - \hat{a} \cos(2\pi t/12) - \hat{b} \sin(2\pi t/12))^2. \quad (4)$$

The \hat{a} and \hat{b} represent the estimates of the Fourier coefficients.

Standard errors for the amplitude and phase are found by finding variances of \hat{a} and \hat{b} , both of which are normally distributed. It is found then that the standard error for the amplitude is

$$SE_{\text{amp}} = \sqrt{2s^2/N}, \quad (5)$$

and the standard error for the phase is

$$SE_{\text{phs}} = \sqrt{2s^2/(N\hat{C}^2)}, \quad (6)$$

where \hat{C} is the estimated amplitude of the annual cycle. The 95% confidence intervals for both the amplitude and phase can then be computed by taking plus/minus two standard errors of the respective quantity.

3.2. Analysis of Second-Moment Statistics

An important characteristic of a random variable, such as surface temperature, is its variability. It is important to measure the amount of this variability (Bulmer 1979). Variability of the surface temperature field is important for many reasons. First of all, knowledge of the geographical distribution of variance in different frequency bands is necessary for our understanding of whether an encountered change is "natural" as opposed to being forced by an external agent. Secondly, the second-moment statistics provide an important measure of the sensitivity of the climate system beyond the standard tests such as the geographical distribution of selected monthly-averaged snapshots or annual means. Finally, they might provide a clue as to the ability of models to predict correctly the climate change due to small, externally imposed forcings (Kim and North 1991).

I looked at several measures of the fluctuations: (1) the variance of the temperature field over many years, i.e., the interannual variability, at each location for the months of January, April, July and October. Each month used represents the mid-month of a season (winter = Dec-Jan-Feb, spring = Mar-Apr-May, etc.); (2) the spatial correlations of the temperature field at selected test points with that of neighboring stations so that correlation contours can be constructed around the test points. Points were selected based on their geographical and meteorological setting in order to depict various features of the Texas climate and to illustrate any effects of continentality present in the region; and (3) the temporal correlation of the temperature field at a lag of one month and one year, i.e. between consecutive data

points and between consecutive years for the months of January, April, July and October for each station. All computations with the data follow the techniques as set forth in Newton (1988).

3.2.1. Geographical Distribution of Variance

The variance of a random variable, as a measure of the dispersion of a set of observations such as monthly surface temperatures, is the sum of the squared deviations from the mean divided by the number of observations:

$$\text{Var}(T(\hat{\mathbf{r}}, t)) = \frac{1}{N} \sum_{i=1}^N (T(\hat{\mathbf{r}}, t_i) - \bar{T}(\hat{\mathbf{r}}))^2, \quad (7)$$

where $\bar{T}(\hat{\mathbf{r}})$ is the temporal mean of $T(\hat{\mathbf{r}}, t_i)$. For each station, the interannual variability is computed in this manner for each of the four months mentioned earlier.

In the remainder of the study, the last 50 years of each station's record were used since this was the minimum record length and equal lengths were needed. Also, respective monthly means were subtracted out in order to remove the annual cycle and its subharmonics, which account for most of the seasonal variance in the temperature record.

3.2.2. Spatial Correlation

The spatial correlation function is calculated according to the following formula:

$$\text{Corr}(T(\hat{\mathbf{r}}_1, t), T(\hat{\mathbf{r}}_2, t)) = \frac{\text{Cov}(T(\hat{\mathbf{r}}_1, t), T(\hat{\mathbf{r}}_2, t))}{\sqrt{\text{Var}(T(\hat{\mathbf{r}}_1, t)) \text{Var}(T(\hat{\mathbf{r}}_2, t))}}, \quad (8)$$

where

$$\text{Cov}(T(\hat{\mathbf{r}}_1, t), T(\hat{\mathbf{r}}_2, t)) = \frac{1}{N} \sum_{t=1}^N (T(\hat{\mathbf{r}}_1, t_i) - \bar{T}(\hat{\mathbf{r}}_1))(T(\hat{\mathbf{r}}_2, t_i) - \bar{T}(\hat{\mathbf{r}}_2)). \quad (9)$$

The spatial correlation function is essentially the spatial pattern of cross-correlation at lag zero between one station and all other stations. Spatial correlation functions were computed for the same four months.

The spatial correlation length scale, in general, increases as the temporal scale becomes larger (Kim and North 1992). Kim and North (1991) used the $1/e \simeq 0.37$ value (e -folding scale) of the correlation for reference. However, since this scale was nearly as large as the region of study, a different reference value was needed. Gaffin (1993) determined that a correlation of approximately 0.86 and higher should be used in obtaining an accurate areal representation for a single station with at least 50% reduction in the standard error of estimate. Therefore, even though this study is not concerned with areal estimates, a correlation of 0.7, which is slightly smaller than twice the e -folding scale, was used as the reference value.

3.2.3. Temporal Correlation

Temporal correlation at a station is calculated according to the following formula:

$$\text{Corr}(T(\hat{\mathbf{r}}, t), T(\hat{\mathbf{r}}, t + \Delta t)) = \frac{\text{Cov}(T(\hat{\mathbf{r}}, t), T(\hat{\mathbf{r}}, t + \Delta t))}{\text{Var}(T(\hat{\mathbf{r}}, t))}, \quad (10)$$

where

$$\text{Cov}(T(\hat{\mathbf{r}}, t), T(\hat{\mathbf{r}}, t + \Delta t)) = \frac{1}{N} \sum_{t=1}^N (T(\hat{\mathbf{r}}, t_i) - \bar{T}(\hat{\mathbf{r}}))(T(\hat{\mathbf{r}}, t_i + \Delta t) - \bar{T}(\hat{\mathbf{r}})). \quad (11)$$

The lag, Δt , used here is either one month or one year.

3.3. Empirical Orthogonal Function Analysis

Empirical orthogonal function (EOF) analysis has been used for many years to study dominant patterns, or modes, of variability in the meteorological and oceanographic fields. The EOF analysis is commonly referred to in the literature as a principal component analysis (PCA). The analysis can be carried out in the direction of both time and space. Many researchers have been particularly interested in

the spatial EOF patterns in various climatological and theoretical studies including Grimmer (1963) and North et al. (1982). These patterns illustrate the spatial distribution of covariability in a meteorological field (Barnett 1978).

There are three main reasons for the EOF analysis. First, it allows the spatio-temporal variability of a large dataset to be represented in terms of a small number of orthogonal modes. These EOF modes may in some cases be identified with dynamical/physical modes and be given physical interpretations (Kidson 1975; North 1984). Although it is not always possible to interpret the EOFs as physically or dynamically plausible modes, the EOFs can be used as a useful set of complete basis functions into which the variability of the underlying field is partitioned (Kim and North 1993).

While the significance of the EOFs and the eigenvalues are very relevant to geophysical studies, there are only a limited number of experiments which have focused on this issue (Preisendorfer and Barnett 1977; North et al. 1982). There are no standard rules widely in use. Barnett (1978) has applied the statistical filtering rules developed by Preisendorfer and Barnett (1977). North et al. (1982) have discussed the problem of degeneracy of eigenfunctions. Namely, when two or more EOFs have almost identical eigenvalues, the EOFs become unstable under slight perturbation due to sampling error, which makes the interpretation of the EOFs difficult. Both of these complex issues will be averted as they are beyond the scope of this study. I examine only the first few modes, which explain most of the variance and which, upon visual inspection, appear to be stable in form and structure. In most cases, the first three EOFs meet these criteria.

3.3.1. Procedure

As in the correlation analyses, the last fifty years of anomaly data for each station have been used so that all the time series are of equal length. To calculate

EOFs, the covariance of the temperature anomaly field among different stations was computed. Covariance is a measure of how two random variables vary relative to one another. The calculation was performed for each pair of stations according to the formula (Newton 1988):

$$\text{Cov}(T(\hat{\mathbf{r}}_1, t)T(\hat{\mathbf{r}}_2, t)) = \frac{1}{N} \sum_{t=1}^N (T(\hat{\mathbf{r}}_1, t) - \bar{T}(\hat{\mathbf{r}}_1))(T(\hat{\mathbf{r}}_2, t) - \bar{T}(\hat{\mathbf{r}}_2)), \quad (12)$$

where $\hat{\mathbf{r}}$ represents a grid point or a station. For a given test point, there are N stations (including itself) at which covariance is to be determined. The covariance computations, then, result in an $N \times N$ matrix. To find an eigenfunction and the corresponding eigenvalue, one diagonalizes the covariance matrix according to

$$\mathbf{C}\phi = \lambda\phi, \quad (13)$$

where \mathbf{C} is a covariance matrix, ϕ is an eigenvector, and λ is an eigenvalue associated with the eigenvector ϕ . Since the covariance matrix is real-valued and symmetric, one finds N such sets of real eigenfunctions and eigenvectors counting the degeneracy. The eigenvectors are orthogonal and form a complete basis set.

The Jacobi rotation method was used to carry out the diagonalization of the covariance matrix (Lorenz 1956). The computer codes were adopted from Press et al. (1986). The eigenvalues were then ordered in size from the largest to the smallest, and the corresponding eigenvectors were arranged accordingly. Lorenz (1956) and later investigators (e.g., Grimmer 1963) noted that the trace (sum of the diagonal elements) of the covariance matrix and the sum of eigenvalues are equal. Since the trace of the covariance matrix is the total variance, the EOF analysis essentially represents the partitioning of total variance in terms of mutually orthogonal eigenfunctions. The eigenvalues show how total variance is partitioned among different modes.

Since meteorological variables are spatially continuum functions, North et al. (1982) considered a general continuum representation of the EOFs:

$$\frac{1}{A} \int_A C(\hat{\mathbf{r}}, \hat{\mathbf{r}}') \phi_\alpha(\hat{\mathbf{r}}') d\hat{\mathbf{r}}' = \lambda_\alpha \phi_\alpha(\hat{\mathbf{r}}), \quad (14)$$

where A is the area of the domain of interest, i.e. the area containing all the stations, and λ_α is the eigenvalue associated with the eigenfunction $\phi_\alpha(\hat{\mathbf{r}})$. The integral extends over the finite domain, and the resulting EOF shapes will depend upon the geometry of this region. Buell (1979) concluded that the EOFs computed over an area with well-defined boundaries will be very strongly influenced by the geometrical shape of the region and to a large extent independent of the region's location. The effect of the shape must also be accounted for prior to the interpretation of the EOFs. Since the state of Texas has a markedly nonuniform geometrical character, I included data from the states of Oklahoma and New Mexico in order to minimize the effects of the domain shape as much as possible. Of course, this cannot be done completely due to the presence of the Gulf of Mexico on the southeastern fringe of the state and to the lack of data over the region of Mexico adjacent to Texas and New Mexico. Nonetheless, additional data from the aforementioned states should help to produce fairly coherent EOF patterns.

3.3.2. Metric Factor for EOF Computations

Buell (1971) indicated that the EOF computation as a matrix problem is better formulated in terms of the Karhunen-Loève integral equation when applied to meteorological fields. The consideration of the area over which the integration is performed then naturally enters in computing the EOFs. The field of surface temperature certainly falls into this category, for it is not confined to an ensemble of discrete points, but rather it is actually a continuous field. From a practical point of view, however, we do not have continuous measurements of temperatures but

a finite number of and often irregularly spaced measurements at discrete stations. Therefore, North et al. (1982) suggested using an appropriate scaling factor which eliminates the geometrical effects of grid spacing. They approximated the integral equation (14) by a finite sum:

$$\frac{1}{A} \sum_{j=1}^N C(\hat{\mathbf{r}}_i, \hat{\mathbf{r}}_j) (\Delta A)_j \phi_\alpha(\hat{\mathbf{r}}_j) = \lambda_\alpha \phi_\alpha(\hat{\mathbf{r}}_i), \quad i = 1, \dots, N, \quad (15)$$

where the $\hat{\mathbf{r}}_i$'s are the N individual grid points and ΔA_i is an area element associated with the point $\hat{\mathbf{r}}_i$.

They further suggested that these elements might be chosen as polygons. This "metric factor" will not affect the scaling of the eigenvalues, but they conjectured that its omission in the computation of EOFs might result in inaccuracies in the shape of the EOFs and the eigenvalues. Therefore, to examine the importance of the metric factor, an area weight was computed for each grid point to carry out the computation in (15). This was compared to the computation without the area weights by means of pattern correlation.

3.3.3. Thiessen Polygons as Area Weights

Geographers routinely use what are known as Thiessen polygons to define artificial areas around a set of points as a method for estimating areal boundaries. Since Thiessen, in 1911, used them to compute more accurate estimates of regional averages of rainfall (Boyle and Dunn 1991), publishing his results in *Monthly Weather Review*, these polygons became widely known by his name. Simple Thiessen polygons can be obtained manually, but there exist several computer programs to compute them rapidly for large areas. The way these polygons are constructed is as follows. Given a set of points representing a set of areas and an outer boundary, Thiessen polygons are created by drawing perpendicular bisectors through the straight lines which join two adjacent points (Boyle and Dunn 1991). The size of each polygon

is determined by the spacing of the grid points. Figure 3 illustrates the method of creating Thiessen polygons. A randomly chosen point in the domain will be closest to the grid point of its respective area, unless it lies on the boundary. The polygons serve to produce a space-exhaustive pattern.

In this study, I used the Geographical Information System (GIS) software package known as ARC/INFO to construct Thiessen polygons for Texas and the surrounding states. The resulting shapes of the areal elements for the stations used in this study are shown in Figure 4. Note the variation in the size of the areas, with most of the smaller polygons confined to the east-central part of Texas where there is a greater density of reporting stations. The software also computed the area of each polygon (Table 1), and it was these areas which were used in evaluating (15). All the EOF calculations in this study include the metric factor unless otherwise stated.

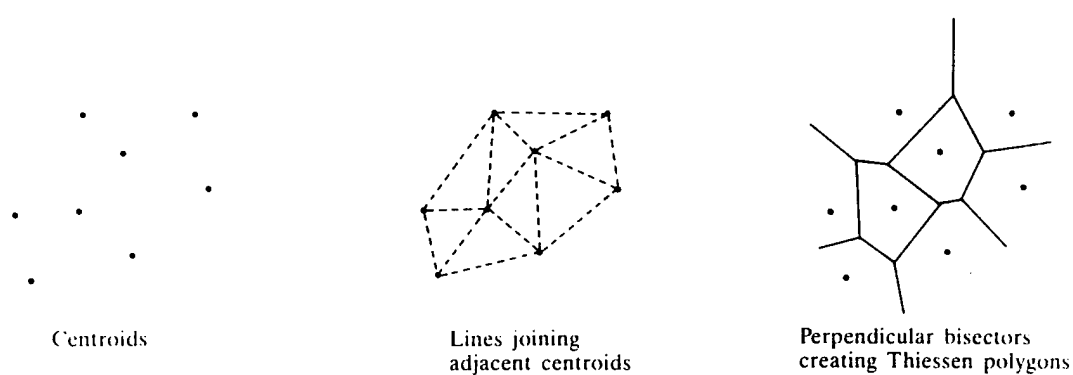


FIG. 3. Procedure for defining Thiessen polygons (from Boyle and Dunn 1991). Stations, or data points, are referred to as centroids in the figure.

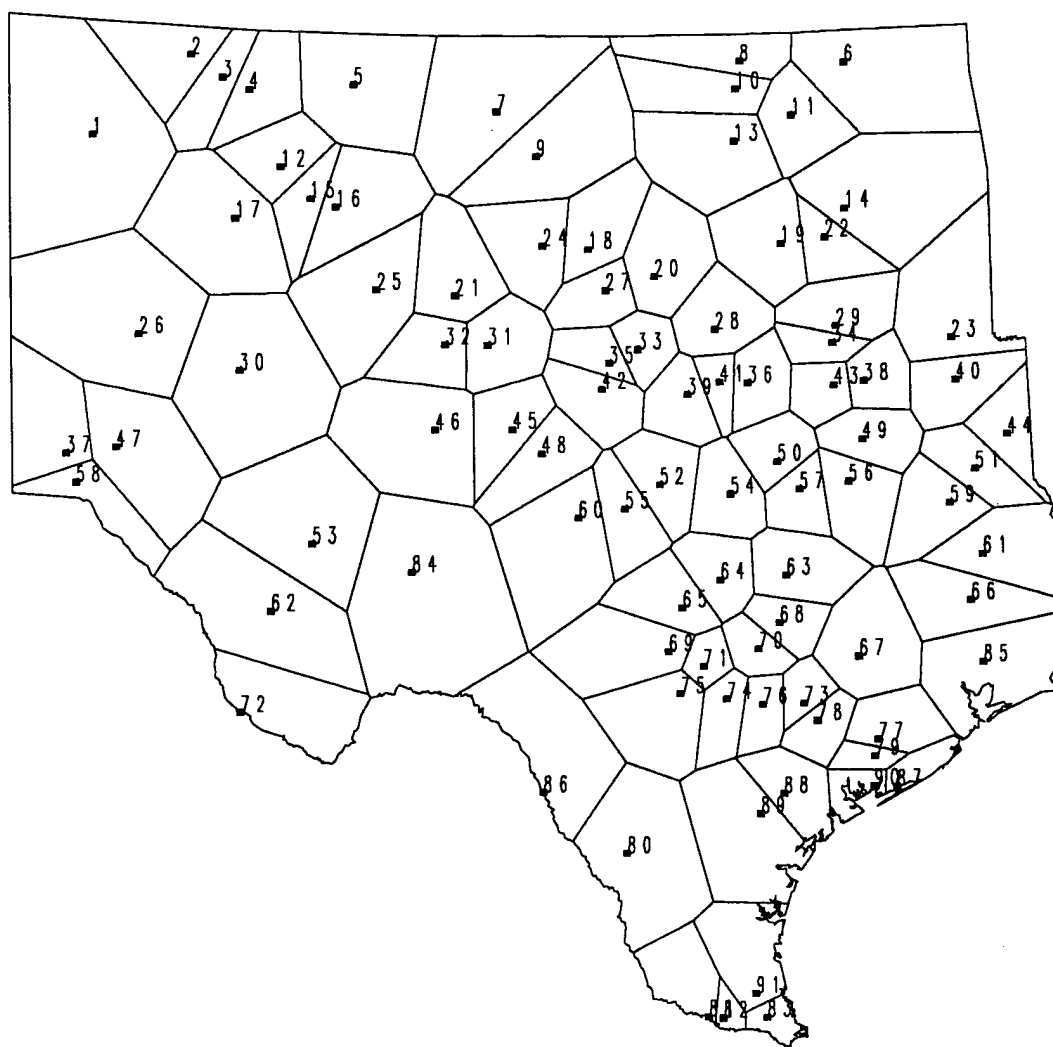


FIG. 4. Plot of the region of study showing each station's location and its area weighting as defined by a Thiessen polygon. Station, or Thiessen, numbers and the area of each polygon are listed in TABLE 1.

4. RESULTS AND DISCUSSION

4.1. Fourier Analysis

Land-sea distribution is one of the main controlling factors for the seasonal cycle of surface temperature over the Earth. Crutcher and Meserve (1970) calculated the amplitude and phase lag of the annual cycle, and the amplitude of the semiannual cycle, of the Northern Hemisphere surface temperature field. The dominating effect of the land masses was readily apparent in the annual cycle analysis. Continental interiors observed phase lags of about 30 days or less, while midoceanic regions showed lags approaching 75 or more days. The Siberian land mass was a prime example of continentality, with amplitudes of about 25°C and phase lags of less than 30 days.

In the analysis of Texas surface temperature, we also expect to see smaller amplitudes and phase lags in mountainous areas, possibly due to an effectively lower local heat capacity and a modification in the outgoing radiation (North et al. 1983).

The amplitude and phase lag of the annual and semiannual cycles of surface temperature were calculated at each station in this study. The analysis was performed for the mean monthly, mean daily maximum, and mean daily minimum time series at each location. The results of the analysis are presented and discussed in the following. In addition, an estimate of the standard error for the amplitude and phase of the annual cycle for mean monthly temperature is presented.

4.1.1. Amplitude of the Annual Cycle

The annual cycle, or the harmonic of period 12 months, for surface temperature is typically the largest of the harmonics in the mid-latitude Northern Hemisphere because of the dominance of the annual insolation cycle (North et al. 1981). The amplitude of the annual cycle of mean monthly temperature over Texas and the

surrounding states exhibits a marked continental signature (Fig. 5). Values range from less than 14°F along the southern Gulf coast to over 22°F in the Panhandle and into much of central and western Oklahoma. As the stations are further away from the coast, so the amplitude of the annual cycle increases. An exception to this statement applies to the regions of higher elevation, most notably the Trans-Pecos. Here amplitudes of less than 16°F appear, values which resemble those found at or near the Gulf coast. In addition, western Texas and New Mexico, regions of increasing elevation from east to west, have amplitudes between 18 and 22°F .

Fig. 6 displays standard error estimates of the amplitude of the annual cycle of mean monthly temperature. Generally, the largest values are found in the interior sections of Texas and in Oklahoma, where the climate is more continental in nature. Smallest values are along the northern Gulf coast. Table 2 gives a complete listing of phase, amplitude and the respective standard error estimates at each station.

The plot of amplitude of the annual cycle of mean daily maximum temperature across Texas is quite similar to that of the mean monthly temperatures in terms of the locations of maxima and minima (Fig. 7).

We see amplitudes in excess of 22°F over some parts of the Texas Panhandle and much of western and central Oklahoma. The lowest values, less than 14°F , hug the coastline of the Gulf of Mexico. There is also a local minimum, a region of fewer than 16°F , in the Trans-Pecos division of the state. A major difference between the two patterns concerns the band of $20\text{--}22^{\circ}\text{F}$ amplitudes, which is confined mostly to the Panhandle and the extreme northern portions of the state for the mean daily maximum temperatures. This possibly indicates that the influence of the Gulf of Mexico extends further inland during the time of maximum temperatures, which is normally mid-to-late afternoon. Such an explanation seems plausible, since it is also the time for the on-shore flow, or sea breeze, to be at its peak strength. It is suspect, however, that the effect of the sea breeze is felt strongly so far inland. The

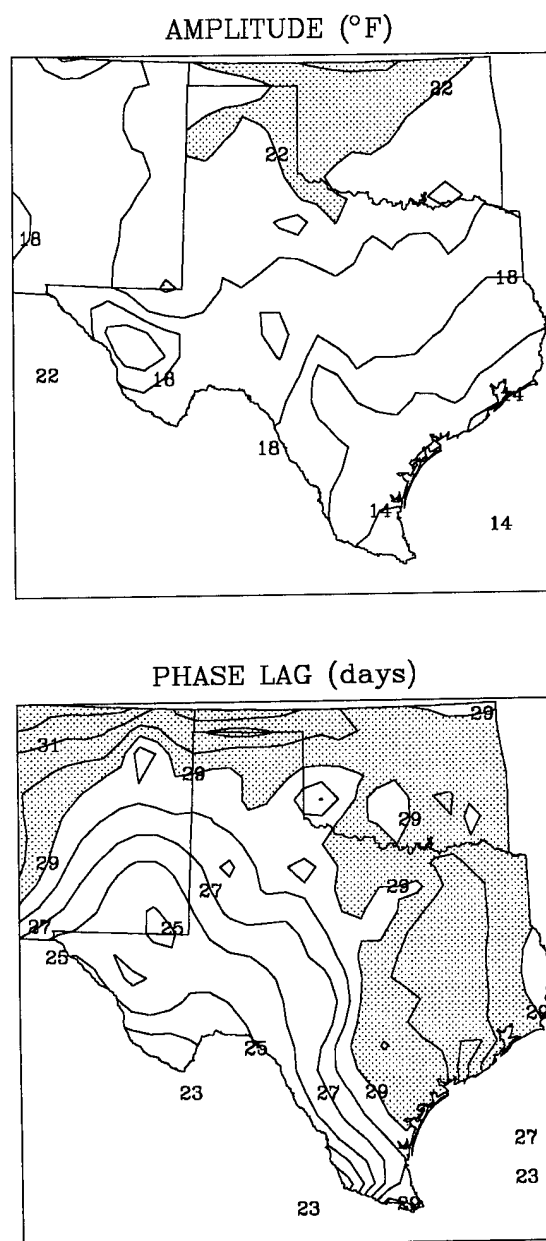


FIG. 5. Plot of amplitude and phase lag of the annual cycle of mean monthly temperature at each station. Amplitude is in $^{\circ}\text{F}$ and phase lag is in days. Phase lag is the difference in phase between the annual cycle of temperature and the annual cycle of insolation. Amplitudes greater than 22°F and phase lags greater than 29 days are shaded.

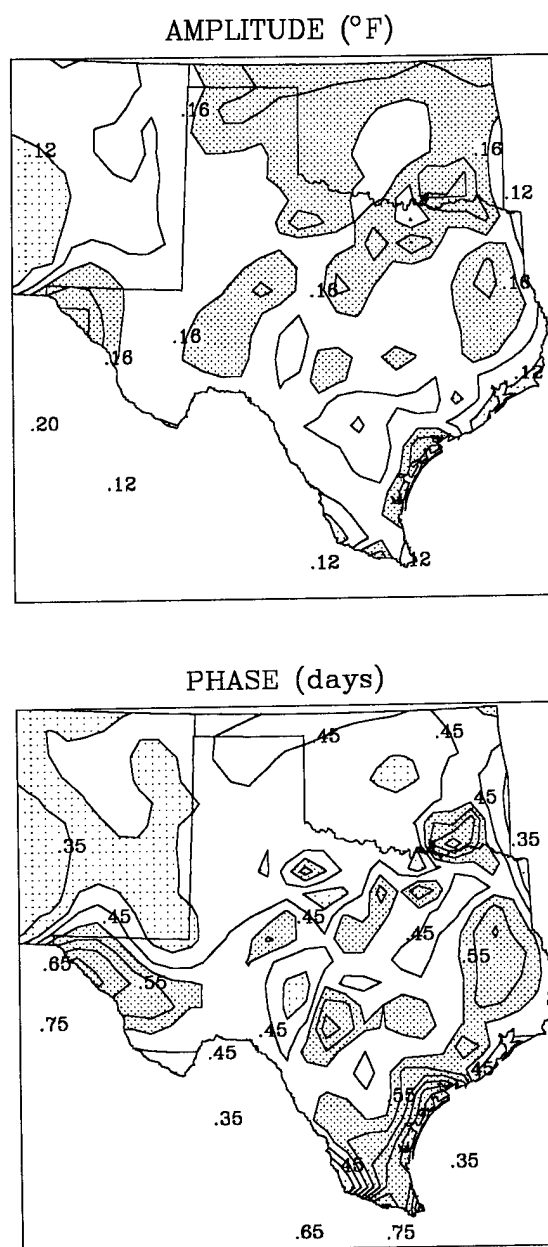


FIG. 6. Plot of standard error for amplitude and phase of the annual cycle of mean monthly temperature at each station. Units are $^{\circ}\text{F}$ for amplitude and days for phase. Darker shading highlights the larger values, lighter shading the lower values, in each plot.

TABLE 2. Phase and amplitude of the annual cycle with an estimate of the standard error for each quantity.

Station	Phase	Std Error	Amplitude	Std Error
Ada, OK	183.24	.44725	20.702	.16160
Austin, TX	182.87	.52388	17.495	.15996
Ballinger, TX	180.32	.44007	19.321	.14840
Beeville, TX	182.74	.52858	14.950	.13792
Bell Ranch, NM	181.58	.37078	21.353	.13818
Blanco, TX	182.87	.50941	17.882	.15898
Boerne, TX	182.39	.49070	16.337	.13992
Brenham, TX	183.53	.47896	17.047	.14250
Bridgeport, TX	182.51	.50001	20.689	.18055
Carrizozo, NM	180.86	.36628	19.402	.12403
Cimarron, NM	183.75	.41451	18.730	.13550
Clayton, NM	184.06	.42712	20.361	.15178
Cleburne, TX	182.62	.45912	19.168	.15360
Clarksville, TX	182.33	.56505	19.775	.19502
Coleman, TX	181.14	.46056	18.376	.14771
Corsicana, TX	183.86	.44764	19.317	.15092
Crosbyton, TX	181.61	.39493	20.421	.14076
Danevang, TX	183.57	.45982	14.742	.11831
Denison Dam, TX	183.22	.52665	20.458	.18805
Eagle Pass, TX	178.66	.46756	17.730	.14468
Encinal, TX	179.71	.52719	16.515	.15196
Enid, OK	183.33	.42093	23.071	.16949
Flatonia, TX	183.31	.50681	16.041	.14190
Fredericksburg, TX	181.21	.57891	16.724	.16898
Frederick, OK	182.53	.43829	21.753	.16640
Goliad, TX	183.12	.62292	14.718	.16002
Graham, TX	182.82	.42739	20.876	.15572
Greenville, TX	183.68	.43238	20.485	.15459
Harlingen, TX	181.49	.65671	12.616	.14460
Haskell, TX	181.72	.40923	20.956	.14967
Henderson, TX	182.82	.61123	17.906	.19102
Henrietta, TX	183.36	.41929	21.723	.15897
Hico, TX	182.11	.47816	18.885	.15760
Hillsboro, TX	183.61	.45005	19.696	.15471
Hallettsville, TX	182.95	.46351	15.752	.12743
Holdenville, OK	183.48	.42900	21.002	.15725
Hollis, OK	181.12	.43635	22.409	.17066
Jacksboro, TX	182.57	.57407	19.689	.19728
Jefferson, OK	183.01	.44031	23.881	.18352
Jemez Springs, NM	183.65	.40295	19.108	.13439
Kaufman, TX	183.90	.43067	19.872	.14937
Kingfisher, OK	182.96	.39888	22.855	.15911
Lamesa, TX	180.68	.42971	20.120	.15090
Lampasas, TX	182.93	.44800	18.620	.14559
La Tuna, TX	179.58	.48218	19.718	.16594
Liberty, TX	182.83	.49078	15.498	.13275
Livingston, TX	182.86	.57376	17.129	.17153
Llano, TX	181.78	.44561	19.212	.14942
Lubbock, TX	180.44	.41657	20.193	.14681
Lufkin, TX	182.05	.51773	17.366	.15692
Luling, TX	182.33	.45669	17.266	.13762
Marshall, TX	182.72	.49045	18.574	.15899
Matagorda, TX	185.02	.54569	14.599	.13904
McAllen, TX	180.70	.75676	12.998	.17168
McCamey, TX	178.74	.48927	19.367	.16538
McKinney, TX	182.65	.56026	19.545	.19111
Memphis, TX	181.99	.43641	21.926	.16700
Miami, TX	182.76	.42225	22.248	.16396

TABLE 2. (Continued)

Station	Phase	Std Error	Amplitude	Std Error
Mission, TX	179.57	.65885	13.560	.15593
Mount Locke, TX	179.22	.59107	14.612	.15074
Mount Pleasant, TX	183.00	.46974	19.601	.16070
Muleshoe, TX	181.09	.41010	20.957	.15000
Munday, TX	181.43	.52147	20.355	.18526
New Braunfels, TX	182.27	.48008	16.642	.13944
Orogrande, NM	179.82	.45861	19.350	.15488
Palacios, TX	183.56	.61607	15.241	.16388
Pauls Valley, OK	182.12	.41894	21.393	.15642
Pawhuska, OK	182.57	.44038	22.526	.17314
Pecos, TX	178.42	.43421	20.224	.15327
Pierce, TX	183.86	.51490	15.416	.13854
Plainview, TX	181.64	.40871	20.220	.14424
Presidio, TX	176.65	.44799	18.763	.14671
Quanah, TX	182.28	.42464	22.405	.16606
Raymondville, TX	180.84	.66622	13.100	.15232
Red River, NM	185.14	.39886	19.495	.13571
Rising Star, TX	182.14	.54385	19.712	.18711
Roscoe, TX	180.48	.53496	19.400	.18114
Roswell, NM	179.06	.38244	20.120	.13430
Rusk, TX	183.30	.59058	17.748	.18294
San Jon, NM	181.82	.39526	21.384	.14752
Santa Rosa, NM	181.52	.41656	19.701	.14323
Seymour, TX	182.22	.46616	22.017	.17913
Sherman, TX	183.37	.43364	20.926	.15837
Snyder, TX	181.17	.44537	20.649	.16050
Spearman, TX	182.89	.48838	22.381	.19077
Springer, NM	181.50	.38783	20.940	.14174
State University, NM	180.46	.36020	19.142	.12034
Stillwater, OK	182.83	.40248	22.422	.15751
Taylor, TX	182.95	.52659	18.255	.16778
Temple, TX	183.58	.45170	18.730	.14766
Tucumcari, NM	182.04	.39347	20.438	.14036

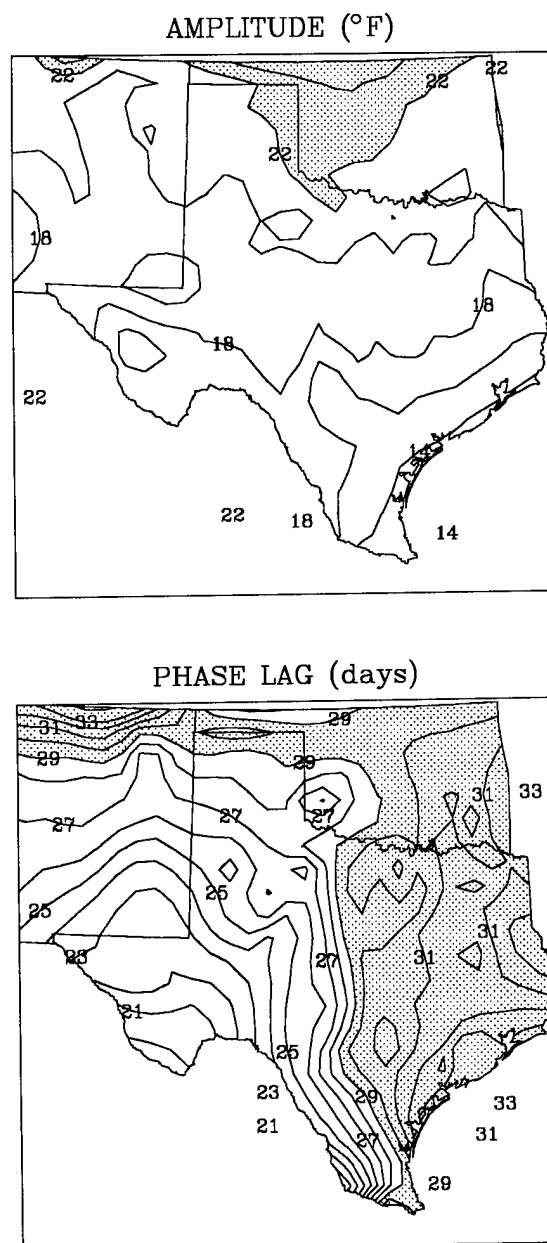


FIG. 7. Same as in FIG. 5, but for mean daily maximum temperature.

high elevation of western Texas, high albedo of eastern New Mexico, or even outside influences may contribute to such a difference.

The amplitude of the annual cycle of mean daily minimum temperature is both qualitatively and quantitatively similar to the other two plots (Fig. 8). Here we see both the maxima and minima at generally the same locations. A slight departure is observed in the isotherms of the 20-22°F. Unlike that of the mean daily maximum temperatures, the 20-22°F region is displaced further southward and westward. Minimum temperature readings normally occur during the early morning hours, about 5-7 a.m. This is also the time for the diminishing sea breeze along the Gulf coast and the onset of the land breeze. Again, this explanation suffers inadequacy in describing the huge north-south swing of the 20-22°F band in the inland fairly remote from the Gulf coast. It is conjectured that some large-scale processes originating outside the region may be responsible for the observed pattern of the amplitudes. Possibly drainage winds down the higher elevations to the west are the culprit.

4.1.2. Phase Lag of the Annual Cycle

Prescott and Collins (1951) noted that the phase lag is smallest, about one month, on the continental basins and highlands, while oceanic regions show lags of approximately one-and-a-half to two months. The observed phase lags of the mean monthly surface temperatures across Texas range from less than 24 days in the Trans-Pecos region of the state to over 30 days in the east (Fig. 5). The effect of the Gulf of Mexico is immediately evident in this figure, for the largest phase lags encompass much of the eastern half of the state, even extending well into the eastern part of Oklahoma. On the other hand, the presence of salient topographical features in the western part of Texas and eastern New Mexico appear to be responsible for the smallest phase lags.

The shape of the phase function bears little resemblance to that of the am-

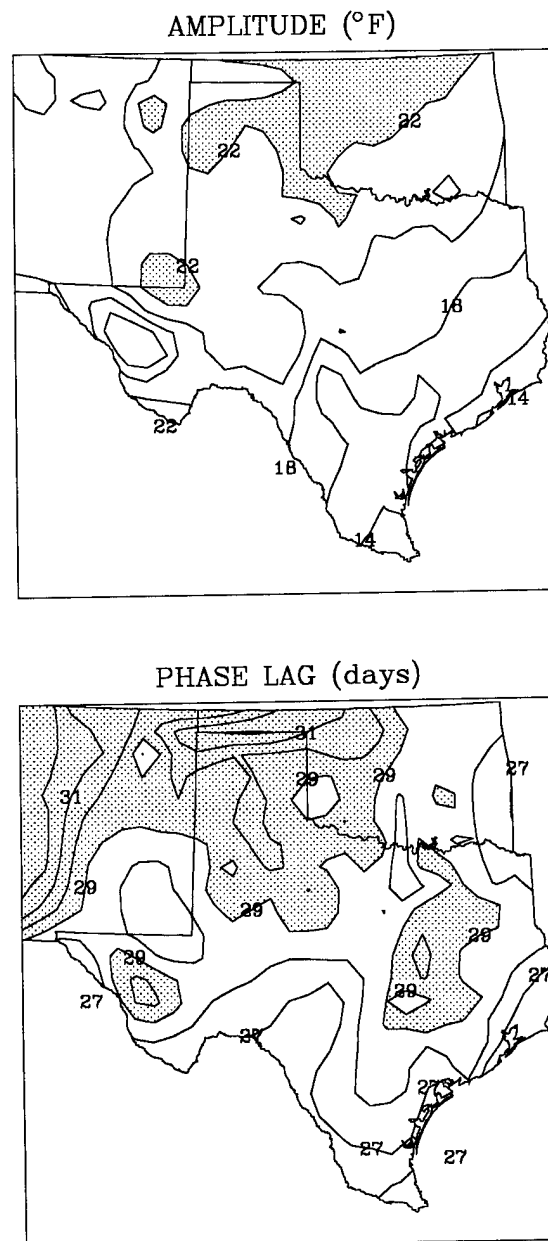


FIG. 8. Same as in FIG. 5, but for mean daily minimum temperature.

plitude of the annual cycle. Nonetheless, the patterns of phase shown here are in good agreement with the work of Prescott and Collins (1951) both qualitatively and quantitatively. The expected decrease in the phase lag with distance from a body of water seems to be a valid assumption only for large continents such as Asia. On a regional scale of the size of Texas, a state whose climate is largely influenced by the presence of the warm Gulf waters during most of the year, local climatological and geographical features seem to play large roles in forming the field of phase lag behind solar radiation of the annual cycle of temperature.

A plot of the estimated standard error for the phase of the annual cycle of mean monthly temperature is shown in Fig. 6. Here we see, for the most part, a decrease in standard error from the coast to inland and mountain locations. However, there exists a region of larger values in the higher elevations of extreme west Texas.

Figure 7 depicts the phase lag of the annual cycle for the mean daily maximum temperatures across Texas. The results are quite similar to those obtained from the mean temperatures in a qualitative sense. However, there is a much greater range of values across the state. Phase lags in excess of 33 days are seen along the northern and central Gulf coast, while lags less than 20 days appear in the Trans-Pecos area of the state. Thus, a greater contrast between continental and marine effects is evident in the signature of the annual cycle of maximum temperature. We see that the phase of the annual cycle of mean daily maximum temperature occurs later in the year for marine-influenced locations, and earlier for non-marine-influenced regions, when compared to that of the mean monthly temperature.

The phase lag of the annual cycle of mean daily minimum temperature behind solar radiation over Texas is shown in Fig. 8. Unlike its companions, this pattern shows a less coherent structure across the state. The range of values is reduced considerably from the previous two, with lags from less than 27 days along much of the Gulf coast and in the Edwards Plateau region of the state to values exceeding

30 days in a sizeable portion of the Panhandle. An explanation for this particular form of the phase lag field may lie in an understanding of the type of synoptic conditions prevalent during the time of minimum temperature, which is typically during the period of 5-7 a.m. Normally, surface winds are at their weakest and sea-level pressure is at or near its maximum diurnal value, while humidity is also at or near its peak reading for the day. Off-shore flows usually develop at night near the coast in response to more rapid cooling of land surfaces than water bodies. This might explain the low coastal phase lags.

4.1.3. Amplitude of the Semiannual Cycle

The semiannual cycle of the surface temperature in the mid-latitude northern Hemisphere is normally much smaller in magnitude than the annual cycle. Observations, smoothed over a $5^\circ \times 5^\circ$ box, show amplitudes of less than 1°C over much of North America (Crutcher and Meserve 1970). North and Coakley (1979) also computed a symmetrized northern Hemisphere average amplitude of 0.8°C .

Focusing on the state of Texas, we observe amplitudes of between 1 and 2°F for the mean monthly temperature field (Fig. 9). The lowest values appear along much of the Gulf Coast and in the higher elevations of the Trans-Pecos and the High Plains. The scales of the maxima and minima seem to indicate that local meteorology is a primary controlling factor for the amplitude of the semiannual cycle.

The amplitude pattern for the semiannual cycle of the mean daily maximum surface temperatures is in close resemblance to that of the mean monthly temperatures (Fig. 10). The former amplitude is slightly higher by about a half degree Fahrenheit.

Figure 11 is a plot of the amplitude of the semiannual cycle for the mean daily minimum temperatures. The pattern is similar to that in Fig. 9. The range of values, however, is smaller, from less than 0.6°F in the Trans-Pecos to greater than

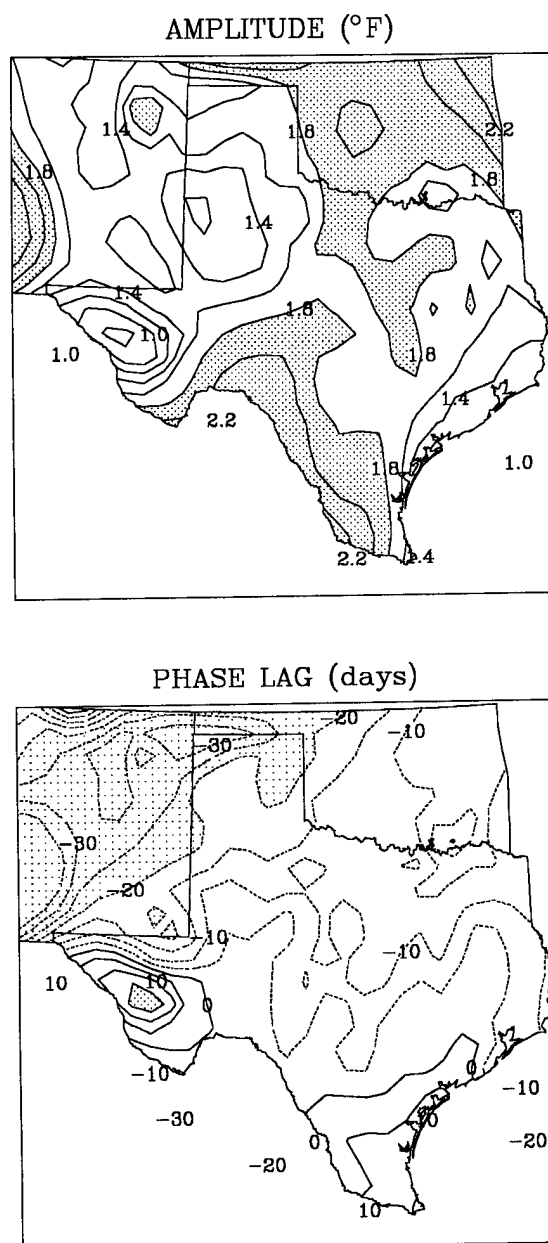


FIG. 9. Plot of amplitude and phase lag of the semiannual cycle of mean monthly temperature at each station. Amplitude is in $^{\circ}\text{F}$ and phase lag is in days. Phase lag is the difference in phase between the semiannual cycle of temperature and the semiannual cycle of insolation. Amplitudes greater than 1.8°F are shaded. Phase lags greater than 15 days and less than -20 days are shaded (darker and lighter, respectively).

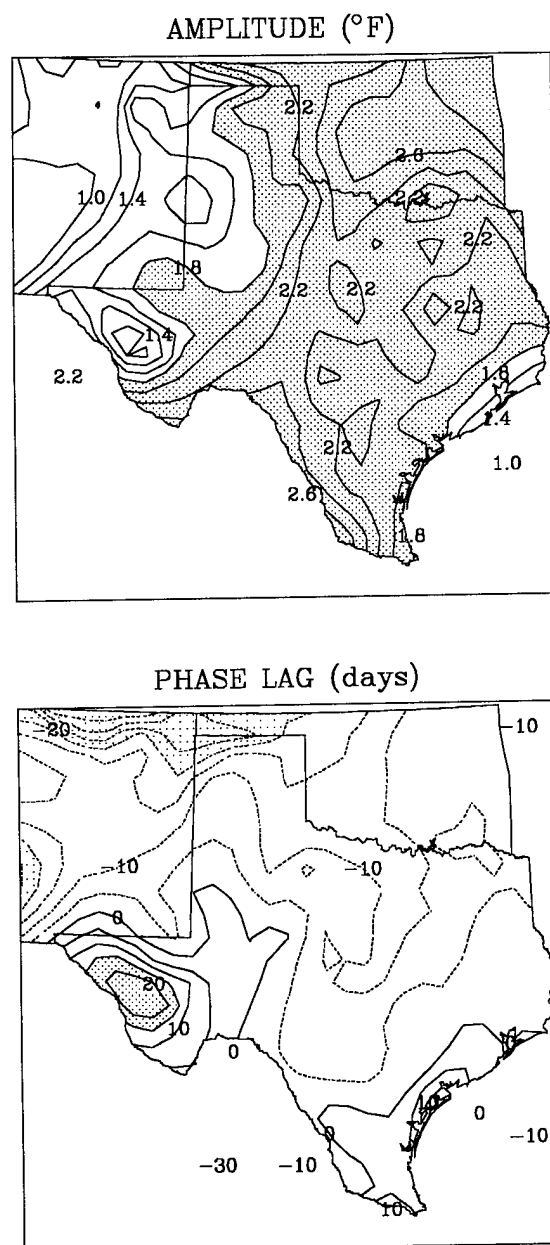


FIG. 10. Same as in FIG. 9, but for mean daily maximum temperature.

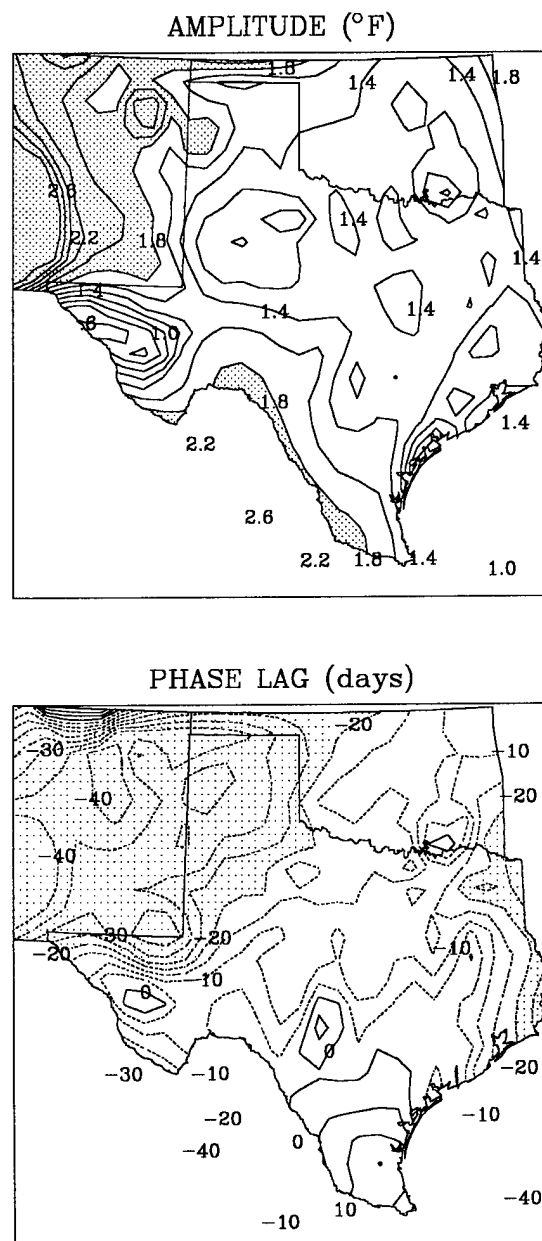


FIG. 11. Same as in FIG. 9, but for mean daily minimum temperature.

1.8°F along the southern portion of the Rio Grande. Again, minima appear along the Gulf Coast and in the highly elevated regions.

4.1.4. Phase Lag of the Semiannual Cycle

The phase lag of the semiannual cycle of the surface temperature is not normally analyzed because its interpretation is somewhat difficult. As shown in Fig. 9, the values range from greater than +15 days in the Trans-Pecos to less than -20 days in the extreme northern Panhandle. There is a general north-south gradient over much of the state, with positive values confined to the southern tip of Texas and negative lags in the northern Panhandle. The gradient becomes west-east in the Trans-Pecos and Edwards Plateau regions, ranging from greater than +15 days to less than -5 days. There is no plausible explanation for the mainly negative lags over Texas. Bear in mind that the computation of the semiannual cycle is rather unstable and that any peculiarities or asymmetry in the annual temperature records will produce an awkward result.

The mean daily maximum temperatures show essentially the same pattern as the mean monthly temperatures (Fig. 10). A difference is in the range of values, with the maximum and the minimum values being about 5 days greater in magnitude. The same gradient exists as well.

The range of phase lags of the mean daily minimum temperatures extends from greater than +10 days in the extreme south to less than -30 days in the Panhandle (Fig. 11). The prominent gradient is now in the south-southeast to north-northwest direction. There also exists a fairly sharp west-east gradient in the eastern part of the state. The Trans-Pecos division is home to a strong north-south gradient, with a local maximum in the heart of the region, and a weak east-west gradient.

4.2. Second-Moment Statistics

Kim and North (1992) noted that land/sea geography plays a vital role in the distribution of various second-moment statistics. Further, dynamical and topographical considerations played almost no role in the results, albeit on a global scale, for both observations and their tested model. It will be interesting to see how these factors influence the distribution on a regional scale.

4.2.1. Geographical Distribution of Variance

The variance distribution over the globe, as computed by Crutcher and Meserve (1970), reveals that the largest variance is located in the interior of vast land masses, while the smallest occurs in tropical areas and on the fringes of continents. Barnett (1978), using many new oceanic observations as compared with earlier studies, found that in the northern Hemisphere the variability over land is roughly 4-6 times larger than over the oceans during the winter seasons and 2-3 times larger on the yearly scale. Kim and North (1992), analyzing the United Kingdom (UK) data set archived at the National Center for Atmospheric Research (NCAR), concluded that the effect of differential heat capacity of land and ocean dominates the pattern of the Earth's surface temperature variability. It is evidenced by the geography of the variance distribution over the globe, which closely resembles the land/sea distribution.

The variance field for mean monthly temperature is displayed in Figure 12 for the months of January, April, July and October. Quite noticeable at first glance is the greater variability in January. This is consistent with synoptic experience, as the winter months typically receive a higher frequency of transient weather systems due to an increased north-south temperature gradient over the continent and a more southerly polar jet stream.

It is interesting that relatively high variance is evident in the eastern one-third

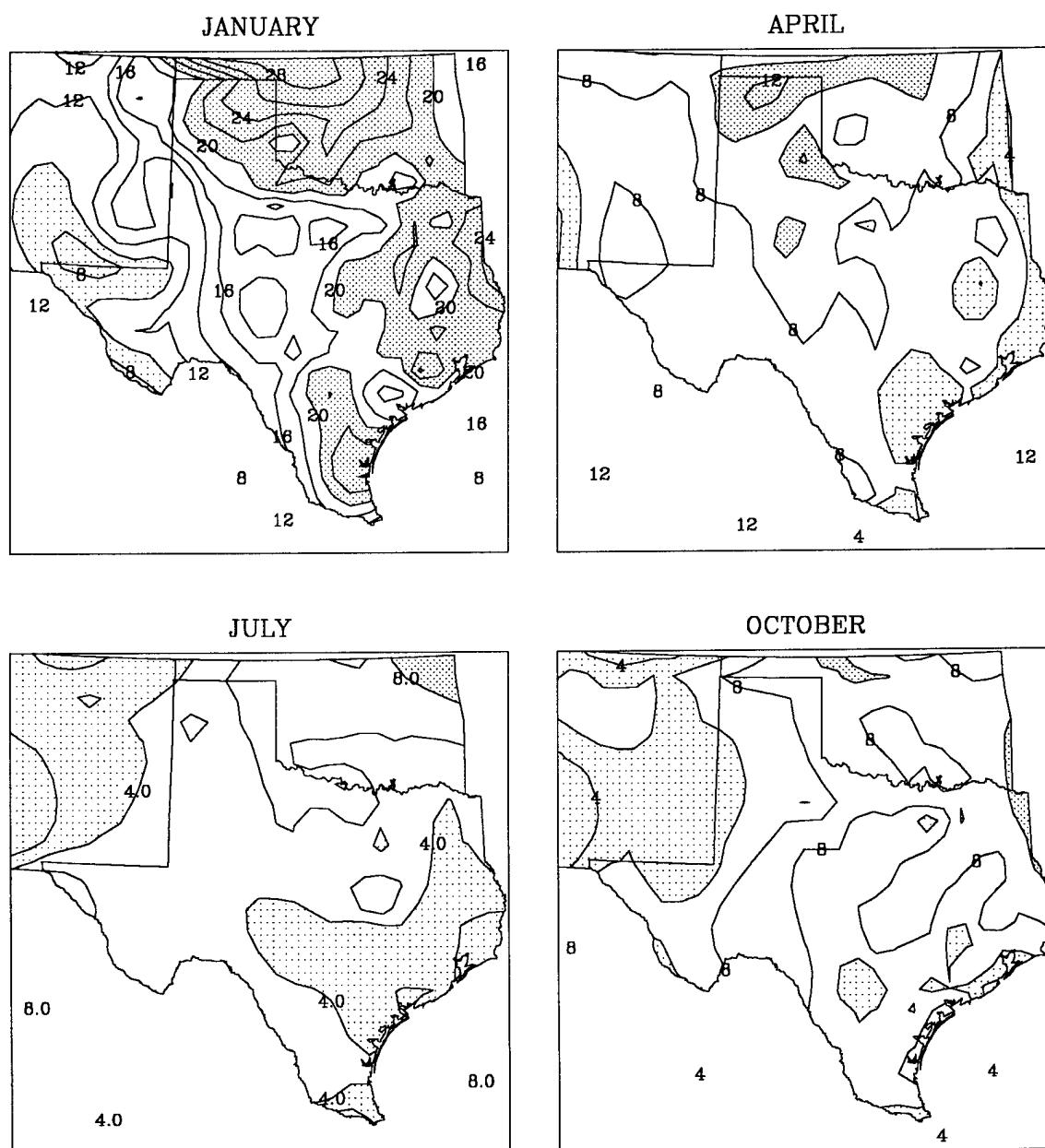


FIG. 12. Distribution of variance of the mean monthly temperature field for the months of January, April, July, and October. Units are $^{\circ}\text{F}^2$. Relatively higher values of variance are indicated by a darker shading, while relatively lower values have a lighter shading.

of the region, while lower values occur in central sections of Texas. An explanation for the former might be found in the fact that the flow from the Gulf of Mexico predominantly affects this portion of the state, bringing warm and moist air well inland. However, this air flow is frequently interrupted during the winter months by surges of cold polar air from the north which move in behind cold fronts dropping out of the Plains east of the Rockies. Once the migratory high pressure cells trailing these systems depart the area, a return flow from the Gulf is established. This air mass confrontation seems to be reflected in the distribution of variance across the eastern part of Texas.

Overall, highest variances are found in the northern part of Oklahoma. This is consistent with the continentality effect, as the region is well displaced from the Gulf of Mexico's influence. One would expect even higher values further to the north in the Great Plains.

Lowest variances are seen in the mountainous regions to the west. These locations are often shielded from the effects of surface weather fluctuations due to their higher elevations.

The month of July experiences the lowest variance of the four months displayed. During the summer, synoptic weather influences are at a minimum in the state. Lowest values are along much of the Gulf coast and well inland from the coast. In addition, low values appear, once again, in the mountainous section of the region. Highest variances are located in northeast Texas and much of Oklahoma. It seems that three of the main climate controls affecting the state, namely the Gulf, or marine influence, the topography, and continentality, are borne out in the geographical distribution of variance during the summer, as well as in the winter.

The months of April and October essentially represent transitional months for the state of Texas in terms of climate. As such, the variance distributions are quite similar, with a rather uniform field across the region. These months are times of the

year when transient weather disturbances occasionally affect the state.

The distribution of variance across Texas for the mean daily maximum temperature field is shown in Figure 13. Here we see quite similar patterns among all four months in terms of location of maxima and minima. Largest variances are in the northern and northeastern portions of the region, corresponding to the Texas Panhandle and much of Oklahoma. Smallest variances are along the upper Gulf coast and in the higher elevations of the west and southwest.

January and July are again those months with the most and least overall variance, respectively, while April and October represent transitional months. However, it appears that the mean daily maximum temperature field preserves the distribution of variance associated with the previously mentioned climate controls throughout the year better than the mean monthly field.

The variance of the mean daily minimum temperature field for the months of January, April, July and October is exhibited in Figure 14. The distribution for the month of January bears a striking resemblance to that of the mean monthly temperature field for the same month. In July, the pattern of coastal variance is less coherent than in its mean monthly counterpart. This could possibly be due to an enhanced land breeze effect during the summer months. The land breeze effect is primarily a nighttime feature of the coastal circulation and, although weaker than the related daytime sea breeze, is felt during the late night and early morning hours, normally the time of minimum daily temperature. In fact, the months of April and October seem to show similar effects which could also be related to the land breeze.

4.2.2. Spatial Correlation

Kim and North (1991) summarized the general patterns of spatial correlation over the globe: (1) The spatial correlation scale of the interannual variability is in the range of 1500-2000 kilometers; and (2) the spatial correlation length scale is

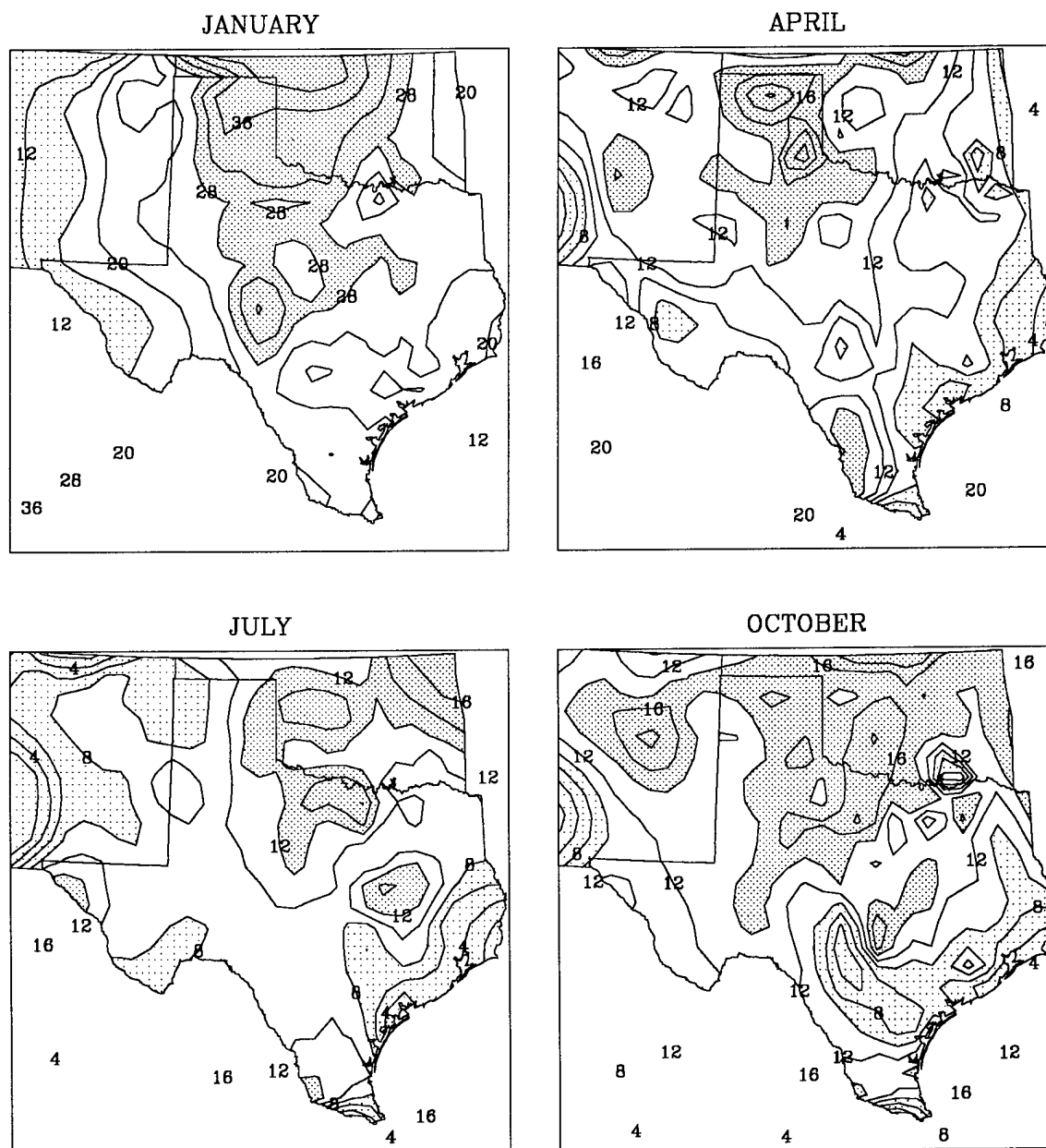


FIG. 13. Same as in FIG. 12, but for mean daily maximum temperature.

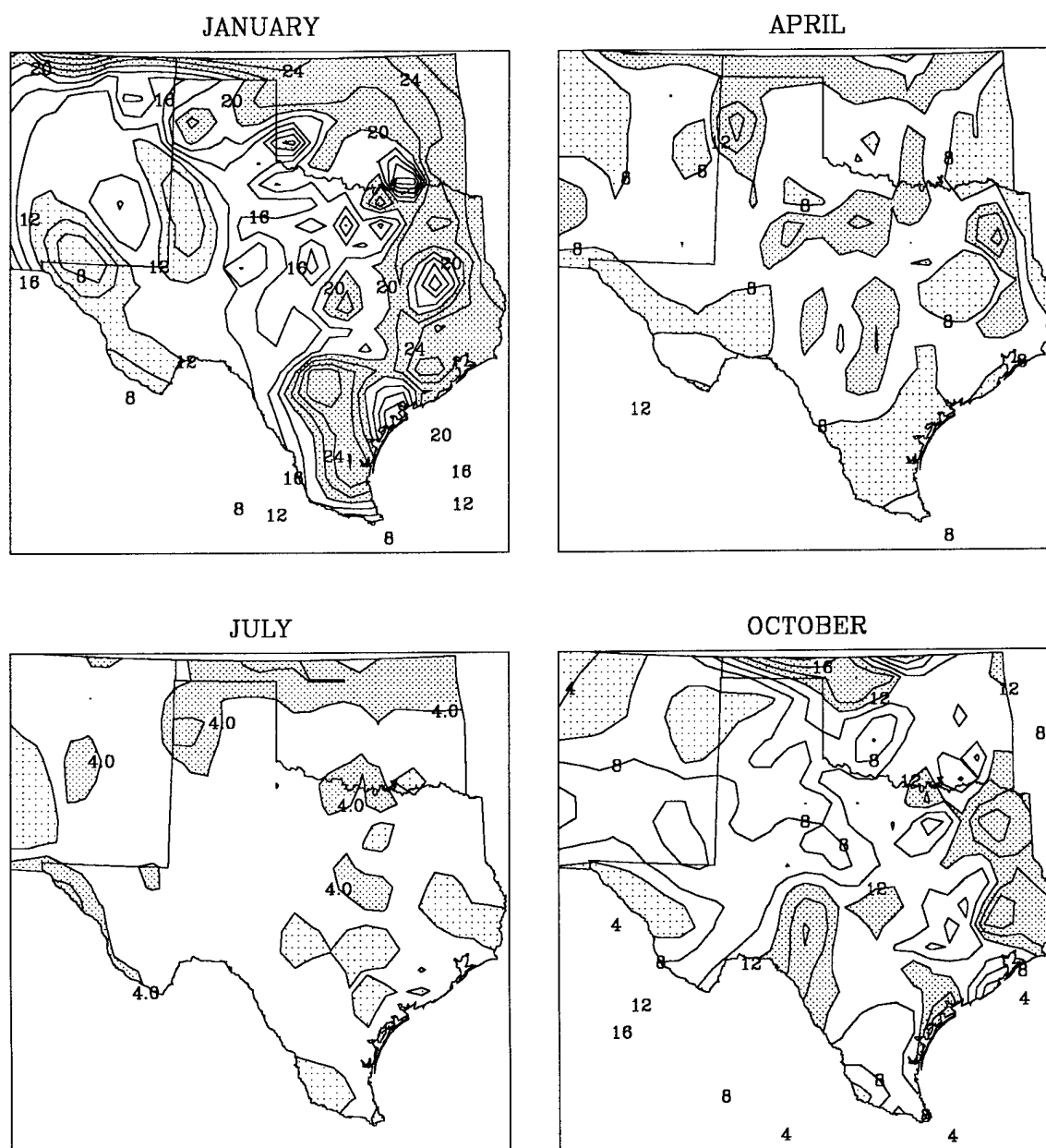


FIG. 14. Same as in FIG. 12, but for mean daily minimum temperature.

larger over land than over the ocean. Their global analysis of spatial correlation functions using the UK data set revealed that the correlation length scale over large continental interiors is larger than that over the ocean. This is due to the different relaxation times of the respective surface media, about one month over land and about 5 years over the open ocean.

The results of the spatial correlation analysis are presented in Figures 15-23. Regions having correlation coefficients of 0.7 or higher are shaded. Each figure contains a plot of the correlation centered around a station in a particular region of the state. Three stations/regions were selected for the purpose of comparison: (1) Pierce, TX/coastal (2) Rising Star, TX/interior (central) (3) Pecos, TX/mountainous region in western Texas. These stations represent regions where significant climatic variations are known to exist, as already discussed. Comparisons will be made on both the spatial and temporal scales for each monthly time series.

Figures 15-17 display the spatial correlation for the mean monthly temperature field for the months of January, April, July and October. Immediately apparent in January is the large region of high correlation for each selected point. The central station is highly correlated with most of Texas and Oklahoma. It appears that stations at lower elevations are well-correlated with each other. Correlation values decrease with increasing elevation. The extent of highly correlated temperatures along the coast reaches well inland during the winter.

In April correlation regions are smaller in size for each point when compared to those of January. By the summer, these areas are even smaller, concomitant with the minimal influence of synoptic-scale weather systems affecting the state of Texas. In fact, since a tropical maritime airmass affects the entire region throughout the season, temperature variations are latitudinal in nature, and correlations decrease correspondingly from the coastal station. Spatial correlations in October are still quite small, except along the coast.

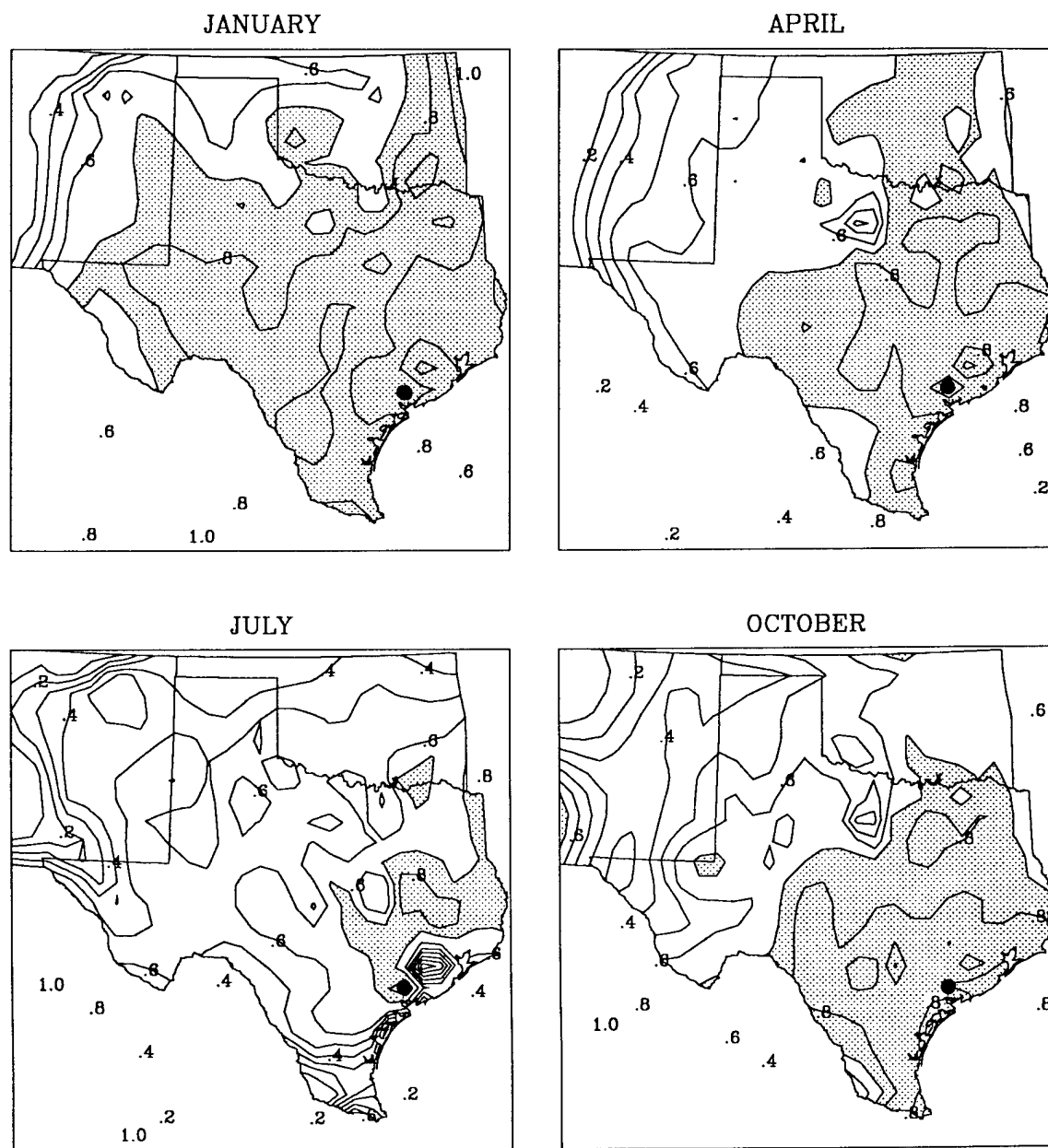


FIG. 15. Plot of spatial correlation function for mean monthly temperature for the months of January, April, July and October. A coastal station is used as the reference point (indicated by black dot). Correlations of 0.7 and higher are shaded.

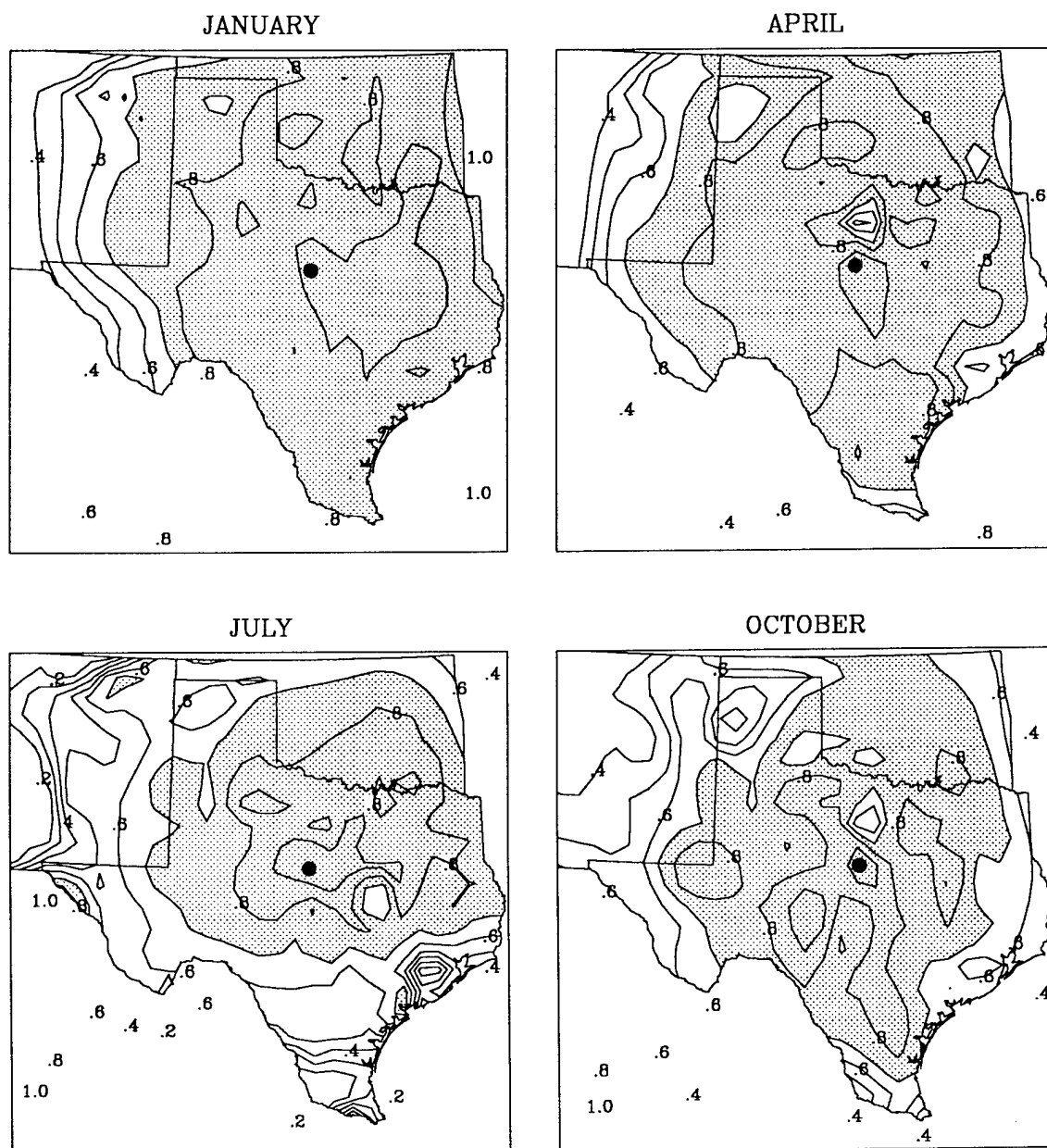


FIG. 16. Same as in FIG. 15, but a station in central Texas is used as the reference point.

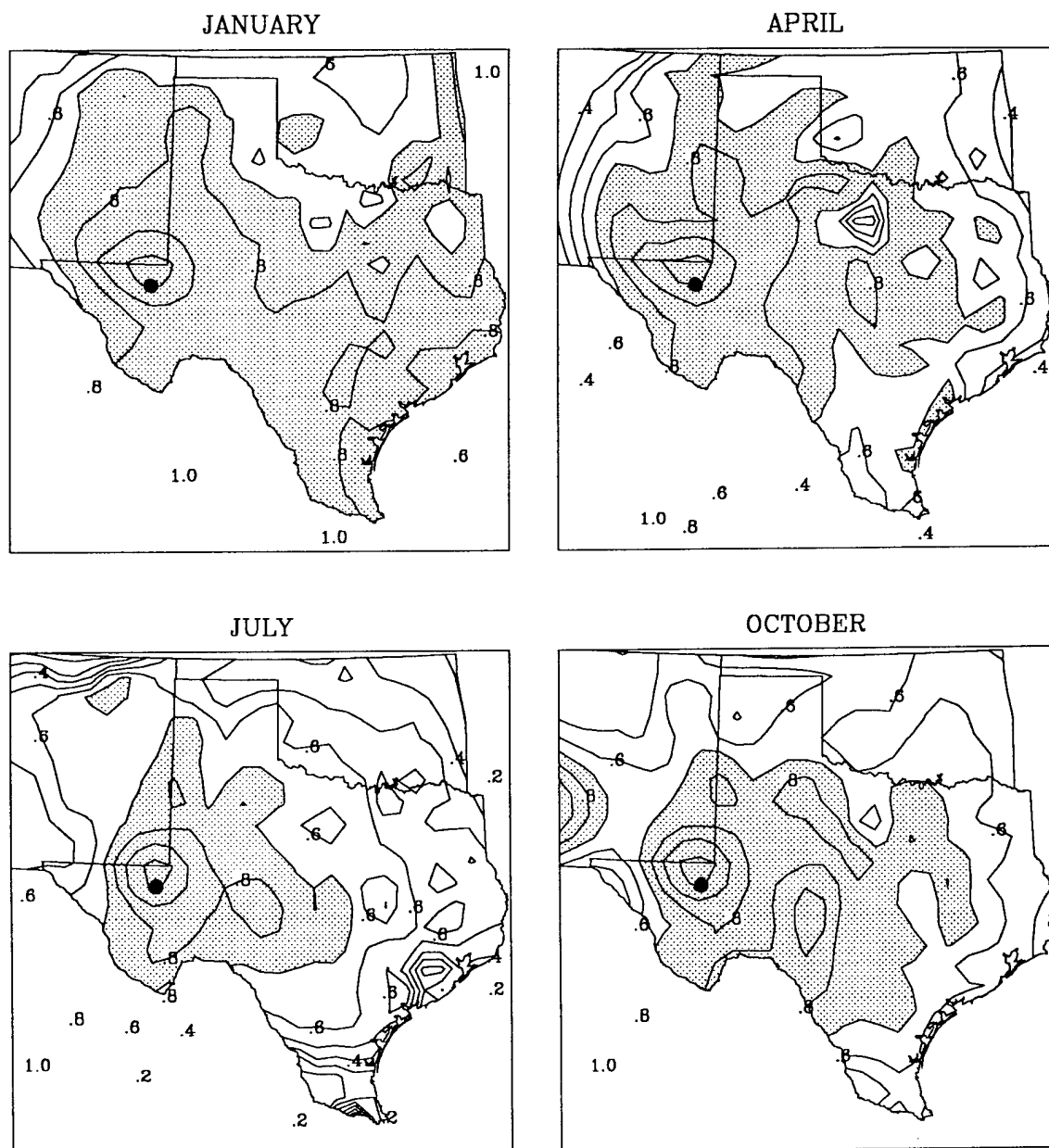


FIG. 17. Same as in FIG. 15, but a station in mountainous west Texas is used as the reference point.

It is intriguing to consider the shape of the spatial correlation function at the test points. Ideally, we expect to see nearly circular isolines around each location. However, we tend to see "branches" protruding out from the higher correlation areas in most of the plots. These "branches" generally extend in a north/south and a northwest/southeast direction. It is possible that the effect of wind flow from the Gulf, which, from experience, favors a southerly or southeasterly direction throughout the year, is producing the shape of the spatial correlation function observed. Another wind flow across the state, although not prevalent, is in a northwesterly direction and is responsible for downsloping conditions in Texas. This may be borne out somewhat in the plots for the mountainous region.

Figures 18-20 show the regions of spatial correlation for the mean daily maximum temperature field over Texas for the same four months of the year. There is a great degree of similarity between these plots and those of the mean monthly field. However, the former expresses slightly larger areas of high correlation. By April, these areas have diminished significantly in size from January, and they are also smaller in size than those of the April mean monthly field. Thus, the correlation of daily maximum temperatures across Texas is not as strong on the spatial scale as that of mean monthly temperatures for the month of April.

The field of spatial correlation in July looks very much like that of the mean monthly temperatures, as was the case in January. By October, though, we see a variety of patterns. The coastal and central points have correlations which are slightly smaller than those of the mean monthly field, while the mountain location is slightly larger. There is much better agreement between the April and October spatial correlation fields of the mean daily maximum temperatures than between those of the mean monthly values.

Figures 21-23 depict the spatial correlation fields for the mean daily minimum temperature time series. In January, the regions of correlation coefficient 0.7 or

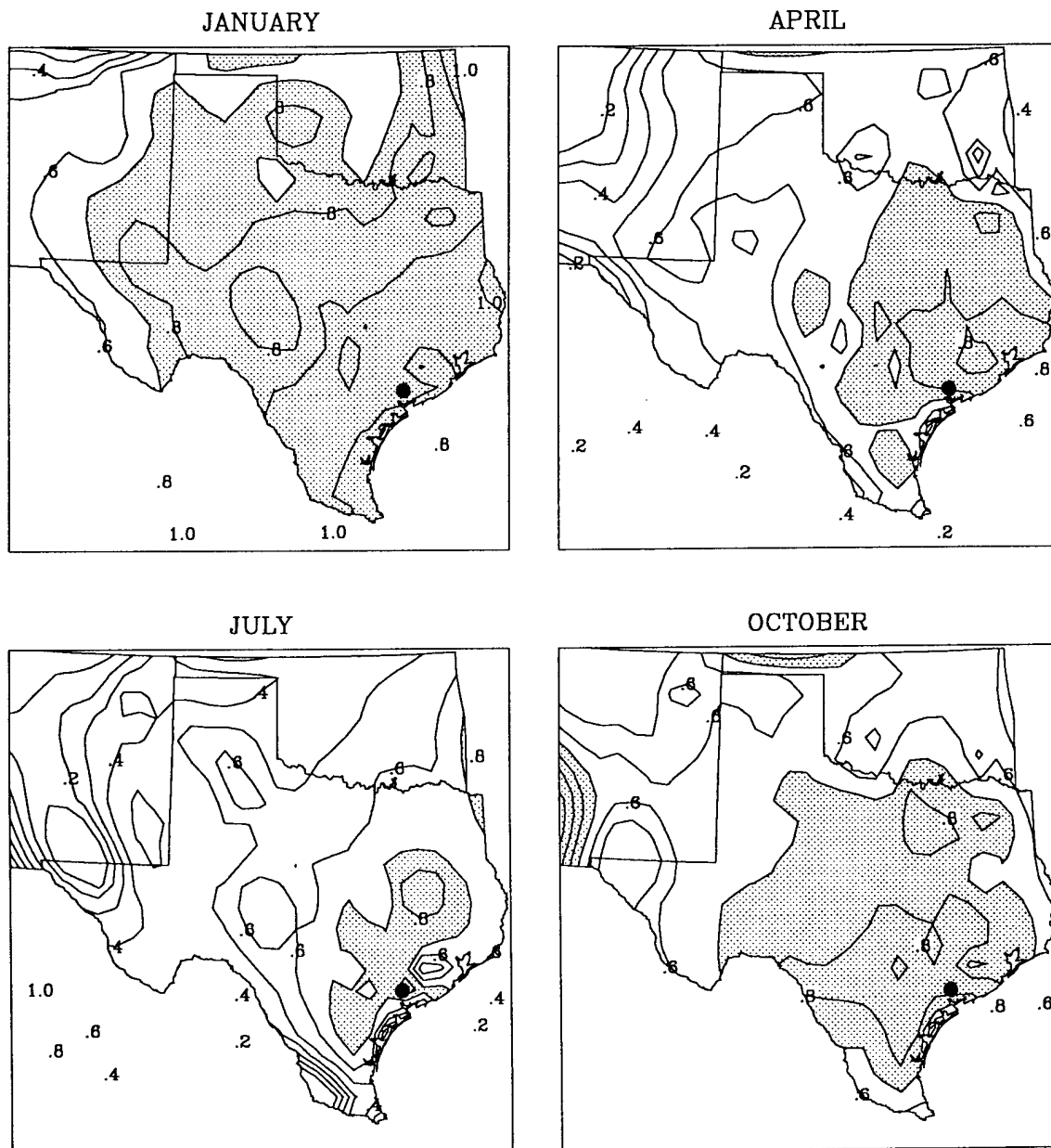


FIG. 18. Plot of spatial correlation function for mean daily maximum temperature for the months of January, April, July and October. A coastal station is used as the reference point (indicated by black dot). Correlations of 0.7 and higher are shaded.

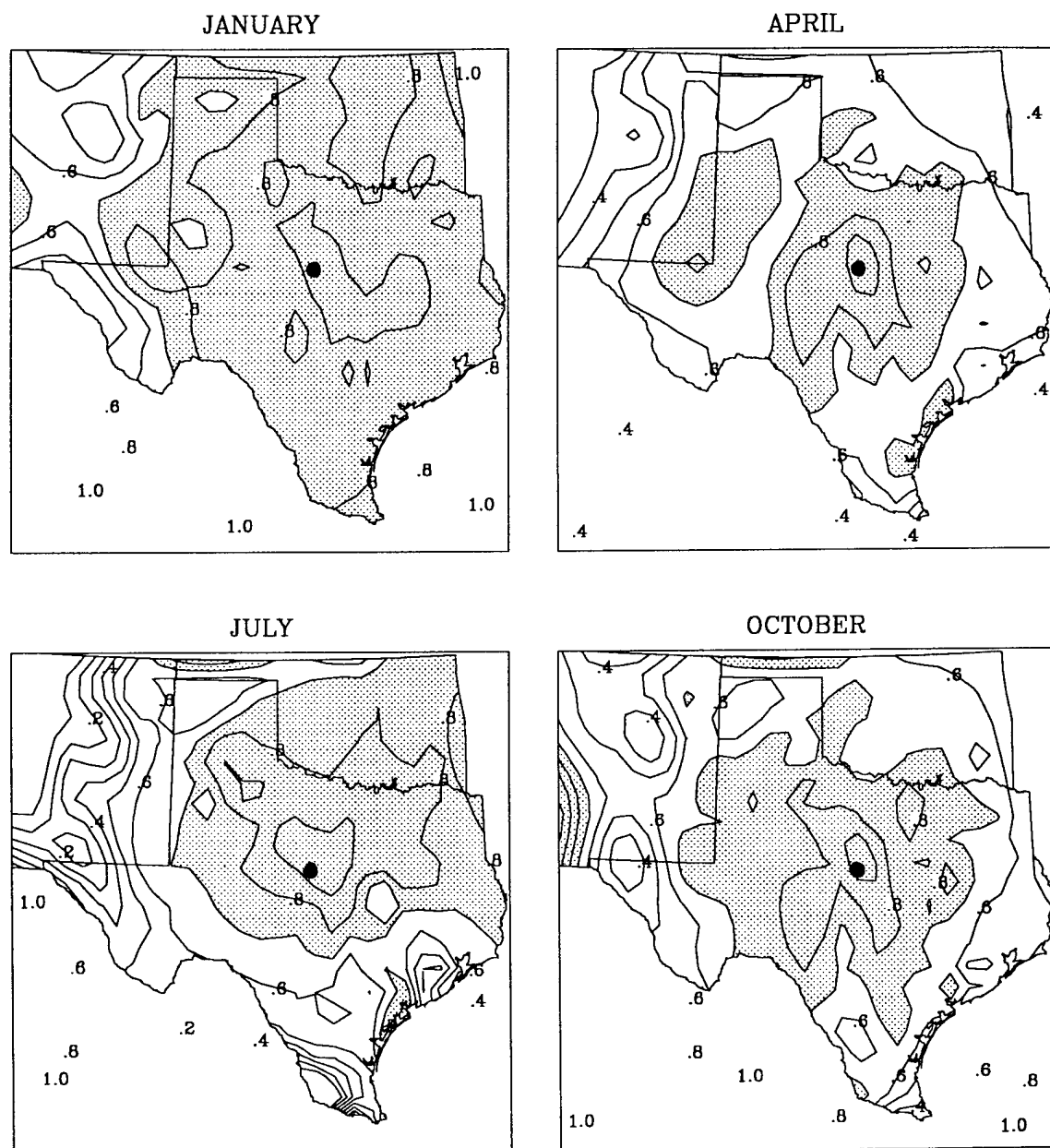


FIG. 19. Same as in FIG. 18, but a station in central Texas is used as the reference point.

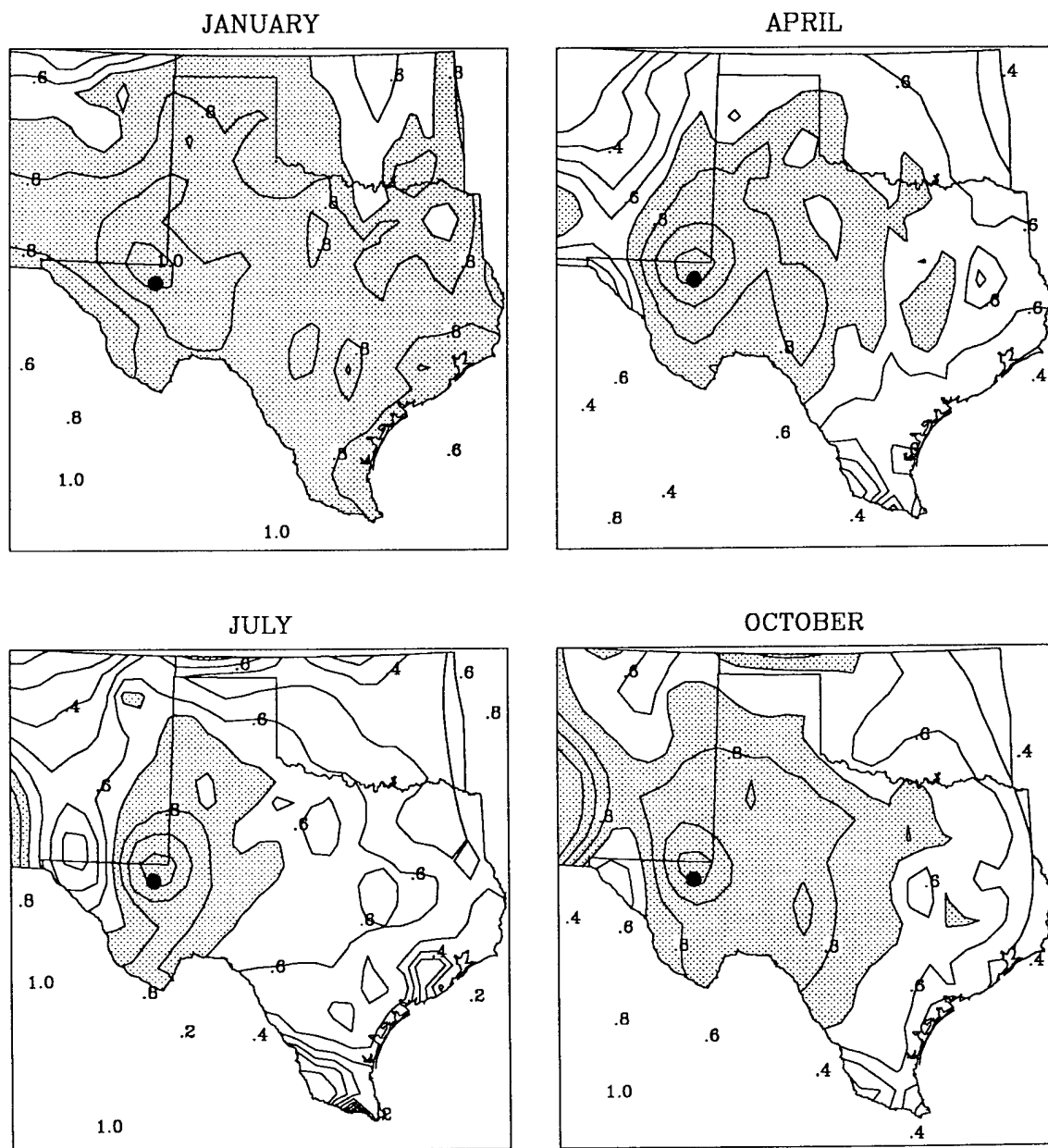


FIG. 20. Same as in FIG. 18, but a station in mountainous west Texas is used as the reference point.

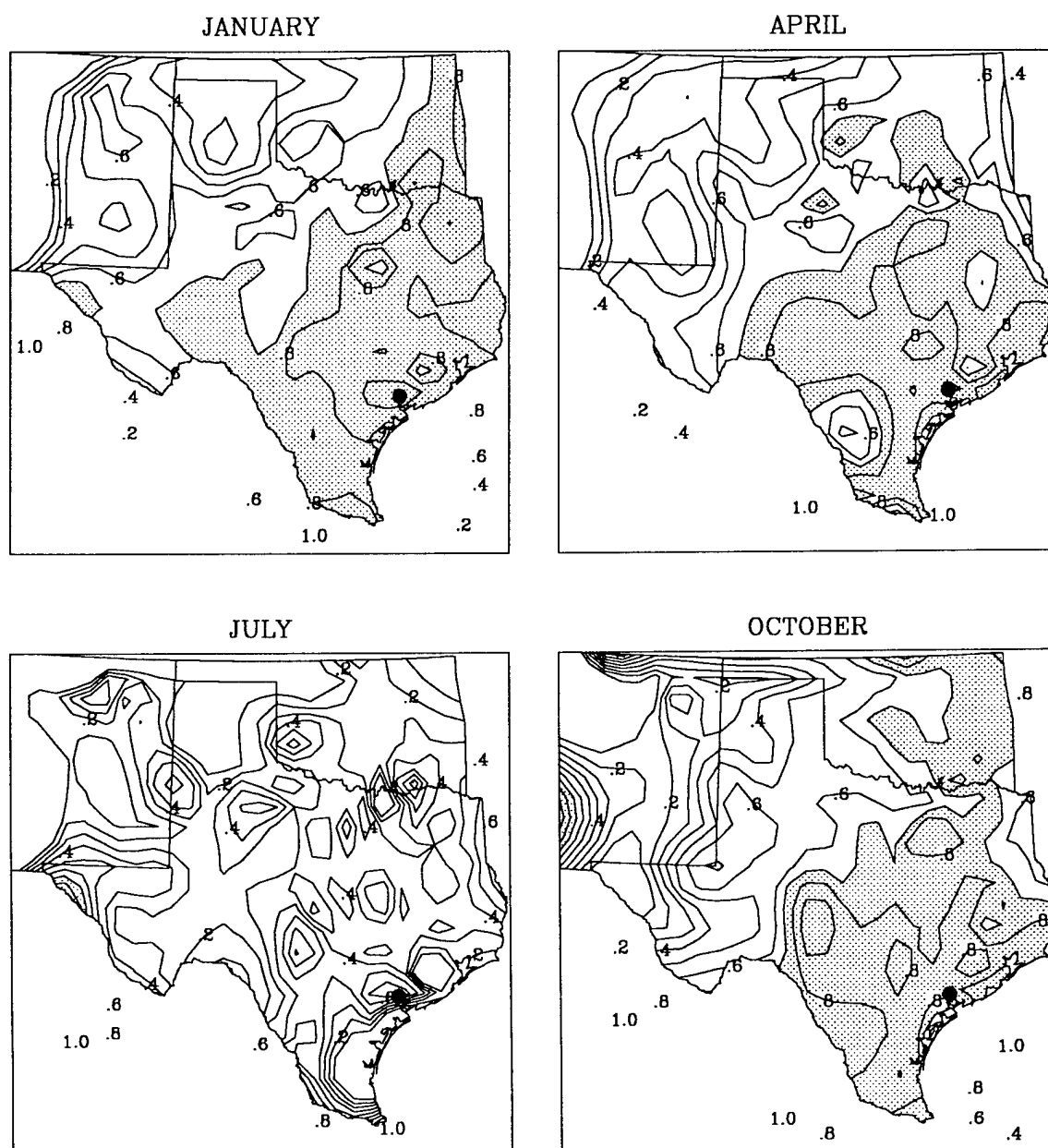


FIG. 21. Plot of spatial correlation function for mean daily minimum temperature for the months of January, April, July and October. A coastal station is used as the reference point (indicated by black dot). Correlations of 0.7 and higher are shaded.

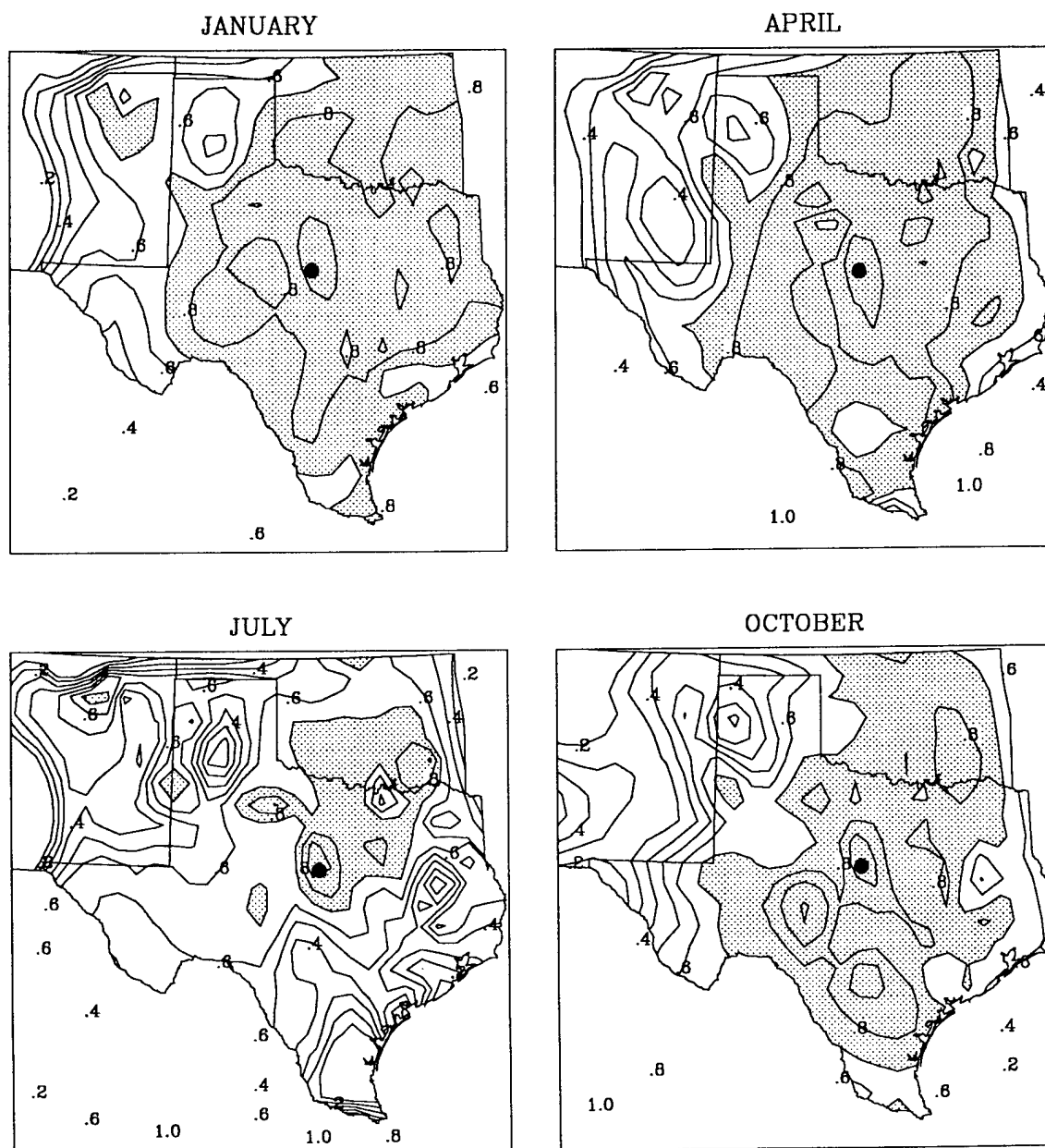


FIG. 22. Same as in FIG. 21, but a station in central Texas is used as the reference point.

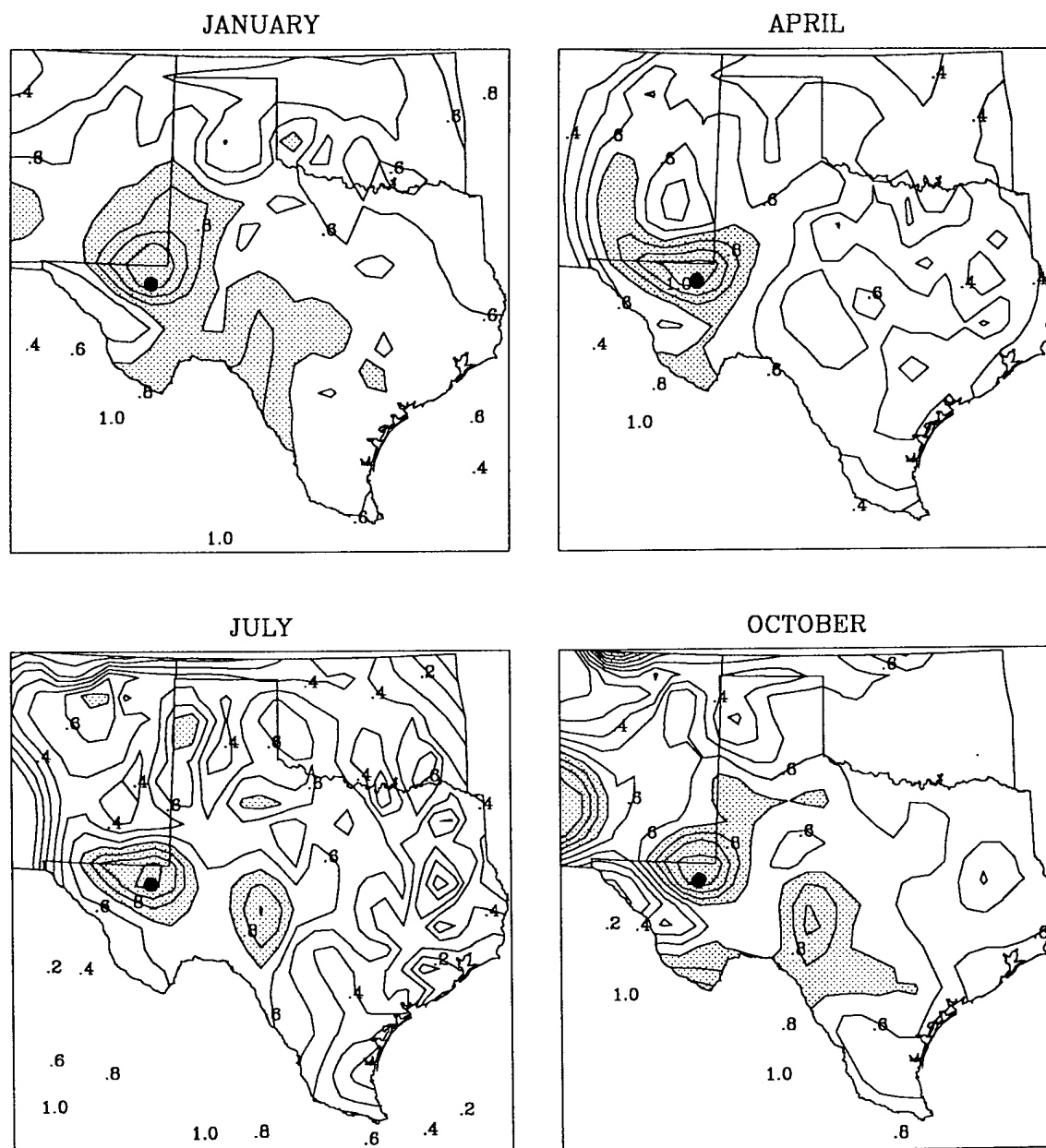


FIG. 23. Same as in FIG. 21, but a station in mountainous west Texas is used as the reference point.

higher are much smaller than those in both the mean monthly and mean daily maximum fields for the same month. This is especially true at both the coastal and mountain locations. This seems to indicate that mean daily minimum temperatures across Texas are not as highly correlated as the mean monthly and the mean daily maximum temperatures during January.

In April the spatial correlation fields slightly resemble those of the mean monthly temperatures for the coastal and central locations, but they are much smaller for the mountain point. However, there appears to be general agreement between the January and April fields of mean daily minimum temperature. By July regions of higher correlation are almost absent in the state. Thus, it appears that mean daily minimum temperatures are subject to latitudinal and local effects which vary across Texas. During the month of October, we see correlation patterns similar to, but slightly smaller than, those of the mean monthly field.

4.2.3. Temporal Correlation

Kim and North (1991) noted that the correlation length scale is shorter over land than over the ocean. The distribution of land mass is an important factor controlling the correlation time scale of the response.

Kim and North (1991) found correlation time scales of about 30 days for an area near Texas in their global analysis using the UK data set. However, initial computations revealed that the correlation length scale over the state of Texas is less than one month. Therefore, since the data used in this study is monthly, it was not possible to rigorously determine the correlation length scale. Instead, temporal correlations were performed for each station using lags of one month, and these correlations were plotted for each time series. In addition, temporal correlations at lags of one year were computed and plotted for each station for the months of January, April, July and October. These results will be presented later.

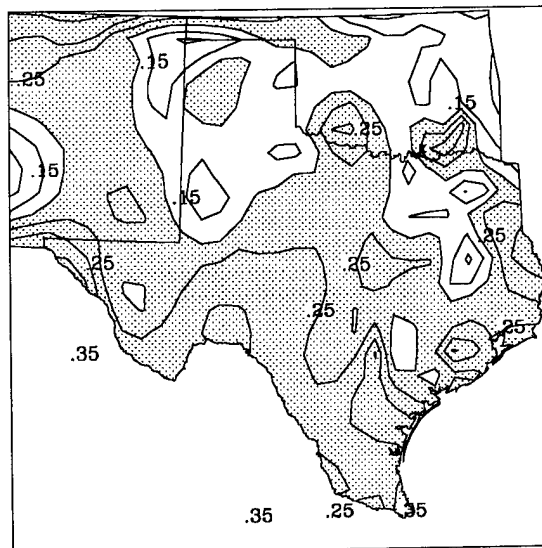
Autocorrelation analysis of meteorological variables such as temperature have been performed for some time (Madden 1977; Shea 1986). These two studies used a lag of one year in order to examine the potential predictability of temperature and other climatic parameters from year to year. Madden (1977) found more significant correlation of mean surface temperature in the summer than in the winter for the Northern Hemisphere with little, if any, relation to the land-mass distribution of the continent. We might expect larger autocorrelations at coastal stations than at interior stations because of their proximity to slowly-changing sea temperatures.

4.2.3.1. One-Month Lag

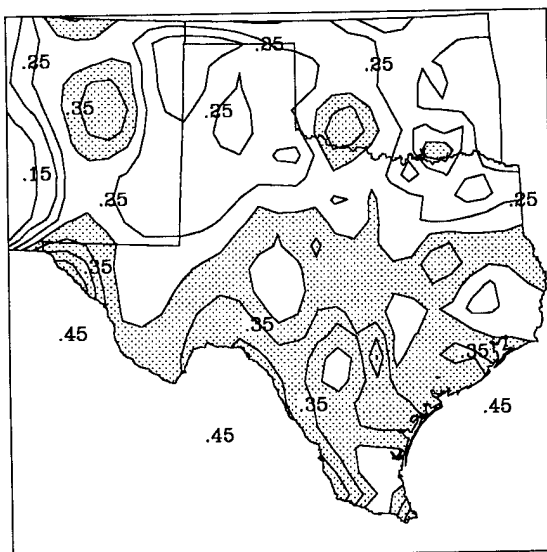
Figure 24 contains spatial plots of temporal correlation at a lag of one month for the mean monthly, mean daily maximum and mean daily minimum temperature time series. Various shading schemes are used to highlight areas of higher correlation coefficients. If we assume the monthly temperature anomalies are normally distributed and successive realizations are independent, we can determine whether the coefficients observed are significantly different from zero. In this case, correlations of approximately .3 or higher are significant at the 95% confidence level, while correlations of .39 or greater can be considered different than zero at the 99% confidence level. However, we cannot readily assume independence among different realizations because serial correlation probably exists between monthly temperatures. Therefore, the threshold coefficients of .3 and .39 most likely should be raised before testing for significance.

Nevertheless, in order to emphasize the aforementioned areas, correlations of .2 and higher were shaded for the mean monthly and mean daily minimum temperature plots; a value of .3 was used for the mean daily maximum plot. In all instances, generally higher temporal correlations are found at stations located in the southern half of the state and in the mountainous region of eastern New Mexico. However, the

MEAN MONTHLY TEMPERATURE



MEAN DAILY MAXIMUM TEMPERATURE



MEAN DAILY MINIMUM TEMPERATURE

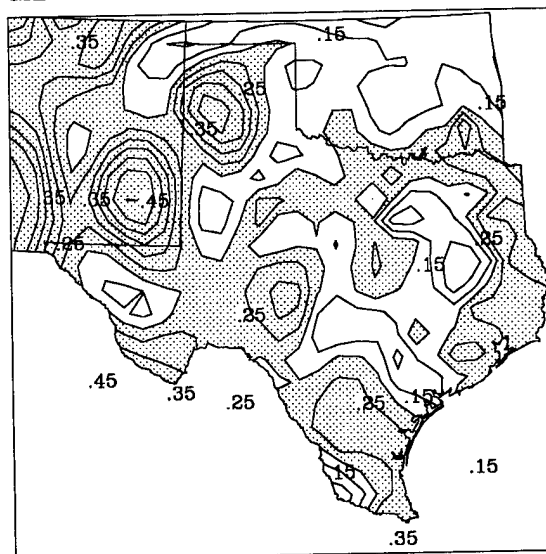


FIG. 24. Plot of the temporal correlation function for a lag of one month for the mean monthly, mean daily maximum, and mean daily minimum temperature field. Correlation coefficients of 0.20 and higher are shaded for the mean monthly and mean daily minimum. Values of 0.30 and higher are shaded for the mean daily maximum.

patterns observed lack in coherence and overall uniformity. It appears that an area of the size of the state of Texas is not large enough to depict distinct differences in temporal correlation across various climatic regimes. Nonetheless, the mean monthly and mean daily minimum charts seem to indicate that inland continental regions favor lower one-month lagged temporal correlations, as might be expected. Most of the lowest correlations are found in Oklahoma and in northern Texas' Panhandle region.

4.2.3.2. One-Year Lag

Figures 25-27 are plots of the one-year lagged correlation coefficients during the months of January, April, July and October for each time series. Since the plots contained maxima and minima of various intensities, giving the field a cluttered and "noisy" appearance, only areas of correlation coefficient .25 and higher and -.25 and lower were contoured. Positive regions were shaded slightly darker than negative regions for distinction.

Immediately apparent in each figure is the area of higher correlations during the month of January. It is by far the largest of all the months for each time series, except the mean daily minimum temperature where July exhibits a rather sizeable region of positive correlations as well.

During January the region of highest correlations for the mean monthly temperature time series (Fig. 25) is located in the northeastern part of Texas, displayed off the Gulf coast, and in eastern Oklahoma. Other months show little or no prominent regions of correlation in the state of Texas.

For the mean daily maximum temperatures (Fig. 26), a large area of high correlation is found in southeastern Texas along the coast and somewhat inland. April shows a few small areas of negative correlation which appear to be local in nature. Other months again show little or no prominent areas in Texas.

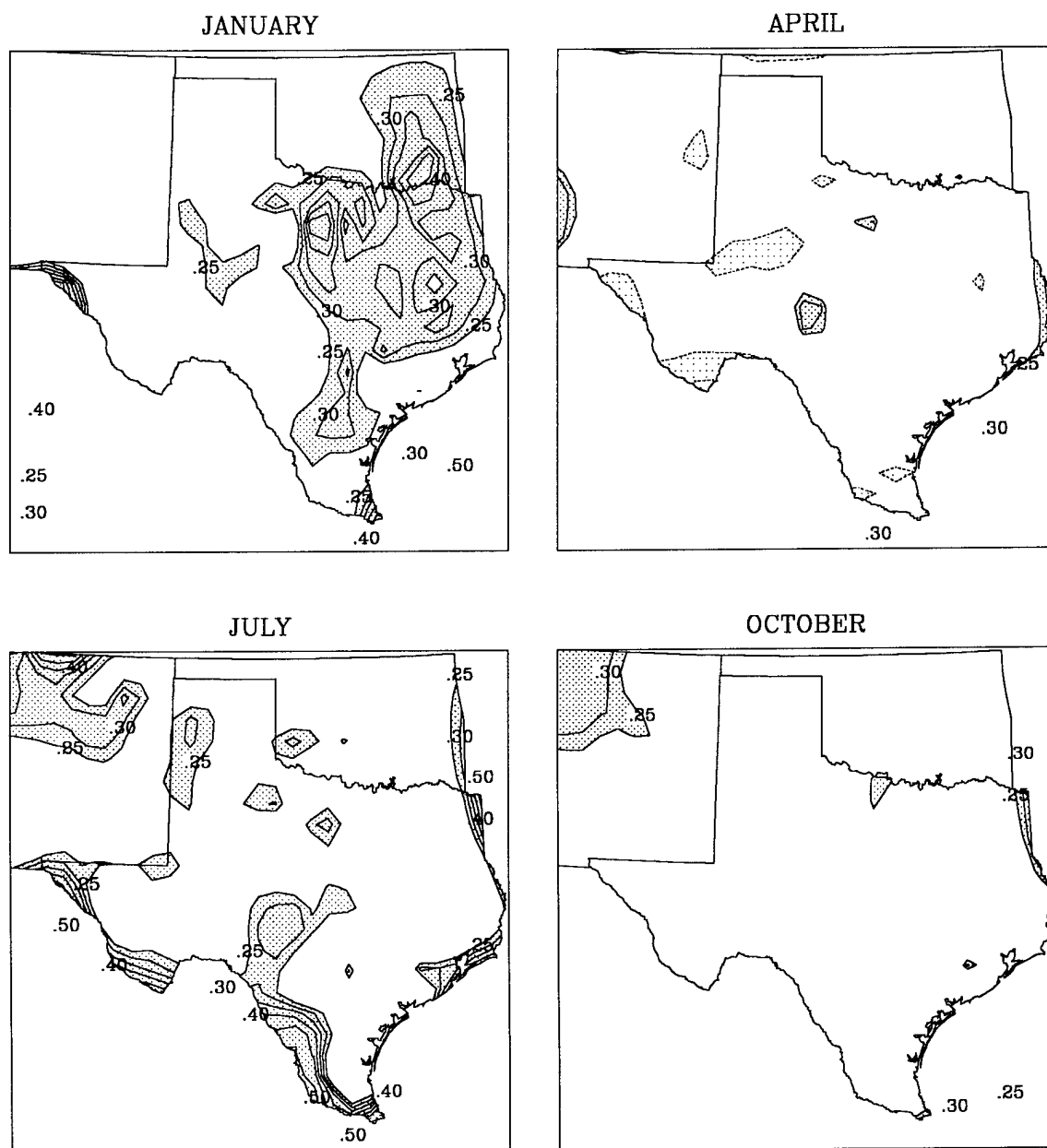


FIG. 25. Plot of the temporal correlation function for a lag of one year for the mean monthly temperature field. The months of January, April, July, and October are shown. Only correlations of 0.25 and greater and -0.25 and less are depicted. The former have a darker shading, the latter a lighter shading.

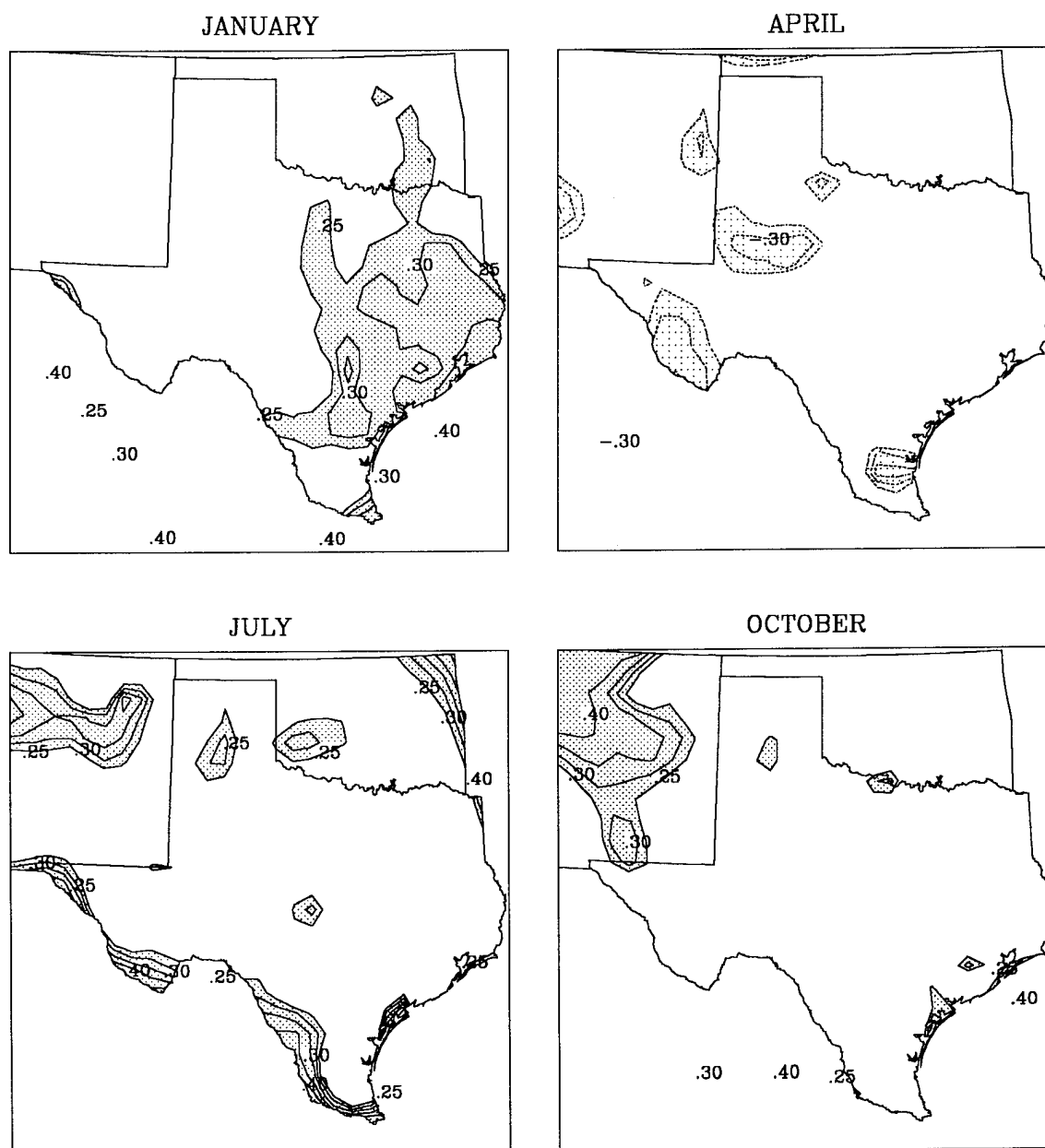


FIG. 26. Same as in FIG. 25, but for mean daily maximum temperature.

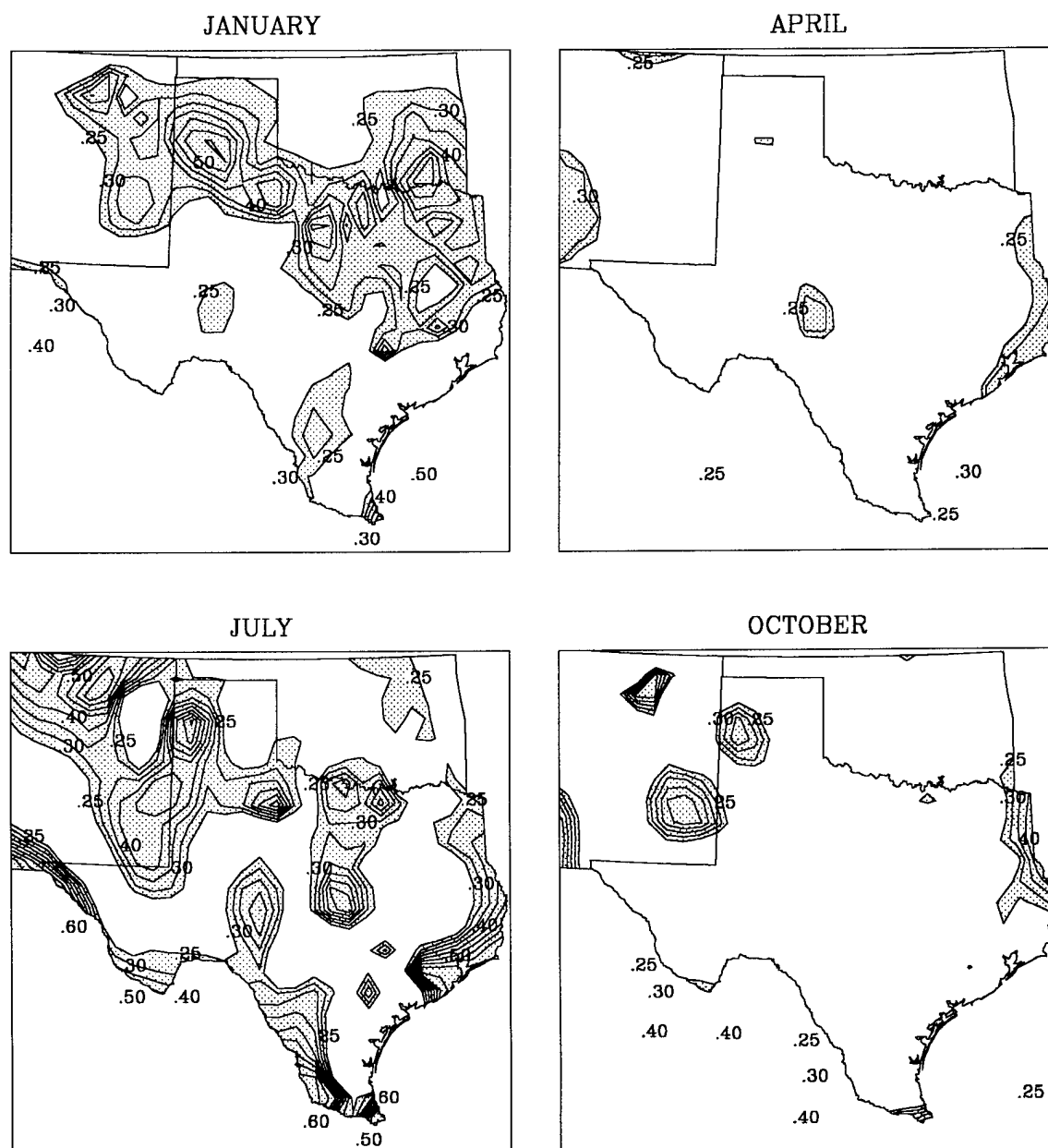


FIG. 27. Same as in FIG. 25, but for mean daily minimum temperature.

Examining the mean daily minimum temperatures (Fig. 27), we see that, as mentioned earlier, both January and July show large regions of positive correlation. During January this area is located to the north and east in Texas, while in July it is scattered into several smaller areas in various parts of the state. Explanations for these particular patterns are elusive. The months of April and October show very little correlation from year to year.

4.3. Empirical Orthogonal Function Analysis

An empirical orthogonal function (EOF) analysis was performed on the 50-year surface temperature anomaly fields for the network of 91 stations. The EOFs of the surface temperature anomaly field calculated in this study were plotted for both the entire year and for the same four months previously used in other analyses. This was done by first determining the value of the function at each grid point for the particular time period chosen. Since there could be as many as 91 EOF patterns for any one time period, only the first several were produced because they contain the most variance.

A pattern correlation between the EOFs computed with and without an area weighting factor was first performed for the months of January, April, July and October for the mean monthly time series. Table 3 contains the correlation matrices. The first several modes appear to be highly correlated. Since these modes are generally the most significant, it seems that the use of an area weighting scheme does not alter the results in a great way. Nevertheless, the metric factor has been used to calculate the EOFs to follow.

It has already been stated how the eigenvalues are related to the variance of the field. Each eigenvalue corresponds to a mode of variability and, if these are arranged in descending order from largest to smallest, the first eigenvalue corresponds to the

TABLE 3. Correlation between the first 8 EOFs computed with and without an area weighting for each station. EOFs were computed for the mean monthly temperature field for January, April, July and October.

Mode #		1	2	3	4	5	6	7	8
January	1	1.00	.00	.02	.00	.00	.00	.00	.00
	2	-.19	-.85	.49	-.03	-.03	.01	-.01	.00
	3	-.19	.58	.79	.00	.02	.02	.00	.03
	4	.08	.13	-.16	-.90	.00	.32	-.07	.10
	5	-.09	.23	.08	-.23	-.82	-.40	.01	-.15
	6	.03	.09	-.03	.25	-.32	.73	-.10	-.37
	7	.05	.02	-.21	.33	-.40	.15	-.31	.57
	8	-.06	.04	.03	-.12	.40	-.37	-.40	-.34
April	1	1.00	.03	-.01	.00	.00	.00	.00	.00
	2	-.26	.96	-.07	-.07	-.01	-.01	-.01	-.01
	3	-.12	-.08	-.96	.21	.13	-.02	.03	-.01
	4	-.10	.21	.17	.86	-.42	-.02	.01	.03
	5	.01	.17	.38	.45	.79	-.05	.01	.00
	6	.06	.05	-.06	.04	.04	.76	.50	.03
	7	.16	-.05	-.18	.09	.06	.44	-.78	.13
	8	-.13	.05	-.07	-.17	.02	-.25	.22	.70
July	1	1.00	.01	-.02	.00	.00	.00	.00	.00
	2	-.11	.98	-.13	-.05	.00	.04	.03	.00
	3	-.25	-.20	-.94	.01	-.11	.01	-.03	.01
	4	-.09	.13	-.05	.94	.25	.04	-.12	.08
	5	-.14	-.11	-.30	-.35	.83	-.14	.03	.08
	6	-.08	-.19	-.08	.11	-.01	.65	.53	.21
	7	-.06	-.05	.12	-.29	.14	.59	-.55	.32
	8	.10	-.04	-.07	-.03	.07	.56	-.30	-.60
October	1	1.00	-.04	.01	.00	.00	.00	.00	.00
	2	-.31	-.90	.29	.04	.02	-.02	.01	-.01
	3	.03	-.46	-.88	.01	-.08	-.06	-.03	-.03
	4	-.09	-.15	-.07	-.93	.28	.09	.03	-.07
	5	.02	.06	-.23	.42	.86	-.06	.03	-.10
	6	.14	.23	.17	-.17	-.03	-.91	.12	-.08
	7	.09	.15	.09	.06	-.26	.18	.23	-.63
	8	.00	-.05	-.19	.08	-.05	.05	.93	.10

most variance, the second to the next greatest portion of variance, etc.

In order to compute the value of the variance associated with each EOF mode, I divided each eigenvalue by the total variance, producing a normalized amount. Since the EOFs are an optimum basis set, no other basis set can explain more of the average variance in the temperature field. Table 4 illustrates how the variability of the surface temperature field is partitioned among the different EOFs. The percent variance and cumulative variance associated with the first eight modes of the mean monthly, mean daily maximum and mean daily minimum temperature time series for the months of January, April, July and October and for the year are shown.

Since most of the variance of the surface temperature anomaly field can be explained by the first few EOFs, only these will be shown. Higher modes generally can be regarded as insignificant because they account for a very small portion of the variance of the field and are usually difficult to distinguish from noise.

Fig. 28-30 are the first four spatial EOFs for the year for each time series. The first three are all quite similar. The first EOF is associated with 60-70% of the total variance of the temperature field, which is a significant portion. The second and third EOFs are associated with about the same amount of variance, approximately 6-9%, and their spatial patterns bear a striking resemblance to each other. Note, however, that they are orthogonal to each other, as required. The fourth EOF is associated with only 2-3% of the total variance, which is a very small portion. It may be difficult to distinguish this EOF from noise. Again, note the shape and content of the pattern, mainly for the mean monthly and mean daily maximum time series. There are now three nodes, and the overall pattern is orthogonal to the others.

Possible explanations or physical interpretations for these patterns are deferred to the following subsections. To provide more insight into the time evolution of the EOFs, the analysis was performed for the same four months used throughout this study. Since there exists a close resemblance between the corresponding EOFs

TABLE 4. Total variance, percent variance, and cumulative percent variance (in parentheses) associated with the first 8 EOFs for January, April, July, October and the entire year. EOFs were computed for (a) mean monthly, (b) mean daily maximum, and (c) mean daily minimum temperature. Units of variance are $(^{\circ}\text{F})^2$.

	Jan	Apr	Jul	Oct	Year
$\sum \text{Var}$	15.3	8.5	4.6	6.8	8.6
1	74.6 (74.6)	69.8 (69.8)	61.8 (61.8)	63.5 (63.5)	68.1 (68.1)
2	8.5 (83.2)	9.2 (79.0)	10.0 (71.8)	11.0 (74.5)	8.8 (76.9)
3	5.8 (89.0)	5.2 (84.1)	6.0 (77.8)	6.7 (81.2)	6.4 (83.3)
(a) 4	1.5 (90.5)	2.8 (86.9)	2.5 (80.3)	2.7 (83.9)	1.8 (85.1)
5	1.1 (91.6)	2.1 (89.0)	2.2 (82.5)	2.3 (86.2)	1.5 (86.5)
6	0.8 (92.3)	1.3 (90.3)	2.0 (84.5)	1.9 (88.1)	1.0 (87.6)
7	0.7 (93.1)	1.0 (91.3)	1.6 (86.1)	1.5 (89.6)	0.8 (88.3)
8	0.7 (93.8)	0.8 (92.1)	1.3 (87.4)	1.1 (90.7)	0.7 (89.1)
$\sum \text{Var}$	23.3	11.9	9.1	12.1	13.7
1	76.4 (76.4)	64.3 (64.3)	59.9 (59.9)	67.0 (67.0)	66.8 (66.8)
2	7.3 (83.7)	10.6 (74.9)	10.1 (70.0)	7.7 (74.7)	8.1 (74.9)
3	4.9 (88.6)	6.2 (81.1)	6.9 (76.9)	6.5 (81.2)	6.8 (81.7)
(b) 4	1.7 (90.3)	3.2 (84.3)	3.3 (80.2)	2.4 (83.6)	2.2 (83.9)
5	1.0 (91.4)	2.3 (86.7)	2.2 (82.4)	2.1 (85.6)	1.3 (85.2)
6	1.0 (92.3)	1.8 (88.5)	1.8 (84.2)	1.9 (87.5)	1.2 (86.4)
7	0.7 (93.1)	1.4 (90.0)	1.6 (85.7)	1.7 (89.3)	1.1 (87.5)
8	0.7 (93.8)	1.2 (91.1)	1.5 (87.2)	1.4 (90.6)	0.9 (88.4)
$\sum \text{Var}$	14.3	9.4	3.1	8.7	8.8
1	64.1 (64.1)	64.1 (64.1)	46.0 (46.0)	59.2 (59.2)	60.4 (60.4)
2	9.6 (73.7)	10.5 (74.6)	8.3 (54.3)	10.2 (69.4)	9.4 (69.8)
3	7.8 (81.4)	4.5 (79.1)	6.9 (61.3)	5.6 (74.9)	5.8 (75.6)
(c) 4	3.1 (84.5)	3.1 (82.2)	5.7 (67.0)	3.4 (78.3)	2.8 (78.3)
5	1.9 (86.5)	2.3 (84.5)	3.6 (70.5)	2.5 (80.9)	2.0 (80.3)
6	1.8 (88.2)	1.6 (86.2)	2.8 (73.3)	2.1 (83.0)	1.7 (82.0)
7	1.4 (89.6)	1.4 (87.6)	2.4 (75.6)	1.9 (84.9)	1.4 (83.4)
8	1.1 (90.7)	1.3 (88.9)	2.2 (77.8)	1.6 (86.5)	1.1 (84.5)

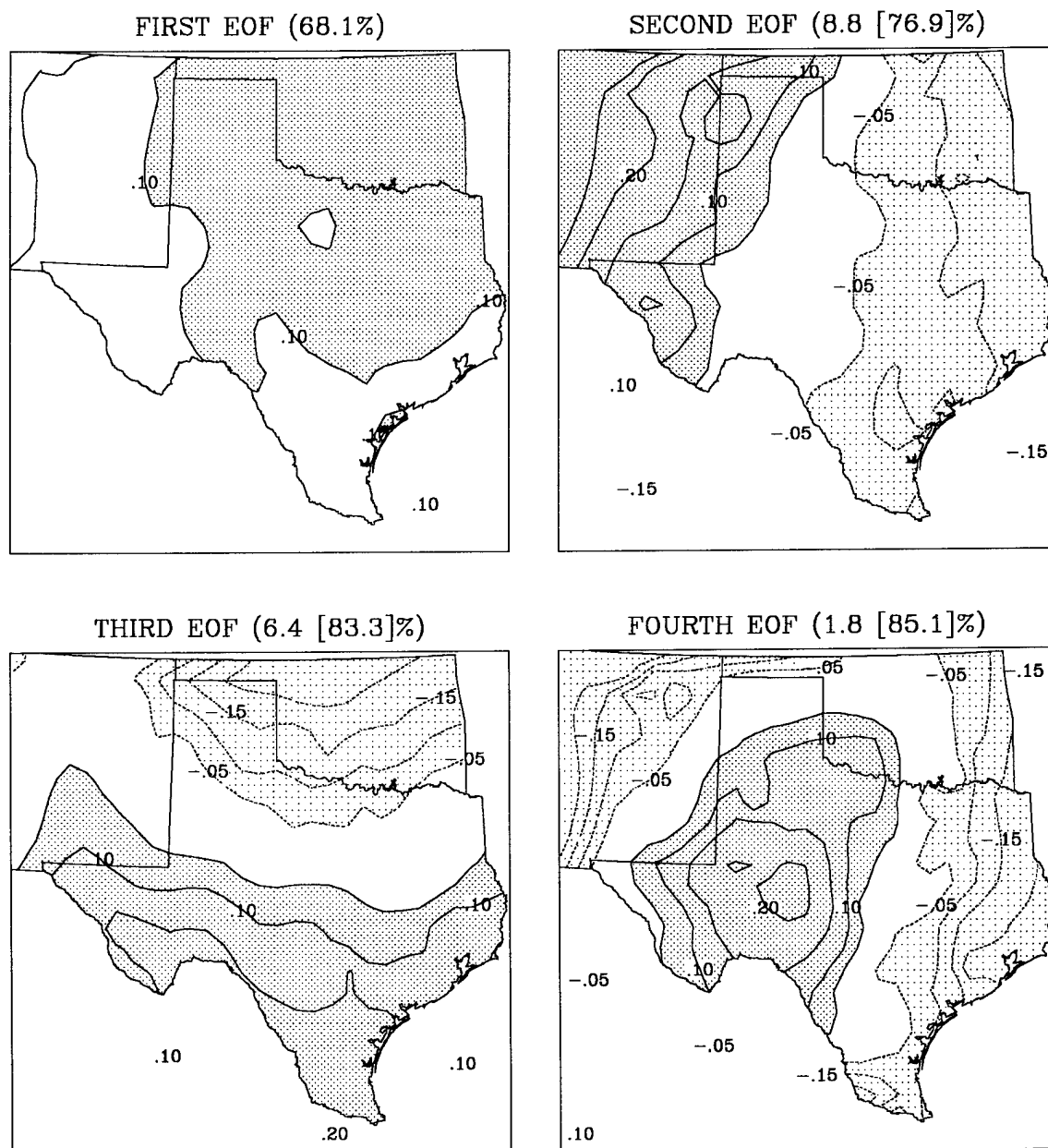


FIG. 28. First four spatial EOFs of mean monthly temperature for the year. Percent variance associated with each EOF is indicated in parentheses. Cumulative percent variance is in brackets. Isolines are non-dimensional. Relatively larger positive values have a darker shading and relatively larger negative values have a lighter shading.

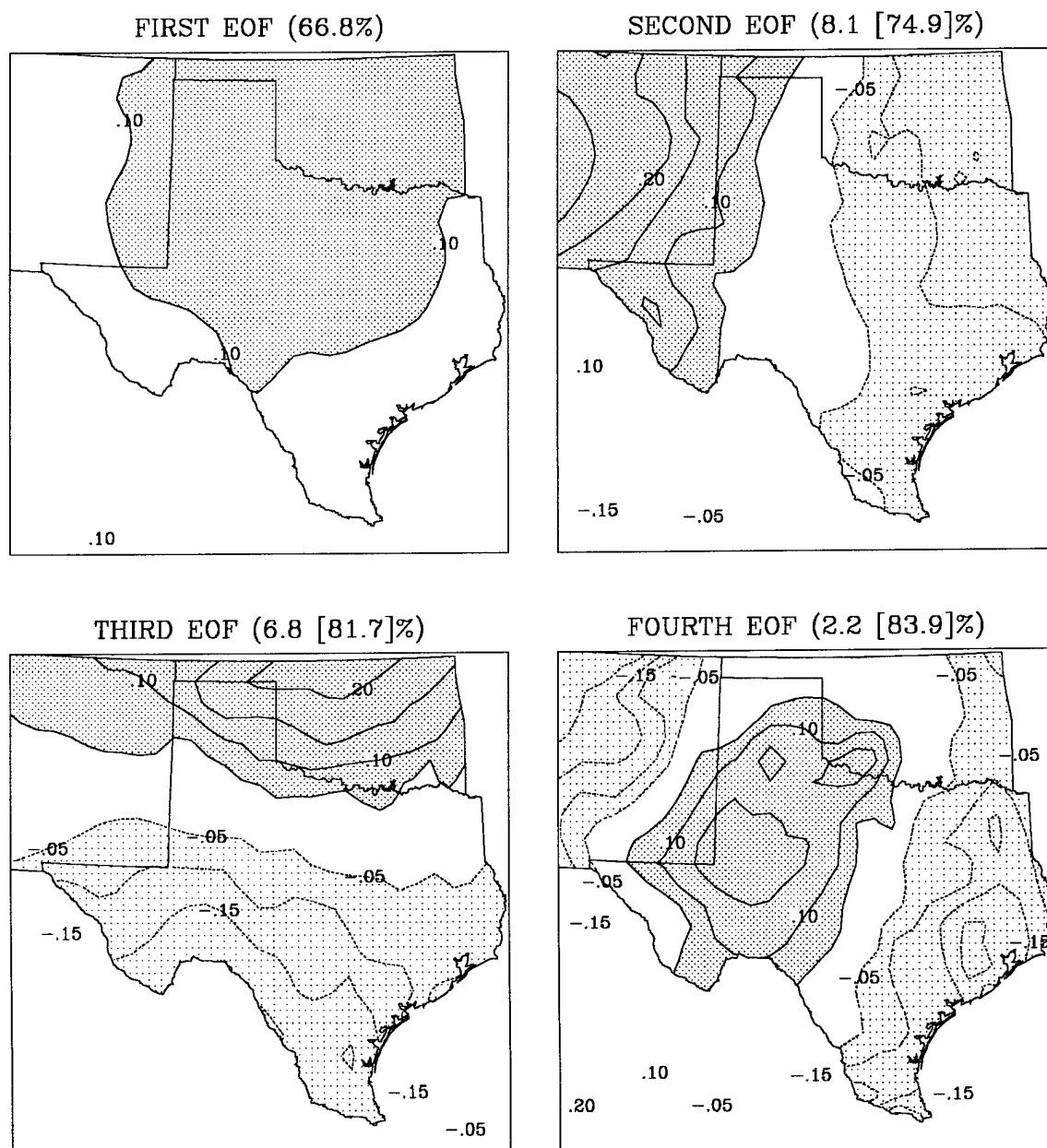
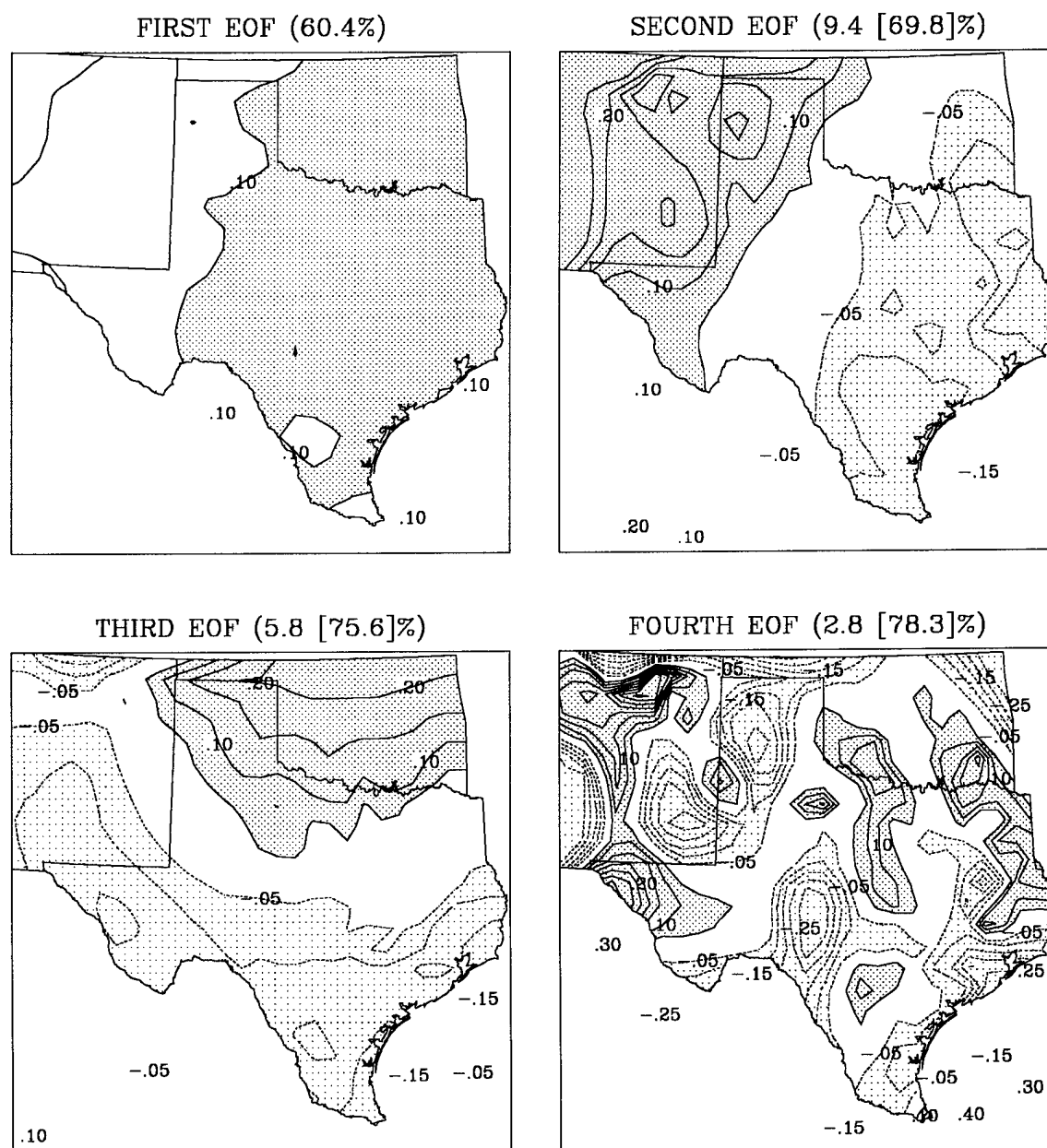


FIG. 29. Same as in FIG. 28, but for mean daily maximum temperature.



of each time series, only those for the mean monthly temperature time series are presented.

The first four EOFs of mean monthly temperature are displayed in Figures 31-34. Between 80 and 90% of the total variance of the field is associated with these four EOFs alone.

4.3.1. First EOF

The first EOF for mean monthly temperature (Fig. 31) produces a fairly uniform and coherent pattern of values across the region. This EOF is associated with between 60 and 75% of the total variance of the temperature anomaly field. The isoline numbers are non-dimensional, but they are all of the same sign. This indicates that most of the variability in Texas is due to outside, or larger-scale, influences and is advected into the state. As a result, it would seem that a mesoscale model for simulating and predicting surface temperature in Texas would not work without knowledge of what is occurring on a scale larger than the state of Texas.

The months of January and October show, for the most part, a higher measure of variability in the eastern one-half to two-thirds of the state. On the other hand, April and July each possess a maximum area of variability which is located in the north and central portions of the state of Texas and into Oklahoma. Decreasing values extend toward the southeast, southwest and west.

Based on synoptic experience in this region, it is possible to speculate why these first EOF patterns exist as they do. Grimmer (1963) and Kidson (1975), and more recently Kim et al. (1984), identified land-sea contrast, or continentality, as the primary mechanism in establishing the observed EOF 1 spatial distribution of covariability. While the earlier studies were performed on a scale much larger than the size of Texas and thus may not be applicable here, the latter was accomplished on a regional scale, namely the state of Oregon. Kim et al. (1984) noted the influence of

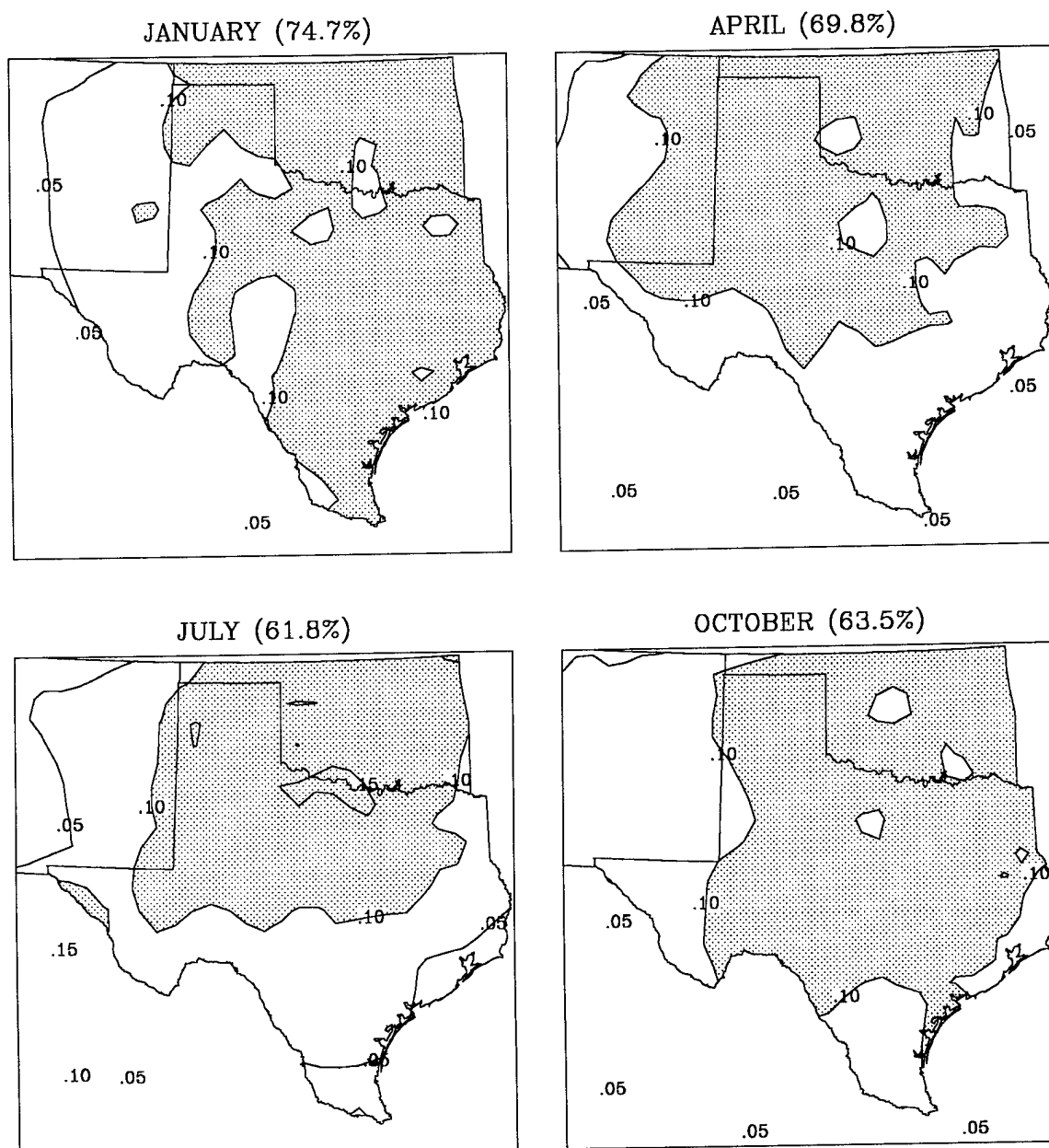


FIG. 31. First spatial EOF for mean monthly temperature for the months of January, April, July and October. Percent variance associated with each month is indicated in parentheses. Isolines are non-dimensional. Values of 0.10 and greater are shaded.

the Pacific Ocean in creating the observed first EOF pattern for surface temperature.

In Texas the Gulf of Mexico is the major control on the state's climate. Predominant wind flow across most of Texas is from the south through southeast around the western flank of the subtropical Bermuda High, bringing moderate Gulf air inland. However, during late fall through early spring, frequent intrusions of polar air, usually associated with transient weather disturbances moving down across the High Plains, east of the Rockies, spread into most of the state, effectively cutting off the flow from the Gulf. These polar air masses even move out over the Gulf itself during the period of October through March.

It appears that EOF 1 for the mean surface temperature anomaly field reflects these two synoptic regimes rather well. In October when the cold air surges, or northers, as they are known locally, are beginning to become a factor in the state's weather, much of Texas is subject to greater anomalous temperatures. Only the coastal regions to the south and southeast and the higher elevations of the Trans-Pecos and New Mexico experience less variability. The mountains to the west serve to inhibit progress of the cooler air from that direction (Orton 1964).

By January, the height of the winter season, the region of greater variability now extends all the way to the Gulf of Mexico. This is the time of the year during which most of the polar intrusions occur. In April, a month during the transitional season of spring, we see that the area of higher variability has now receded inland. The Gulf flow has regained its dominant role. A wider region of lower variability exists along the coast and even well inland at locations which are more influenced by the Gulf air (Griffiths et al. 1987).

During the month of July, a marked continentality effect is evident. The region of greatest variability is confined to the north-central half of the state and to most of Oklahoma. It seems that larger diurnal ranges of surface temperature in this area outweigh the moderating effect of the Gulf waters. However, the latter's influence is

certainly felt along the coast and a few miles inland, where anomalous temperatures appear to be absent.

Even though only the months of January, April, July and October are depicted, the remaining months' first EOFs represent intermediate patterns of the variability just discussed and thus strongly support the explanation put forth.

4.3.2. Second EOF

The second EOF for mean monthly surface temperature anomalies (Fig. 32) consists of two distinct nodes or centers of action which are present throughout the year. This EOF is associated with 8-11% of the total variance, which makes the cumulative variance 71-83% for the first two EOFs combined.

This EOF pattern, and possibly the third EOF as well, may be associated with latitudinal shifts in the westerlies and to the amplitude and position of long waves over the United States. Grimmer (1963) and Kidson (1975) both noted that the second and third EOFs could be considered indices of the atmospheric circulation. Since the winter months in Texas are more susceptible to transient disturbances brought in by steering upper-level jet streams, one might expect to notice the response of the surface temperature anomaly field to this forcing more readily during this season.

The January pattern of EOF 2 shows an area of cold anomalies located in Oklahoma and northeastern Texas with a region of warm anomalies confined to the western one-third of the state and to New Mexico. This configuration could be linked to the position of a major long-wave trough over eastern North America and a high-pressure ridge over the western United States.

One might also consider upslope/downslope winds in Texas as possible contributors to the variance of the second mode. Recall the second EOF for the year and its orientation (Fig. 28). In fact, most of the monthly EOFs have this same pattern

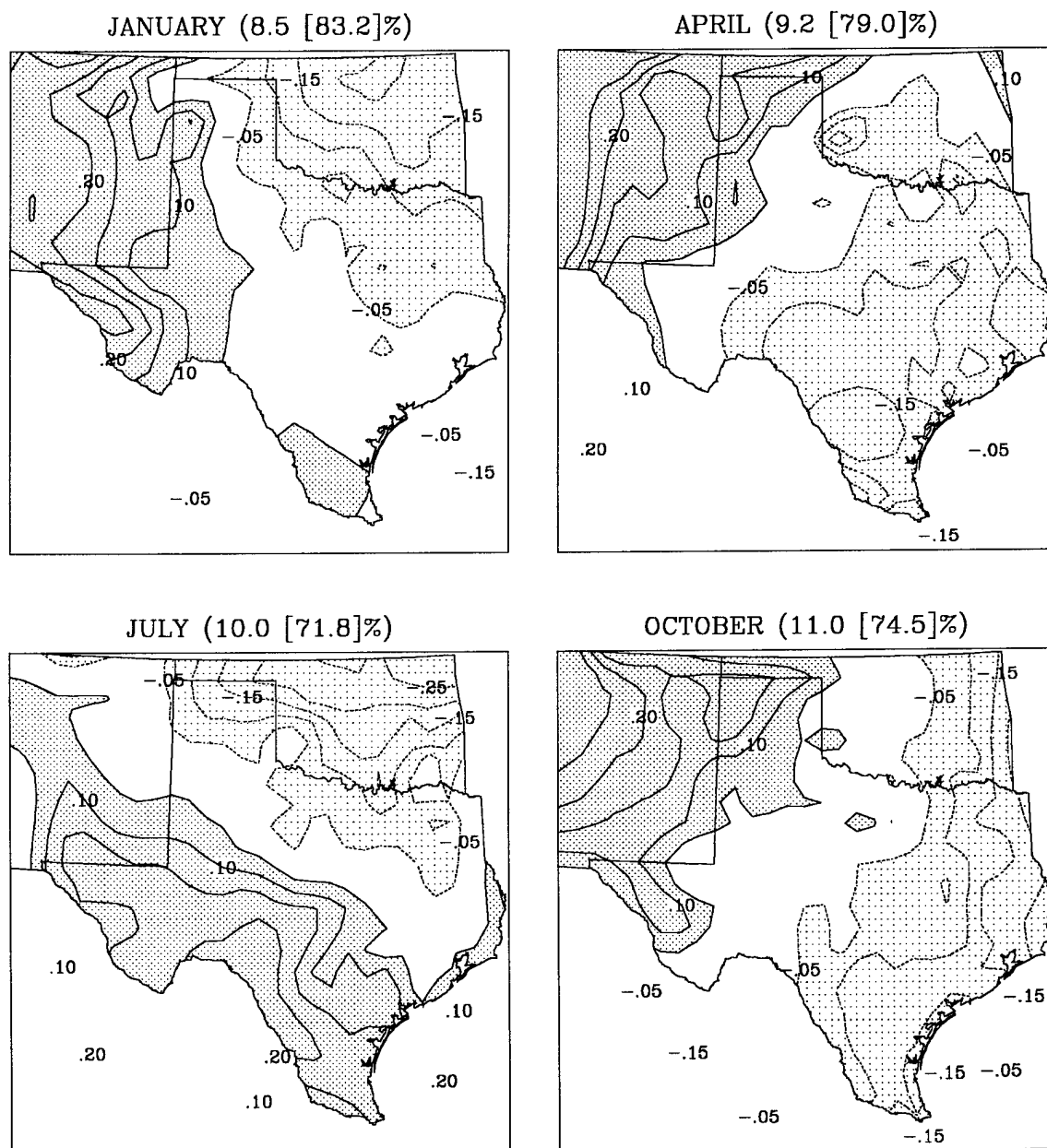


FIG. 32. Second spatial EOF for mean monthly temperature for the months of January, April, July and October. Percent variance associated with each month is indicated in parentheses. Cumulative percent variance for the first two EOFs is in brackets. Values greater than 0.05 (darker shading) and less than -0.05 (lighter shading) are highlighted.

throughout the year. What is quite interesting is that this configuration bears a striking similarity to the orography of the region of study (Fig. 1).

We must be careful not to read too much into this EOF, or try to extract too much information from it. After all, since it accounts for only 8-11% of the total variance, which amounts to about 1.5°F^2 in January, it could well be associated with sampling or measurement error alone. However, it is still intriguing to speculate as to why the pattern chose to orient itself with the orography.

4.3.3. Third EOF

The third EOF for mean monthly surface temperature anomalies (Fig. 33) is associated with only 5-6% of the total variance. With variance for January being about 15°F^2 , this means that the third EOF accounts for less than 1°F^2 of variance of the anomaly field. This is probably not much larger than the error associated with sampling. Nevertheless, the patterns illustrated by this EOF resemble those of EOF 2 (Fig. 32) in that there are primarily two centers of action, both of which seem to be stable and coherent in structure.

The pattern orientations in this EOF are constrained to be orthogonal to those of the second EOF. Because the variance explained is also quite small for both modes, it is possible that these two modes could be interchanged rather easily due to instability of the eigenvalues. Kim and North (1993) noted that when adjacent eigenvalues are close to each other in magnitude, the two corresponding EOFs can mix under slight perturbations. Any two adjacent EOFs could thus switch their positions and merge or intermingle in the presence of sampling or other kinds of errors. This fact leads further credence to the possibility that orography may be responsible for the next highest mode of variability mainly from its influence in producing upslope/downslope flow and the resulting temperature changes. Thus, this third EOF may simply be a result of the geometry of the region under study

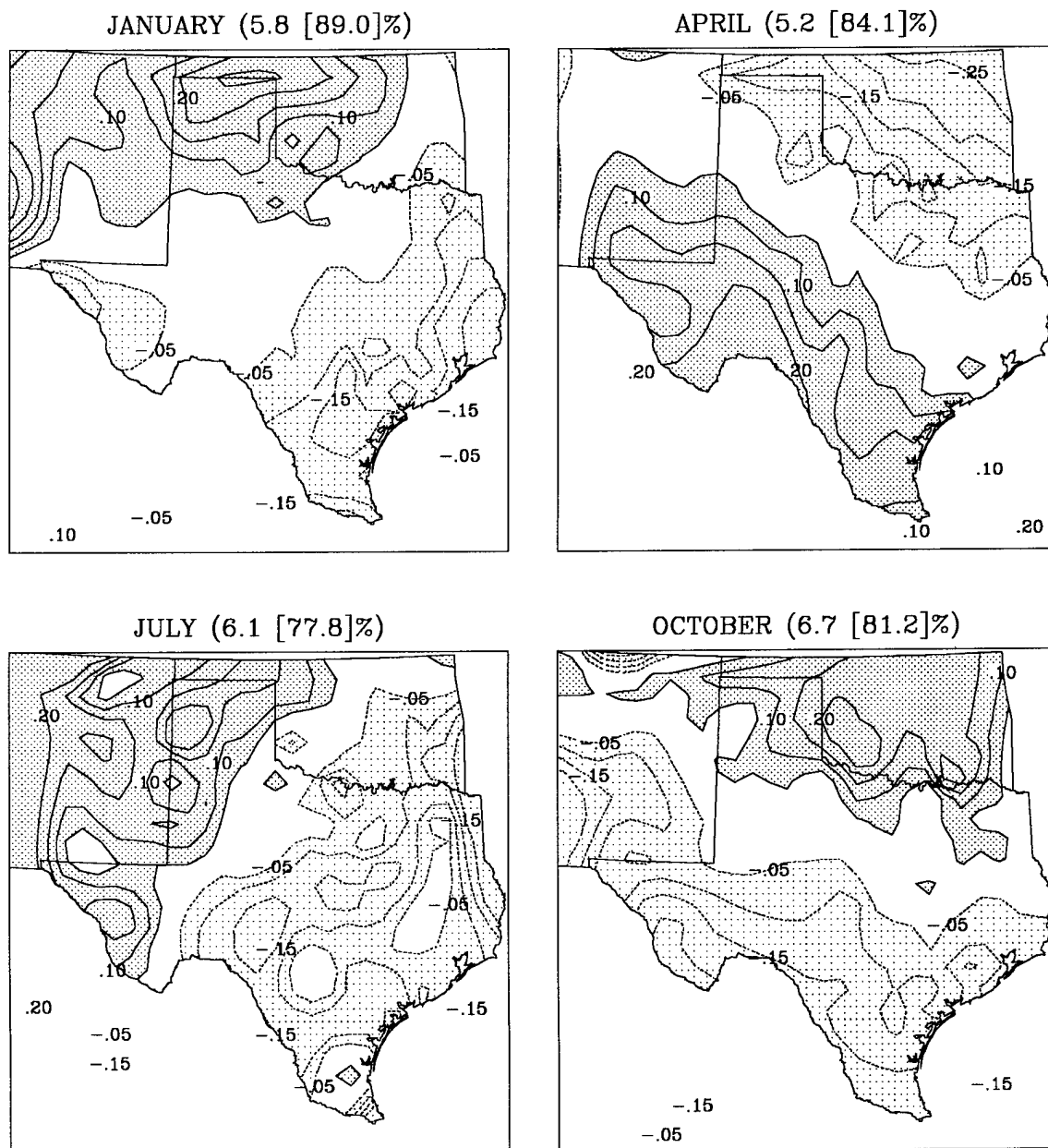


FIG. 33. Third spatial EOF for mean monthly temperature for the months of January, April, July and October. Percent variance associated with each month is indicated in parentheses. Cumulative percent variance for the first three EOFs is in brackets. Shading scheme follows that of FIG. 32.

and have no intrinsic physical meaning at all.

4.3.4. Fourth EOF

The fourth EOF for mean monthly temperature (Fig. 34) is associated with little variance and the spatial patterns depicted appear to be linked to mesoscale and local effects in Texas. However, this EOF is hard to distinguish from noise and any explanations for what is observed are difficult to render.

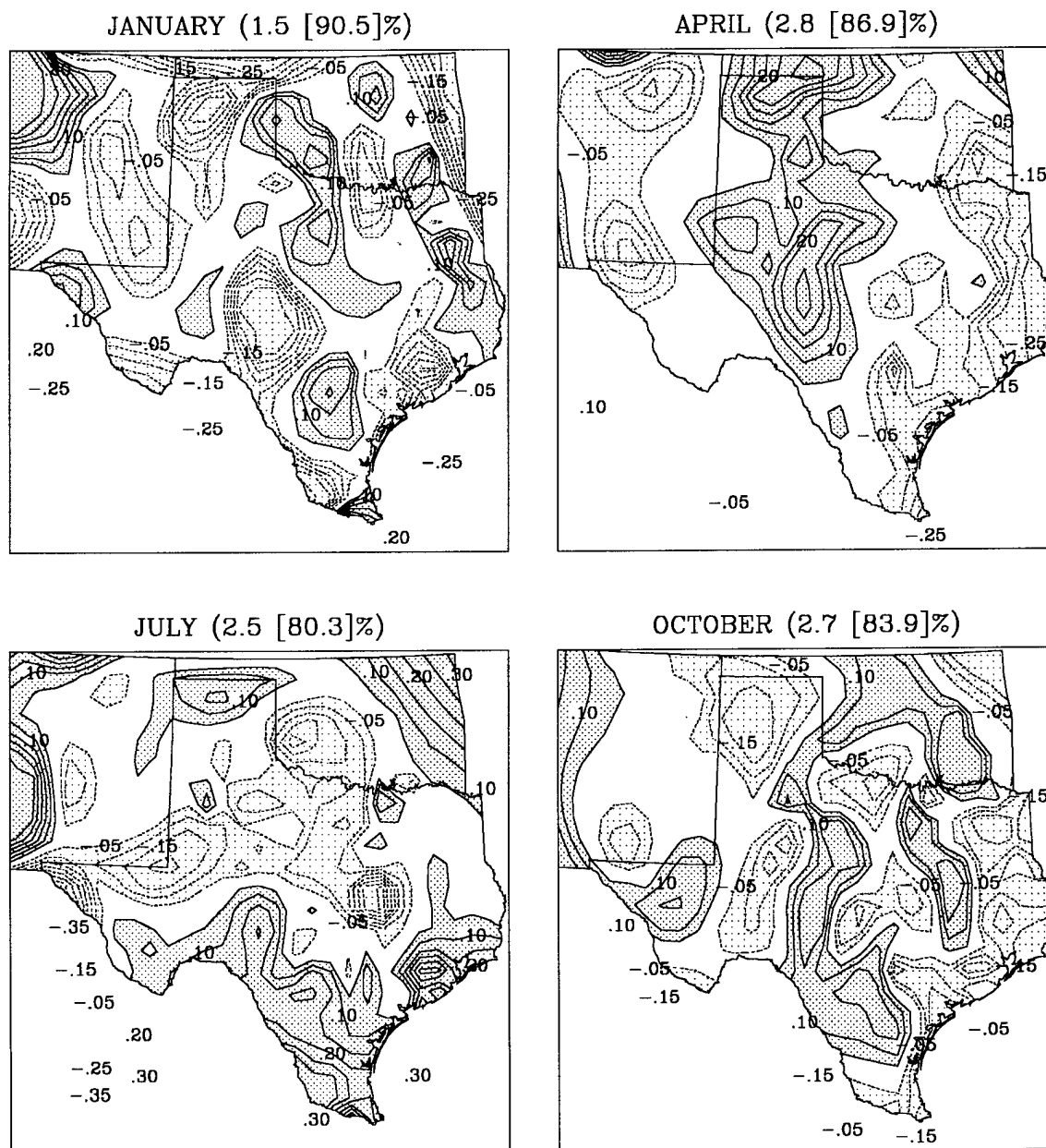


FIG. 34. Fourth spatial EOF for mean monthly temperature for the months of January, April, July and October. Percent variance associated with each month is indicated in parentheses. Cumulative percent variance for the first four EOFs is in brackets. Shading scheme follows that of FIG. 32.

5. SUMMARY AND CONCLUSIONS

This research effort has focused on the fluctuations of surface temperature in Texas on both the spatial and temporal scales. Section 1 introduced the problem and discussed previous research in the area. A main objective of the present study was to examine the variability of the surface temperature field on a regional or local scale. The state of Texas was an ideal location for such a study because of its diversity in climate and its vast network of stations with long historical records.

In section 2, the datasets used in this analysis were discussed. Three time series were actually examined. Besides the standard mean monthly temperature which is a staple of much research, the mean daily maximum and mean daily minimum temperature time series were also analyzed. Possible sources of problems with the data were mentioned, but they were assumed to be not significant enough to affect the final results.

Section 3 was a detailed account of the various methods of analysis used to study temperature and its temporal and spatial fluctuations. Fourier analysis served to isolate the annual and semiannual cycles of surface temperature, from which an amplitude and phase could be computed at each station. It was also applied to insolation, and the resulting phase of insolation was subtracted from that of the annual and semiannual cycles to determine the phase lag of temperature behind solar radiation at each station.

Second-moment statistics were also used to study the variability of surface temperature in Texas. Interannual variability was measured by computing the variance in monthly surface temperature for the months constituting the midpoint of each season, namely January, April, July and October. Spatial correlation, or cross-correlation at lag zero, was calculated around three test sites, each situated in a different climatic region of the state. Finally, temporal correlation, or autocorre-

lation at various lags, was determined. Both one-month and one-year lags were used.

EOF analysis was then performed on the surface temperature anomaly field to determine the dominant modes of variability and the percent variance associated with each mode. EOFs were computed in two ways: with and without the use of an area weighting, or metric, factor. The former takes into account the irregular spacing of grid points used to estimate the continuous surface temperature field and was suggested by North et al. (1982). EOFs were calculated from both yearly and monthly data.

Results from each type of analysis were presented in the form of plots and tables in section 4. In many cases, it was possible to identify the effect of various climate controls on the distribution of surface temperature across Texas. The Gulf of Mexico plays a dominant role in producing the climate of the state, and this fact is borne out in many ways when surface temperature variability is examined. A secondary mechanism, namely the effect of orography on wind flow, seems to also lend some assistance in causing Texas temperatures to fluctuate from their long-term mean values.

From the Fourier analysis, largest amplitudes of the annual cycle are found well inland, where the climate is more continental in nature. Smallest amplitudes are seen along the coast and in the mountainous regions of the state. Largest phase lags of the annual cycle of temperature behind solar radiation are located in the eastern part of Texas. It is this region which is under the influence of the warm, moist Gulf flow throughout most of the year. Smallest lags are found in the higher elevations. It seems that amplitude is a better index of continentality than phase lag in the state of Texas.

Interannual variability is found to be greatest in the month of January, decreasing to a minimum in July. During the winter month, largest variances are in the

eastern part of the state and well inland. In the other months examined, a gradient of variance generally exists from the coast to the interior portions of Texas.

As expected, the spatial correlation length scale was found to be largest in January and smallest in July. The higher frequency of synoptic-scale weather features entering the state in winter seems to be responsible for this difference. Summers in Texas are characterized by mesoscale events, producing the smaller spatial correlations. The length scale is also found to be largest at the inland test site, where a more continental-type climate exists. The coastal point possesses the smallest length scale of the three points examined. This is where the climate is more marine in nature, being near the Gulf of Mexico.

Generally, poor temporal correlation exists across Texas for lags of both one month and one year. Largest values of the latter exist in the eastern part of Texas during the month of January.

The use of area weighting for the EOF computation does not significantly affect the results for the first few modes, which carry the most significance. Nevertheless, these weights, which were defined by Thiessen polygons, were used to compute all the EOFs in this study.

The first four EOFs of monthly surface temperature in Texas are associated with 80-90% of the total variance. The first EOF alone is related to 60-75% of the variance, depending on the season. January's first EOF is associated with more variance than that of July.

This first EOF is a result of primarily large-scale processes. It can be linked to competing airmasses over the state from late fall through early spring and possibly to the effect of continentality in Texas during the summer. The second EOF pattern of yearly temperature data closely resembles the orography of Texas and can be linked to upslope/downslope flow. The shape and pattern of the third EOF appears to be related to the geometry of the state. Since the variance associated with the

second and third EOFs is quite similar, their eigenvalues are unstable and can be easily interchanged. Higher modes of the surface temperature variability are difficult to distinguish from noise and are probably not significant.

This study has applied the methods commonly used in the analysis of temperature fluctuations to the state of Texas. The variability of surface temperature was examined on both the spatial and temporal scales. Large scale processes are found to be responsible for producing the observed distribution of the various parameters studied.

REFERENCES

- Barnett, T. P., 1978: Estimating variability of surface air temperature in the Northern Hemisphere. *Mon. Wea. Rev.*, **106**, 1353–1367.
- Boyle, P. J., and C. E. Dunn, 1991: Redefinition of enumeration district centroids: A test of their accuracy by using Thiessen polygons. *Environ. Plan. A*, **23**, 1111–1119.
- Buell, C. E., 1971: Integral equation representation for factor analysis. *J. Atmos. Sci.*, **28**, 1502–1505.
- Buell, C. E., 1979: On the physical interpretation of empirical orthogonal functions. *Preprints 6th Conf. on Probability and Statistics in Atmospheric Sciences*, Banff, Amer. Meteor. Soc., 112–117.
- Bulmer, M. G., 1979: *Principles of Statistics*, Dover Publications, Inc., New York, 252 pp.
- Climatological Data Annual Summary, New Mexico, 1988–1992*: National Climatic Data Center, Asheville, North Carolina.
- Crutcher, H. L., and J. M. Meserve, 1970: Selected level heights, temperatures, and dew points for the northern hemisphere. *Rep. NAV AIR 50-1C-52 (revised)*, Chief of Nav. Oper., Washington, D.C.
- Driscoll, D. M., P. B. Rice, and J. M. Yee Fong, 1994: Spatial variation of climatic aspects of temperature: Interdiurnal variability and lag. *Int. J. Climatol.*, **14**, 1001–1008.
- Gaffin, D. M., 1993: Comparison of point and areal estimates of temporal fluctuations of climatic elements: A case study for Texas. M.S. Thesis, Dept. Meteor., Texas A&M University, 115 pp.
- Giorgi, F., G. T. Bates, and S. J. Nieman, 1993: The multiyear surface climatology of a regional atmospheric model over the western United States. *J. Clim.*, **6**, 75–95.
- Griffiths, J. F., and D. M. Driscoll, 1982: *Survey of Climatology*, Bell & Howell Company, 358 pp.
- Griffiths, J. F., J. Bryan, and L. G. Shrout, 1987: *The Climates of Texas Counties*, Natural Fibers Information Center, University of Texas, Austin, 569 pp.
- Grimmer, M., 1963: The space-filtering of monthly surface temperature anomaly data in terms of pattern, using empirical orthogonal functions. *Quart. J. Roy. Meteor. Soc.*, **89**, 395–408.
- Hsu, C.-P. F., and J. M. Wallace, 1976: The global distribution of the annual and semiannual cycles in precipitation. *Mon. Wea. Rev.*, **104**, 1093–1101.

- Hyde, W. T., T. J. Crowley, K.-Y. Kim, and G. R. North, 1989: Comparison of GCM and energy balance model simulations of seasonal temperature changes over the past 18,000 years. *J. Clim.*, **2**, 864–887.
- Kendrew, W. G., 1953: *The Climates of the Continents*, 4th ed., Clarendon Press, 607 pp.
- Kidson, J. W., 1975: Eigenvector analysis of monthly mean surface data. *Mon. Wea. Rev.*, **103**, 177–186.
- Kim, J.-W., J.-T. Chang, N. L. Baker, D. S. Wilks, and W. L. Gates, 1984: The statistical problem of climate inversion: Determination of the relationship between local and large-scale climate. *Mon. Wea. Rev.*, **112**, 2069–2077.
- Kim, K.-Y., 1988: *Documentation for the LINEBM Package*. Applied Research Corporation Technical Report, 44 pp. (available from the author at the CSRP, Dept. Meteor., Texas A&M University)
- Kim, K.-Y., and G. R. North, 1991: Surface temperature fluctuations in a stochastic climate model. *J. Geophys. Res.*, **96**, 18 573–18 580.
- Kim, K.-Y., and G. R. North, 1992: Seasonal cycle and second-moment statistics of a simple coupled climate system. *J. Geophys. Res.*, **97**, 20 437–20 448.
- Kim, K.-Y., and G. R. North, 1993: EOF analysis of surface temperature field in a stochastic climate model. *J. Clim.*, **6**, 1681–1690.
- Kirkyla, K. I., and S. Hameed, 1989: Harmonic analysis of the seasonal cycle in precipitation over the United States: A comparison between observations and a general circulation model. *J. Clim.*, **2**, 1463–1475.
- Kutzbach, J. E., 1967: Empirical eigenvectors of sea-level pressure, surface temperature and precipitation complexes over North America. *J. Appl. Meteor.*, **6**, 791–802.
- Lorenz, E. N., 1956: Empirical orthogonal functions and statistical weather prediction. Sci. Rep. No. 1, Statistical Forecasting Project, Contract AF19(604)-1566, Dept. of Meteorology, M.I.T., 49 pp.
- Madden, R. A., 1977: Estimates of the autocorrelations and spectra of seasonal mean temperatures over North America. *Mon. Wea. Rev.*, **105**, 9–18.
- Newton, H. J., 1988: *TIMESLAB: A Time Series Analysis Laboratory*, Wadsworth and Brooks, Pacific Grove, California, 623 pp.
- North, G. R., 1984: Empirical orthogonal functions and normal modes. *J. Atmos. Sci.*, **41**, 879–887.
- North, G. R., and J. A. Coakley, 1979: Differences between seasonal and mean annual energy balance model calculations of climate and climate sensitivity. *J. Atmos. Sci.*, **36**, 1189–1204.

- North, G. R., R. F. Cahalan, and J. A. Coakley, 1981: Energy balance climate models. *Rev. Geophys. Space Phys.*, **19**, 91-121.
- North, G. R., T. L. Bell, R. F. Cahalan, and F. J. Moeng, 1982: Sampling errors in the estimation of empirical orthogonal functions. *Mon. Wea. Rev.*, **110**, 699-706.
- North, G. R., J. G. Mengel, and D. A. Short, 1983: Simple energy balance model resolving the seasons and the continents: Application to the astronomical theory of the ice ages. *J. Geophys. Res.*, **88**, 6576-6586.
- Orton, R. B., 1964: *The Climate of Texas and the Adjacent Gulf Waters*, U.S. Dept. of Commerce, Weather Bureau, Washington D.C., 195 pp.
- Preisendorfer, R. W., and T. P. Barnett, 1977: Significance tests for empirical orthogonal functions. *Preprints Fifth Conf. Probability and Statistics*, Las Vegas, Amer. Meteor. Soc., 169-172.
- Preisendorfer, R. W., and T. P. Barnett, 1983: Numerical model-reality intercomparison tests using small-sample statistics. *J. Atmos. Sci.*, **40**, 1884-1896.
- Prescott, J. A., and J. A. Collins, 1951: The lag of temperature behind solar radiation. *Quart. J. Roy. Meteor. Soc.*, **77**, 121-126.
- Press, W. H., B. P. Flannery, S. A. Teukolsky, and W. T. Vetterling, 1986: *Numerical Recipes*, Cambridge University Press, 818 pp.
- Rubincam, D. P., 1994: Insolation in terms of Earth's orbital parameters. *Theoret. and Appl. Climatol.*, **48**, 195-202.
- Shea, D. J., 1986: Climatological Atlas: 1950-1979. Surface Air Temperature, Precipitation, Sea-Level Pressure, and Sea-Surface Temperature (45°S - 90°N). NCAR/TN-269+STR, 35 pp. plus 158 figures and 10 fiche.
- Weinberger, H. F., 1965: *A First Course in Partial Differential Equations*, John Wiley & Sons, New York, 446 pp.
- White, G. H., and J. M. Wallace, 1978: The global distribution of the annual and semiannual cycles in surface temperature. *Mon. Wea. Rev.*, **106**, 901-906.

VITA

Anthony David Moninski was born on April 16, 1965, in Dudley, Massachusetts, and resided there until 1983. Upon graduating from Shepherd Hill Regional High School in 1983, where he was named class salutatorian, he attended the Pennsylvania State University. He graduated with a Bachelor of Science degree in meteorology and was appointed as a Second Lieutenant in the United States Air Force in 1987.

Anthony was assigned to Beale Air Force Base in California in 1988, where he served as a Wing Weather Officer to the 9th Strategic Reconnaissance Wing in support of SR-71 and U-2 spy aircraft. In 1990 he was reassigned to Kelley Barracks outside of Stuttgart, Germany as the assistant staff weather officer to the Commanding General of the US Army's Seventh Corps. There he provided meteorological support for wartime operations in southern Germany.

Anthony was promoted to the rank of Captain in 1991. In 1992 he was reassigned to Headquarters Fifth Corps in Frankfurt, Germany, serving in the same capacity as in his prior assignment.

In 1993 Captain Moninski was accepted into the Air Force Institute of Technology's advanced degree program to pursue a Master of Science degree in meteorology at Texas A&M University. He performed research toward this end in the area of regional climatology under the direction of Dr. Gerald R. North. During his time there he completed the Air Force's Squadron Officer School in correspondence and was appointed to a Regular commission.

Captain Moninski will be assigned to the Air Force Environmental Technical Applications Center, Simulation and Techniques Branch, at Scott Air Force Base in Illinois upon completion of the master's degree program. His permanent address is 71 Airport Road, Dudley, Massachusetts 01571-0343.